République Algérienne Démocratique et Populaire

Ministère de l'Enseignement Supérieur et de la Recherche Scientifique

École Nationale Polytechnique

Département d'Automatique

Laboratoire de Commande des Processus

Thèse de Doctorat en Science en Génie Électrique

Option : Automatique

Présenté par

CHOUDAR Adel

Magister de L'université de Sétif

Intitulé

A Local Energy Management and Coordinated Control of an Active PV Generator Connected to an Electric Smart Microgrid

Soutenu le 02/07/2017

Directeur de Thèse	BOUKHETALA Djamel	Professeur	ENP
Co-Directeur de thèse	BARKAT Saïd	MCA	Univ. M'Sila
Président du jury	BOUDJEMA Fares	Professeur	ENP
Examinateurs	BERKOUK El Madjid	Professeur	ENP
	GROUNI Saïd	Professeur	UMB Boumerdes
	RADJEAI Hammoud	Professeur	UFA Sétif
	RAHMANI Lazhar	Professeur	UFA Sétif

ENP 2017

République Algérienne Démocratique et Populaire

Ministère de l'Enseignement Supérieur et de la Recherche Scientifique

École Nationale Polytechnique

Département d'Automatique

Laboratoire de Commande des Processus

Thèse de Doctorat en Science en Génie Électrique

Option : Automatique

Présenté par

CHOUDAR Adel

Magister de L'université de Sétif

Intitulé

A Local Energy Management and Coordinated Control of an Active PV Generator Connected to an Electric Smart Microgrid

Soutenu le 02/07/2017

Directeur de Thèse	BOUKHETALA Djamel	Professeur	ENP
Co-Directeur de thèse	BARKAT Saïd	MCA	Univ. M'Sila
Président du jury	BOUDJEMA Fares	Professeur	ENP
Examinateurs	BERKOUK El Madjid	Professeur	ENP
	GROUNI Saïd	Professeur	UMB Boumerdes
	RADJEAI Hammoud	Professeur	UFA Sétif
	RAHMANI Lazhar	Professeur	UFA Sétif

ENP 2017

Acknowledgements

I would like to take this opportunity to express my thanks to everyone who contributed to this work.

My sincere thanks go to my supervisors, **Pr. Djamel BOUKHETALA** (Pr: ENP, Alger) and **Dr. Saïd Barkat** (MCA: université de M'sila), for their confidence in me throughout this project and for their valuable guidance, discussions and insightful comments during the study. I would also like to thank my brother **Mr. Samir GASSAB** (Doctorant: université de sétif), for his moral support and very enjoyable scientific discussions.

For their participation in the scientific evaluation of this work, I would also like to thank members of the jury: Professor **Fares BOUDJEMA (ENP),** Professor **Lazhar RAHMANI,** Professor **HAMOUD Radjeai (UFA),** Professor **El Madjid BERKOUK (ENP)**, and Professor **Saïd GROUNI (UMB).**

Finally, I am infinitely grateful to all my families for their moral support, to my parents for their continuous encouragement.

Abstract

ملخص – هذا العمل يركز على استراتيجية إدارة و تسيير الطاقة، بغرض تحسين عمل نظام كهروضوئي فعال موصول بشبكة التوزيع. الشبكة الذكية المصغرة هي شبكة ذكية في نطاق صغير، وقد تكون قائمة بذاتها أو موصولة بالشبكة. ويستند النظام المقترح على مولد كهروضوئي، بطاريات حمض الرصاص ومكثفات فائقة. تستخدم ثلاثة محولات طاقة لربط عناصر النظام الكهروضوئي إلى مكثف الارتباط المشترك. تدير استراتيجية التسيير تدفق الطاقة بين المحولات والشبكة من خلال مكثف الارتباط المشترك من أجل تلبية متطلبات مدير شبكة الكهرباء. وتستخدم البطاريات كمصدر للطاقة، لتحقيق الاستقرار والسماح للنظام الكهروضوئي الفعال بالعمل على انتاج طاقة ثابتة ومستقرة، لتخميد موجات الذروة في الطلب على الكهرباء وتخزين الفائض من الطاقة الآتي من المولد الكهروضوئي. وتستخدم المكثفات الفائقة كمعدلات كاقة فائقة السرعة في : الحد من التيارات العالية المتبادلة مع البطاريات، مراقبة وتعديل توتر مكثف الارتباط المشترك عند حدوث انقطاع عن الشبكة، تزويد الشبكة بطاقة ثابتة مهما كانت الإضطرابات القادمة من المولد الكهروضوئي، و هذا بتصفيتها. يتم عرض طرق تشغيل عديدة لإدارة تدفقات الطاقة محليا ما بين مختلف المصادر، مع الأخذ بعين الاعتبار: حالة الشحن للبطاريات ، ومستوى التوترللمكثفات الفائقة، الطاقة الكهروضوئية المتاحة و كمية الطلب على الطاقة من طرف مدير (مسير) الشبكة.

كلمات مفتاحية: شبكة ذكية مصغرة، موارد الطاقة الموزعة، التخزين الموزع، نظام كهروضوئي فعال، تسيير الطاقة، طريقة الحد من الطاقة الكهروضوئية، بطاريات حمض الرصاص، المكثفات الفائقة.

Résumé - Le travail présenté dans cette thèse concerne la proposition d'une stratégie de gestion de l'énergie afin d'optimiser le fonctionnement d'un système photovoltaïque actif (APS) connecté à un micro-réseau. Un micro-réseau est un réseau intelligent à petite échelle, qui peut être autonome (isolé) ou connecté au réseau électrique. Le système étudié est basé sur : un générateur photovoltaïque, des batteries au plomb et des ultra-condensateurs. Trois convertisseurs sont utilisés pour relier les éléments de l'APS à un bus-DC. La stratégie de gestion présentée gère le flux de puissance entre les convertisseurs et le réseau par le biais d'un bus-DC afin de maintenir la demande de puissance du gestionnaire réseau. Les batteries sont utilisées comme source d'énergie de longue durée pour stabiliser et permettre aux unités de l'APS de fonctionner à une puissance constante et stable, amortissant les pics de pointe dans la demande d'électricité et stockant l'excès d'énergie du générateur photovoltaïque. Les ultra-condensateurs sont utilisés comme un régulateur rapide de puissance pour limiter le courant échangé avec les batteries, réguler la tension du bus-DC quand le mode d'ilotage est choisi, ils (ultra condensateurs) permettent de fournir une puissance lisse au réseau tout en filtrant les fluctuations de la puissance PV intermittente et celle de la charge. Plusieurs modes de fonctionnement sont présentés pour gérer localement les flux de puissance entre les différentes sources, en tenant compte de l'état de charge des batteries (SOC), du niveau de tension des ultra-condensateurs (Lev), de la puissance PV disponible et de la demande d'énergie des opérateurs réseau.

Mots clés : Microréseau ; ressources énergétiques distribuées ; Stockage distribué ; Système photovoltaïque actif ; Gestion de l'énergie ; Mode limitation PV ; Batteries au plomb ; Ultra-condensateur.

Abstract -The presented work focuses on energy management strategy, to optimize the operation of a grid connected active PV system (APS) in a microgrid. A microgrid is a smart grid in a small scale which can be stand-alone or grid-tied. The proposed system is based on a photovoltaic generator, batteries and ultra-capacitors. Three converters are used to interface the elements of the APS to a common DC-link capacitor. The presented control strategy manages the power flow between the converters and the grid through the DC-link in order to maintain the grid power demand coming from the grid operator. Batteries are used as an energy source, to stabilize and permit the APS units to run at a constant and stable output power, damping peak surges in electricity demand and to store the excess of energy from the PV array. Ultra-capacitors are used as a fast power regulator to: limit the battery's current, regulate the DC-link voltage when the disconnection mode occurs and to deliver a smooth power to the grid, despite primary source and load fluctuations. Several operating modes are presented to manage locally the power flows between the various sources, taking into account the state of charge of batteries (SOC), the energy level of ultra-capacitors (Lev), the available PV power and the power demand from the grid operator.

Keywords: Microgrid; Distributed energy resources; Distributed storage; Active PV system; Energy management; PV limitation mode; Batteries; Ultra-capacitor.

Contents

Contents

Abbreviations

Abbreviations

PV	Photovoltaic
APG	Active PV generator
COM	Control of the operating mode
CCV	Calculation of the control variables
AC	Automatic control
ACU	Automatic control unit
SC	Switching control
SCU	Switching control unit
PCU	Power control unit
PWM	Pulse width modulation
NOM	Normal operating mode
PLS	PV limitation strategy
MPPT	Maximum power point tracking
IM	Islanding mode
FUCM	Full ultra-capacitor mode
EUCM	Empty ultra-capacitor mode
SOC	State of charge
Lev	Voltage level of the ultra-capacitors
FBM	Full battery mode
SU	Storage units
DPC	Direct power control
GFS	Grid following strategy
PDS	Power dispatching strategy
DERs	Distributed energy resources
IT	Information technology
PCC	Point of common coupling
T&D	Transmission and distribution
EV	Electric vehicle

General Introduction

General Introduction

Importance of renewable resources

With the accelerated consumption of the fossil fuel resources in our modern society (Fig.1), a sudden instability can appear may be much faster than we can foresee today. At the same time, the use of fossil fuels contributes to global pollution and climate change [Abb11].

Fig.2 shows the evolution of the final energy consumption by sector in the EU. A statistical analysis shows that the biggest consumers are the transport, the residential and industry sectors [Ecp14]. In addition, much of the energy is consumed in the form of electrical energy [Iea14].

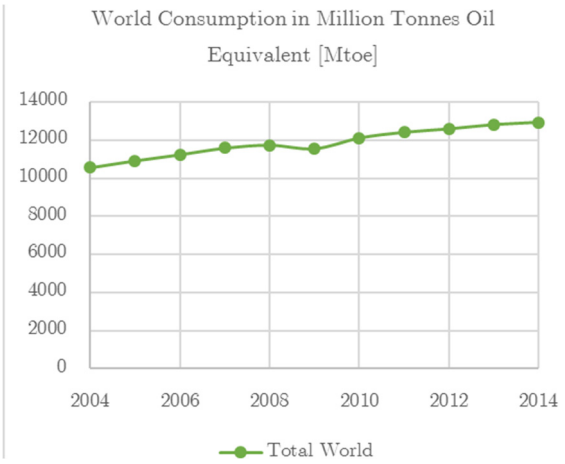

Fig.1. Final Energy Consumption in the World [Bp15]

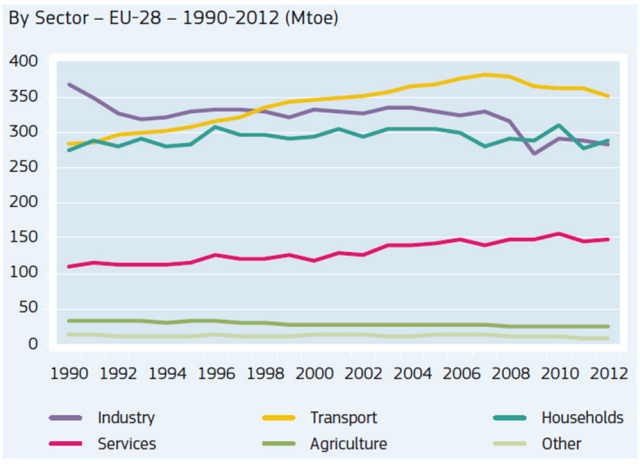

Fig.2. Final Energy Consumption by Sector in the EU [Ecp14]

The electricity is suffering from a constraint irrefutable: At any moment, electrical systems must ensure a balance between production and consumption, while maintaining a satisfactory voltage. Historically, grid reliability was mainly assured by having excess capacity in the system with unidirectional flow to dispersed consumers from centrally dispatched large power plants.

Objectives for future electrical Grids (smart grids)

The massive development of distributed generation (DG) requires changing the architecture of electrical networks and their technical and economic management system. According to the scenarios of their development, these new networks should facilitate bidirectional flows of electric power, and a decentralized network monitoring, integrating intelligence on all levels: large producers, small producers, domestic, and consumers. These

changes lead to the concept of intelligent electrical networks (smart grids), and a new trend of non-centralized energy production close to the end-user by using DG such as photovoltaic systems, wind turbines and other non-conventional sources and their integration into the distribution network forming a localized microgrid [Hat07] [Lis10] [Vel14] [Mot14] [Pal14].

The concept of smart grid is based on the integration of a communication infrastructure and a variety of automation technologies and digital communication services into the electrical infrastructure. The Web can be used as a platform for the incremental addition of new grid applications and their integration with utility systems and external systems and users. The Smart Grid transforms the current grid to one that operates functions more cooperatively, responsively and organically. Bidirectional flow of energy transfers and bidirectional flow of information, coupled with new management capabilities will pave the way for a range of new features and applications that will improve [Lu10]:

- the capacity through the supply of electricity by integration of renewable sources for the huge demand,
- the reliability, through a high quality electricity available whenever it is needed with no interruptions
- the efficiency, through the energy saving from production and transport to consumption of electricity and the best use of resources, i.e. maximize benefits and minimize costs,
- the sustainability, through the use of low carbon energy sources.
- For distribution system operators, first features concern the control of power flows for a better solicitation of assets, the peak shaving, and the deployment of renewable energies. Three levels of innovation can be identified:
  - the improvement of physical infrastructures,
  - the development of customer interfaces in order to refine the management of small dispersed producers and the load demand (communicating meters, wired or not communication network, sensors, communication box, …),
  - the use of grid technologies to improve the energy management of the entire electrical system. This last point and more precisely the design of advanced energy management systems for integrating more PV generators is the general topic of this work.

Limitation of the renewable resources

Nowadays, renewable energies are considered as a fundamental solution for greenhouse gases emissions. Fueled by economic, environmental, and social drivers, the penetration of photovoltaic generators rises in distribution networks. Thanks to its operation without noise and gas emission, it can be easily installed outdoor and on roofs. However, the development of grid-connected PV generation is limited by the intermittent nature and time lag between the production and the consumption. Massive deployments of PV systems complicate the balancing between production and consumption that may cause blackouts if it is disturbed.

Solutions and research themes to be developed

Since the PV power generation is intermittent, PV generator cannot be used directly as a power source because of the lack of the stability, reliability, and controllability. The topic of this thesis is to transform this ineffective PV generator into an active generator by integrating a distributed storage (DS) and a local energy management system for the coordination of inner sources (Fig.3). DS technologies are used in microgrid applications where the generation of the microgrid cannot be exactly matched. DS enhances the overall performance of microgrid systems in three ways. First, it stabilizes and permits DG units to run at a constant and stable output, despite load fluctuations. Secondly, it provides the ride through capability when there is fluctuant primary energy (PV, wind...). Thirdly, it permits DG to seamlessly operate as a dispatchable unit. Moreover, power systems can benefit from energy storage by damping the peak surges in electricity demand, facing short time power disturbances, providing outage ride-through while backup generators respond, and storing energy for future demand [Kro08] [Mot14] [Zha14].

There are several forms of energy storage available that can be used in microgrids, including batteries, ultra-capacitors, and flywheels. Batteries store electrical energy in the form of chemical energy. Many utility connections for batteries have bidirectional converters, which allow energy to be stored and taken from the batteries. Ultra-capacitors are electrical energy storage devices that offer high power density and extremely high cycling capability.

In this thesis, we will propose an enhanced management strategy for a PV based active system. The electrical power required by the grid operator is given as a reference to the microgrid input. The proposed strategy should properly distribute the entire power reference between the system parts. Many constrains are taken into account in the repartition philosophy, such as the availability of the PV power (variable with the solar irradiation), the power demand given by the grid operator and the state of charge of both storage elements

(when they are fully charged, we should not store the power, conversely, when they are empty, we should recharge them), etc. Finally, according to these constraints, a suitable operating mode is selected; then, the proposed strategy of management will calculate and dispatch the power references to the dedicated controllers of the different sources (PV, Bat, and UC).

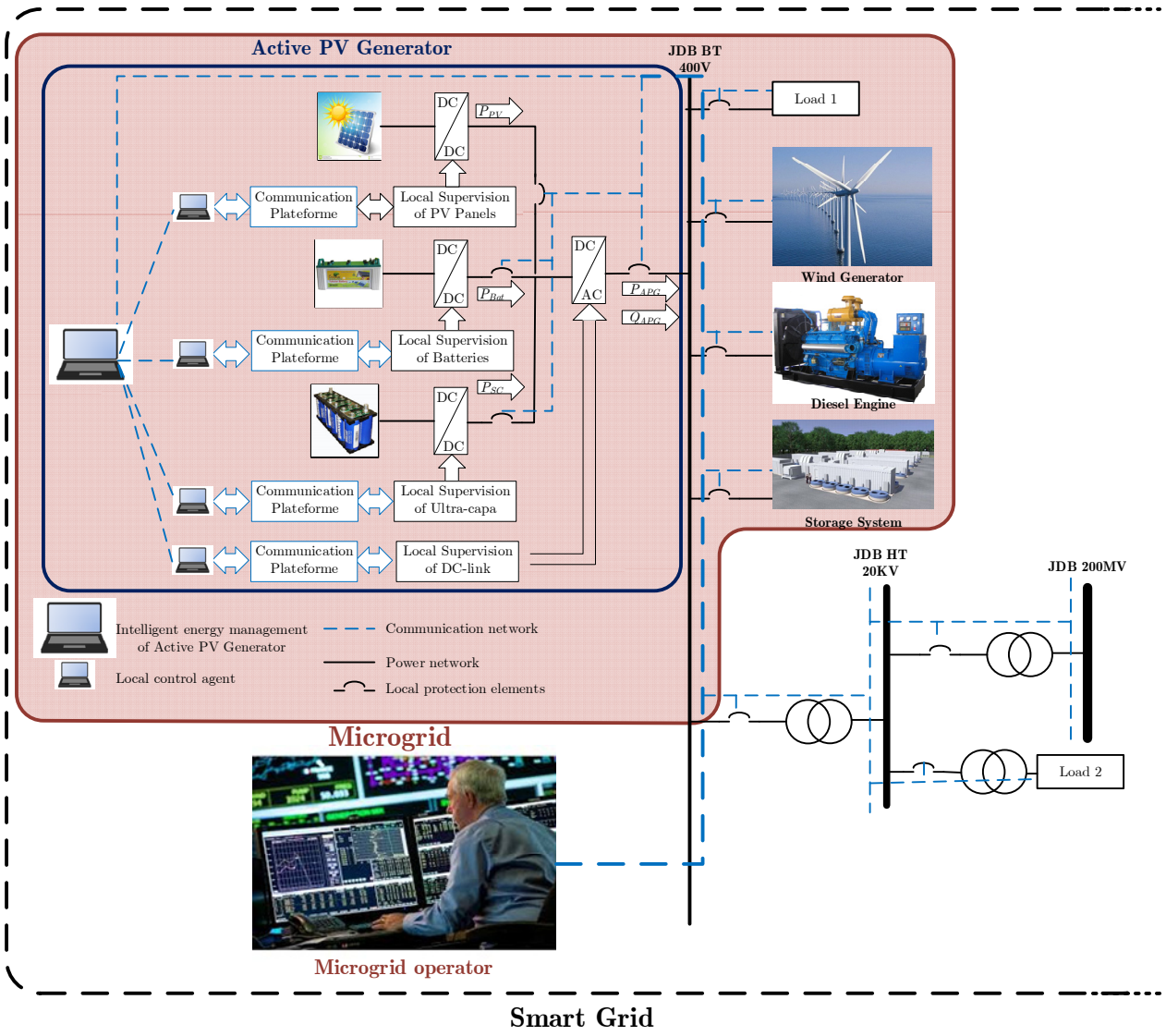

Fig.3. Global scheme of a smart grid includes the studied microgrid.

Thesis organization

This thesis is organized as follows:

In the first chapter, we will commence the work by giving a state of the art on smart microgrids, clarify their components, types and associated benefits, and give some European project examples.

In the second chapter, different forms of renewable energy and different kinds of electrical storage technologies will be presented. A hybrid system based on PV panels, lead acid batteries and ultra-capacitors will be proposed, and each source inside this hybrid generator is described and modeled.

The third chapter consists of the modeling of the power converters with average values, the automatic control laws for all the dedicated power converters (DC-DC boost converter, DC-DC buck&boost bidirectional converter and grid inverter), and the switching control technics.

In the last chapter, a hierarchical control structure is used and the design of the control system, including the power balancing strategies and energy management strategies are detailed. The objective is to set up an active PV generator, which can work like a classical power plant; e.g., it must supply the power references coming from a grid operator.

This management system implements several algorithms in order to provide the power demanded by the main operator of the microgrid. At the same time, it allows to extract the maximum PV power in certain cases, to limit this power if necessary and to respect the storage capacity and the power limits for each of the storage elements in order to optimize their lifetimes. A low-pass filtering method for the internal distribution of the power references will be proposed.

Chapter 01

Chapter 01

1.1. Introduction to Microgrids

a. What is smart grids?

Definitions vary, but broadly speaking, smart grid is used to describe electricity networks having bidirectional communication and power flow capability across the generation sources (conventional and renewable) and demand loads from all types of customers.

Smart grids are fundamentally important for transforming today's electricity grids in order to address growing demand; renewable, intermittent, and distributed generation; and environmental pressures. Microgrids are an integral part of this transformation. However, as in all transformations, there are challenges as well as opportunities.

b. What is microgrid?

The microgrid, as defined by the U.S. Department of Energy, is ''a group of interconnected loads and distributed energy resources (DERs) with clearly defined electrical boundaries that acts as a single controllable entity with respect to the grid and can connect and disconnect from the grid to enable it to operate in both grid-connected or island modes'' [DE12]. Based on this definition, DER installations could be considered as a microgrid if comprised of three distinct characteristics: they must have electrical boundaries that are clearly defined, there must exist a master controller to control and operate DERs and loads as a single controllable entity, and the installed generation capacity must exceed the peak critical load thus it could be disconnected from the utility grid, i.e., the islanded mode, and seamlessly supply local critical loads. These characteristics further present microgrids as small-scale power systems with the ability of self-supply and islanding which could generate, distribute, and regulate the flow of electricity to local customers. Microgrids are more than just backup generation. Backup generation units have existed for quite some time to provide a temporary supply of electricity to local loads when the supply of electricity from the utility grid is interrupted. Microgrids, however, provide a wider range of benefits and are significantly more flexible than backup generation. The concept of microgrids dates back to 1882 when Thomas Edison built his first power plant. Edison's company installed 50 DC microgrids in four years. At that time centrally controlled and operated utility grids were not yet formed.

With the utility grid subsequently utilizing large centralized power plants, which benefited from the economies of scale, and significantly increasing transmission connections for reliability purposes, the electric grid turned into a monopolistic utility by connecting isolated microgrids, and these microgrids faded away. There is a new wave in recent years, however, to deploy microgrids, which is driven in part by the need for higher reliability and power quality, advancements in power electronics and DER technologies, and a more engaging generation of electricity consumers [EPRI01].

The main microgrid components include loads, DERs, master controller, smart switches, protective devices, as well as communication, control, and automation systems. Microgrid loads are commonly categorized into two types: fixed and flexible (also known as adjustable or responsive). Fixed loads cannot be altered and must be satisfied under normal operating conditions while flexible loads are responsive to controlling signals. Flexible loads could be curtailed (i.e., curtailable loads) or deferred (i.e., shiftable loads) in response to economic incentives or islanding requirements. DERs consist of distributed generation units (DG) and distributed energy storage systems (ESS) which could be installed at electric utility facilities and/or electricity consumers' premises. Microgrid DGs are either dispatchable or non-dispatchable. Dispatchable units can be controlled by the microgrid master controller and are subject to technical constraints depending on the type of unit, such as capacity limits, ramping limits, minimum on/off time limits, and fuel and emission limits. The microgrid master controller, on the contrary, cannot control Non-dispatchable units, since the input source is uncontrollable. Non-dispatchable units are mainly renewable DGs, typically solar and wind, which produce a volatile and intermittent output power. The intermittency indicates that the generation is not always available and the volatility indicates that the generation is fluctuating in different time scales. These characteristics negatively affect the non-dispatchable unit generation and increase the forecast error; therefore, these units are commonly reinforced with ESS. The primary application of ESS is to coordinate with DGs to guarantee the microgrid generation adequacy. They can also be used for energy arbitrage, where the stored energy at low price hours is generated back to the microgrid when the market price is high. The ESS also plays a major role in microgrid islanding applications. Smart switches and protective devices manage the connection between DERs and loads in the microgrid by connecting/disconnecting line flows. When there is a fault in part of the microgrid, smart switches and protective devices disconnect the problem area and reroute the power,

preventing the fault from propagating in the microgrid. The switch at the point of common coupling (PCC) performs microgrid islanding by disconnecting the microgrid from the utility grid. The microgrid scheduling in interconnected and islanded modes is performed by the microgrid master controller based on economic and security considerations. The master controller determines the microgrid interaction with the utility grid, the decision to switch between interconnected and islanded modes, and optimal operation of local resources. Communications, control, and automation systems are also used to implement these control actions and to ensure constant, effective, and reliable interaction among microgrid components. Microgrids offer significant benefits for the customers and the utility grid as a whole: improved reliability by introducing self-healing at the local distribution network; higher power quality by managing local loads; reduction in carbon emission by the diversification of energy sources; economic operation by reducing transmission and distribution (T&D) costs; utilization of less costly renewable DGs; and offering energy efficiency by responding to real-time market prices. The islanding capability is the most salient feature of a microgrid, which is enabled by using switches at the PCC, and allows the microgrid to be disconnected from the utility grid in case of upstream disturbances or voltage fluctuations. During utility grid disturbances, the microgrid is transferred from the grid-connected to the islanded mode and a reliable and uninterrupted supply of consumer loads is offered by local DERs. The islanded microgrid would be resynchronized with the utility grid once the disturbance is removed [GEI15], [Mass15]. The installed microgrid capacity is estimated to grow from the 1.1 GW in 2012 to 4.7 GW in 2017 with an estimated market opportunity of $17.3 billion [Sur14]. Considering the growing interest in microgrid deployment, the research on microgrids has significantly increased over the past few years.

By 2020, around 50 billion devices of various kinds could potentially be connected to each other worldwide [MFE13]. Given that there are already 6 billion mobile phones in the world today, even this figure may prove to be too conservative. Electricity grids will be the foundation of this “constellation of microgrids” supplying power to practically all of the other components in one form or another and exploiting the new possibilities that state-of-the-art, efficient information and communication technology (ICT) offers. The sum of these possibilities is often what the words smart grid means and consists in optimally managing the energy all across the system through the coordination of microgrid operations.

Electricity companies have always adopted these types of ideas to some extent, but traditionally, communication has been a one-way process and was limited to connections with a relatively small number of dispatchable generating points. Most consumption data have so far been forecast and subsequently reconciled financially through meter readings with significant time lag. Distribution operators have very limited access to real-time meter data to monitor whether the system is operating, as it should. With the smart grid, communication becomes multidimensional, with information flowing among numerous devices and stakeholders and consumption points connecting with the system in real time. This allows the entire system to be operated more flexibly, facilitating the penetration of low-carbon technologies like electric vehicles or intermittently available renewable energy. Smart grids are also likely to drive deregulation by bringing choices and incentives to consumers of electricity, similar to those already in place in other domains such as telecommunications. The cost of electricity is likely to reflect the impacts of real-time energy prices, which fluctuate hour by hour or even minute by minute. However, the cost of electricity will be packaged commercially to bring net value and convenience to end consumers. In this context, microgrids have been called the impatient upstarts of our energy future. While many microgrid projects share important characteristics beyond their common name, there are equally important differences across the growing number of microgrids around the world. The purpose of this chapter is to: Clarify all the terms relating with the concepts of microgrids; Give a state of the art for the microgrids; Present several European microgrids, focusing on their roles relative to each other and to the overall energy ecosystem.

c. Why Microgrids?

The business objectives of microgrids spring from the confluence of a growing demand for clean, reliable, and economic energy and recent major technology innovation in distributed renewable energy, telecommunications, information technology (IT)/automation, and customer empowerment for customized energy services. These factors are facilitating a shift from classical centralized power systems toward increasingly modular, decentralized microgrids. The major benefits of microgrids include [MEE13]:

- Providing energy services tailored to the requirements of microgrid end users, such as service continuity in times of main grid outage and increased renewable generation;
- operating more efficiently and reliably within the microgrid, as compared with dedicated backup generation in a classical microgrid model;

- enabling parallel operations with the main grid for improved financial performance through economic exchange of energy and ancillary services between the two;
- enabling parallel operations with the main grid for improved service reliability through coordinated response during emergency situations to serve critical loads and to reduce outage impacts;
- enabling innovation in new energy technology and services that have broad societal impact beyond local energy delivery.

d. Types of Microgrids

There are several effective types of microgrids, UGE has done a lot of research to look into possible situations for microgrids, and the company has found three of the most promising microgrid markets.

Telecoms towers: These work in remote locations where microgrids can provide consistent power to base stations.

Single buildings: This could work especially well for civic facilities like hospitals, schools, and fire stations, which can be used to produce energy during times of disaster.

Communities: This is mostly in developing countries with remote locations, where a microgrid can provide about 100 households with all the energy they need throughout the day. A solar energy system with batteries could provide electricity for 50 households in a remote village [MEE13].

1.2. European Microgrid Project Examples [MEE13]

In this section, we present current European microgrid projects. We have selected one microgrid project from each of the following classes of microgrids for comprehensive discussion:

- European utility microgrids
- European city microgrids
- European industrial microgrids.

1.2.1. Grid4EU

Grid4EU is the joint project of a consortium comprised of 27 partners in 12 EU member states. Fig.1.1. shows the landscape of the various Grid4EU projects. ERDF

(Electricité Réseau Distribution France) is the program coordinator for the Grid4EU project in France, and ENEL (Ente Nazionale per l'Energia Elettrica) is the technical director in Italy, with an overall budget of more than €50 million.

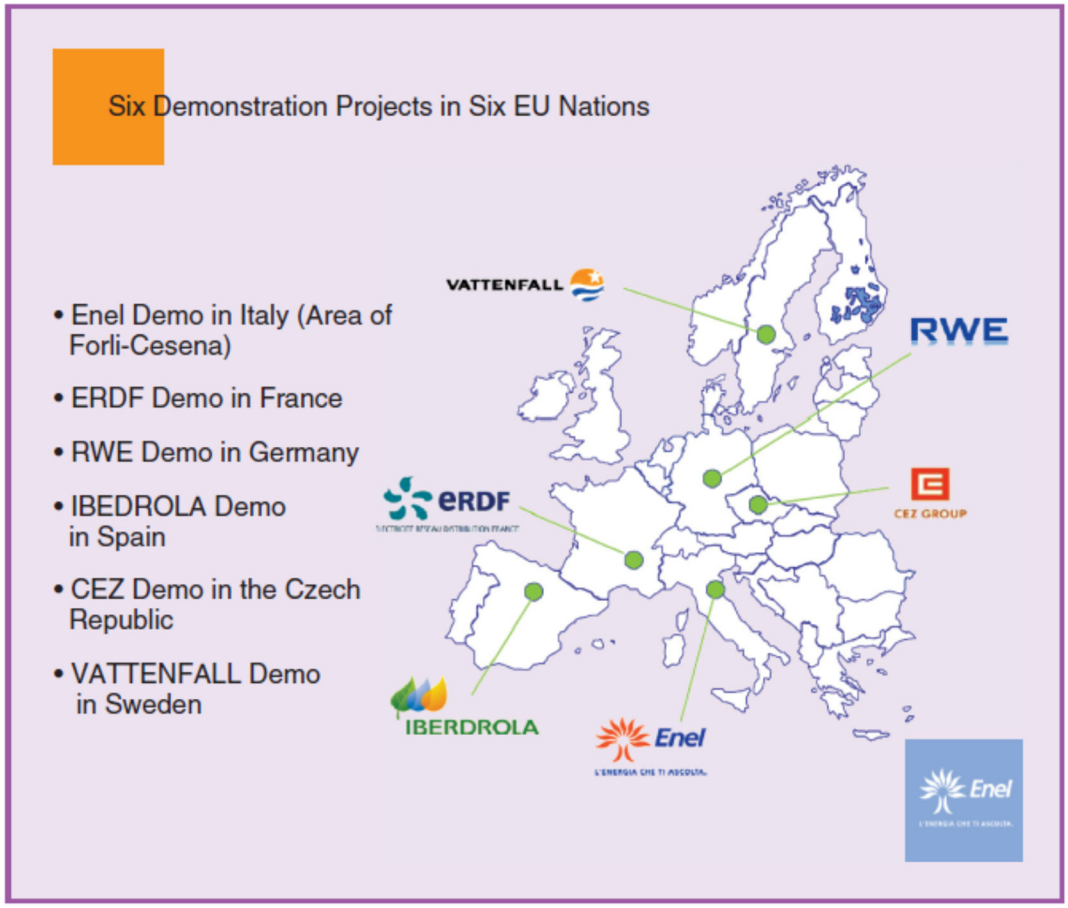

Fig.1.1. Six Grid4EU demonstration projects in six EU nations. (http://www.grid4eu/overview.aspx).

1.2.2. NiceGrid: A Utility Microgrid

The NiceGrid microgrid project is one of the six smart grid projects of the European Union's Grid4EU program, whose partners include Alstom, EDF, ERDF, and others. The microgrid is located in the municipality of Carros, in southeastern France. The project is designed to test an innovative architecture for medium and low-voltage (MV/LV) distribution microgrids with high concentrations of photovoltaic (PV) generators together with smart houses capable of managing their electricity needs. More than 1,500 residential, commercial, and industrial end users are participating in this microgrid project initiative. The project is expected to last four years. Beyond that period, it is planned to be a living laboratory for the region. It should be noted that the Nice region in southeastern France is connected to the bulk power grid through a somewhat fragile transmission corridor, as shown in Fig.1.2. The project is designed to study and test the economic, technical, and social issues related to the microgrids of the future. These include the optimization and

use of MV/LV networks with massive, decentralized, and intermittent insertion of renewable energy sources (principally PV), as well as the behavior of customers, who become agents for their own production, consumption, and storage of electricity. The specific objectives of the NiceGrid project are to:

- optimize the operation of an MV/LV electrical network with a major integration of solar power generation and electricity storage capacities in both grid-connected mode and islanded mode;
- test the islanding of a microgrid based on solar power generation and electricity storage;
- guarantee continuity of supply and reduce potential constraints on the high-voltage transmission lines of the area;
- encourage customers to be proactive in managing the production, consumption, and storage of electricity. The microgrid region includes the Carros industrial district and Carros le Neuf, the existing residential district. The microgrid network topology consists of two substations and several feeders and secondary substations, as depicted in Fig.1.3.

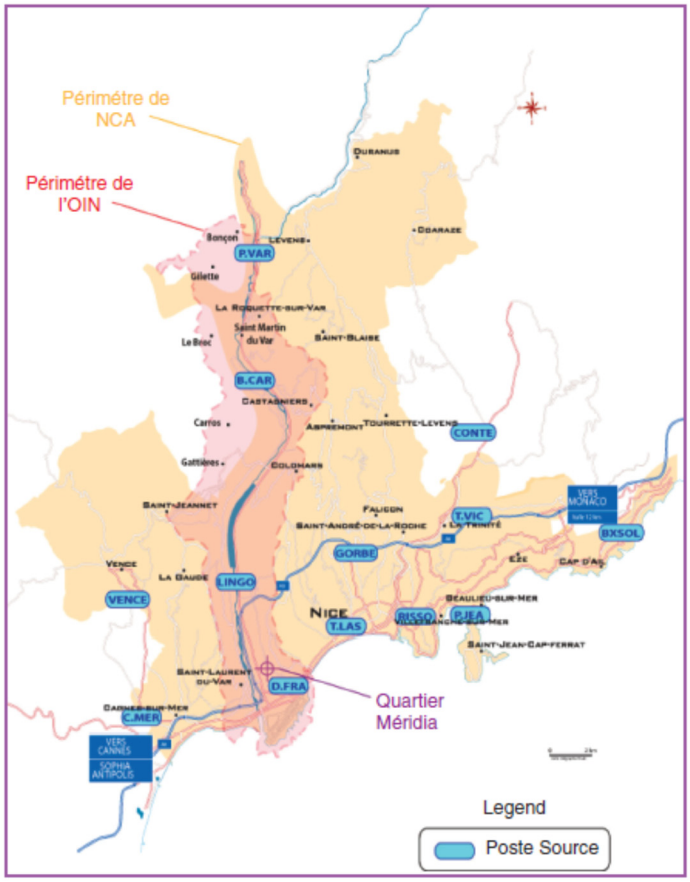

Fig.1.2. The French regional transmission system serving Nice and the surrounding area (source: European Institute for Energy Research).

Key technical challenges of the project include the smooth insertion and management of decentralized and intermittent renewable energy into the distribution grid. The project integrates storage systems with distributed hierarchical decision tiers in the microgrid control and communication architecture.

Another challenge of the project is to enable consumers to become active participants in the local energy balance via distributed resources (DR). A new model of interactions among energy actors (DER asset owners, consumers, commercial aggregators, retailers, and the distribution system operators (DSO)) at the cluster microgrid level is designed a part of the microgrid study. In summary, the microgrid project will test programs of dynamic DER management to :

- enhance the integration of solar power generation into the existing distribution grid;
- ensure the security of energy supply at the local level;
- reduce consumption levels during peak demands;
- study the islanding of a neighborhood based on solar generation and electrical storage.

1.2.3. IssyGrid: A City Microgrid

Coordinated Through Cloud Services France's first smart grid ecodistrict, IssyGrid, is a city microgrid project aimed at optimizing energy usage in the French city of Issy-les-Moulineaux, near Paris. With a consortium of industrial partners led by the French group Bouygues, Alstom and EMBIX (joint venture of Bouygues Immobilier) are contributing the project's smart grid dimension through energy monitoring and control technology that will let the district keep its carbon footprint and energy costs to a minimum. The IssyGrid project is currently being deployed starting from the city's business center with renewable and storage devices. As part of this interconnection, a new cloudbased service is being launched at the city level in Issy-les-Moulineaux to inform end users about their carbon efficiency and link them to future DR programs as well as future multimodal transportation services. This project scheme is illustrated in Fig.1.4. The project's main environmental features are targeted at reducing building energy consumption, integrating more than 1.000m^2 of solar generation and integrating a fleet of electric vehicles in the city. All of this is aimed at reducing greenhouse-gas emissions while keeping energy costs down. During 2012, the project's focus was on indoor and outdoor infrastructure (for example, EV charging points) and ecocity monitoring. The project will ultimately feature all the components of a "smart city," including PV and cogeneration,

energy storage, smart street lighting, EV charging spots, and more, as shown in Fig.1.4. The smart ecocity coverage area will be gradually extended from its initial base

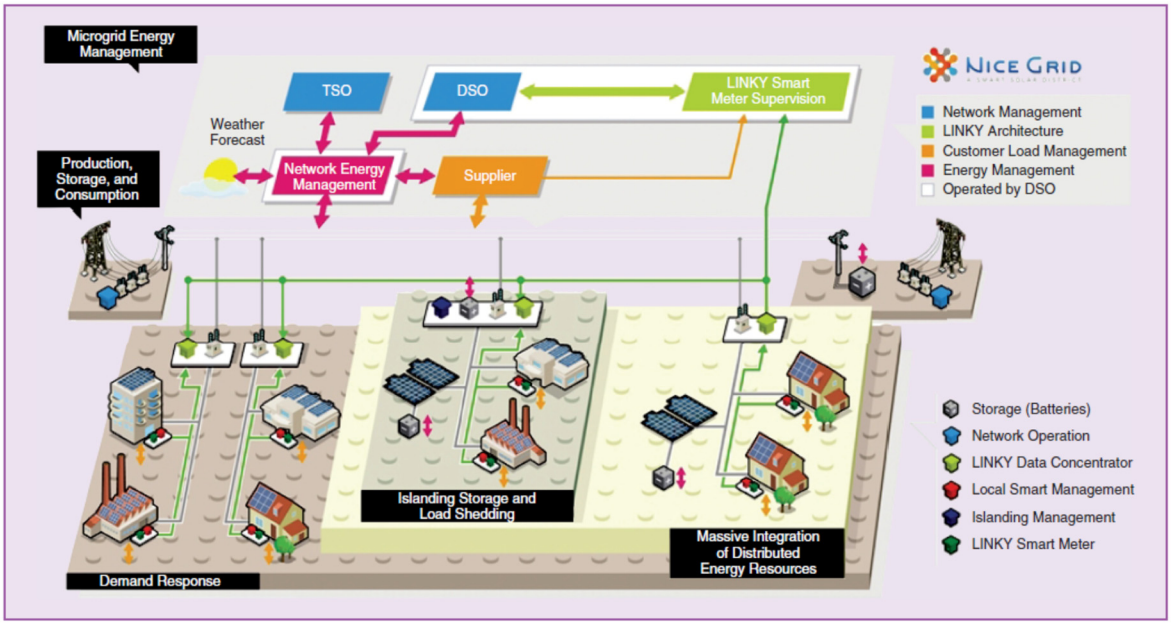

Fig.1.3. NiceGrid microgrid network topology (source: Alstom Grid).

in the Seine Ouest district to the entire city of Issy-les-Moulineaux. IssyGrid will cover the needs of nearly 10,000 people in a 160.000m^2 area. The key objectives of the project are:

- integration and optimization of distributed CO2- free power sources through distributed generation.

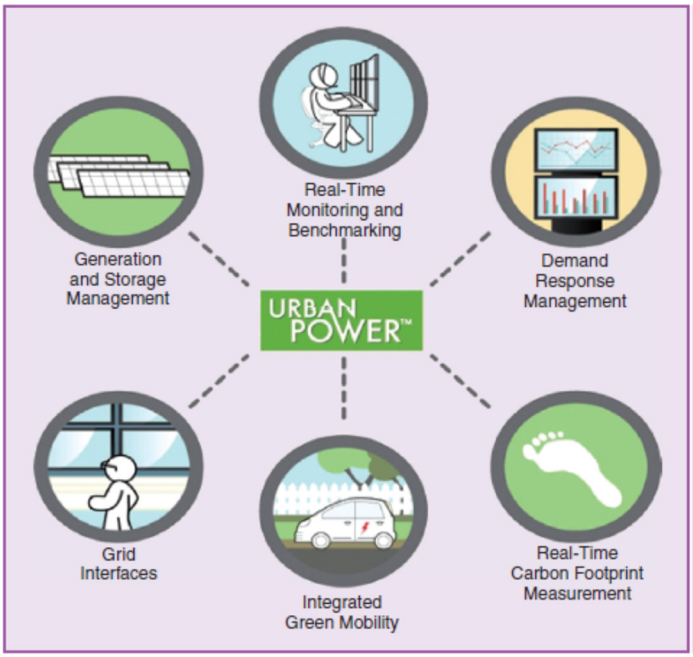

Fig.1.4. IssyGrid's Urban Power project scheme (source: Alstom Grid).

- optimization of energy and transportation resources through CO2 emission planning and monitoring; generation, load, and storage balancing within city nodes; management of congestion in city infrastructures; and management of critical infrastructure availability.

1.2.4. Réflexe : An Industrial VPP and Microgrid

The Réflexe project, considered in its entirety, forms a VPP by integrating renewable generation, storage, and DR among several industrial sites. In addition, some of the large industrial sites connected to the grid could potentially operate as microgrids. Though the overall project in its current form is a VPP. The VPP scheme shown in Fig.1.5 will integrate many diverse and widespread sources of decentralized generation, storage, and consumption. The VPP will therefore have to manage considerable amounts of information in real time using a communication network in parallel with a power network. Key project objectives include

- reducing carbon emissions through renewable integration;
- optimizing the overall cost of operation through DR in a VPP framework;
- realizing additional revenue streams through integration with deregulated markets.

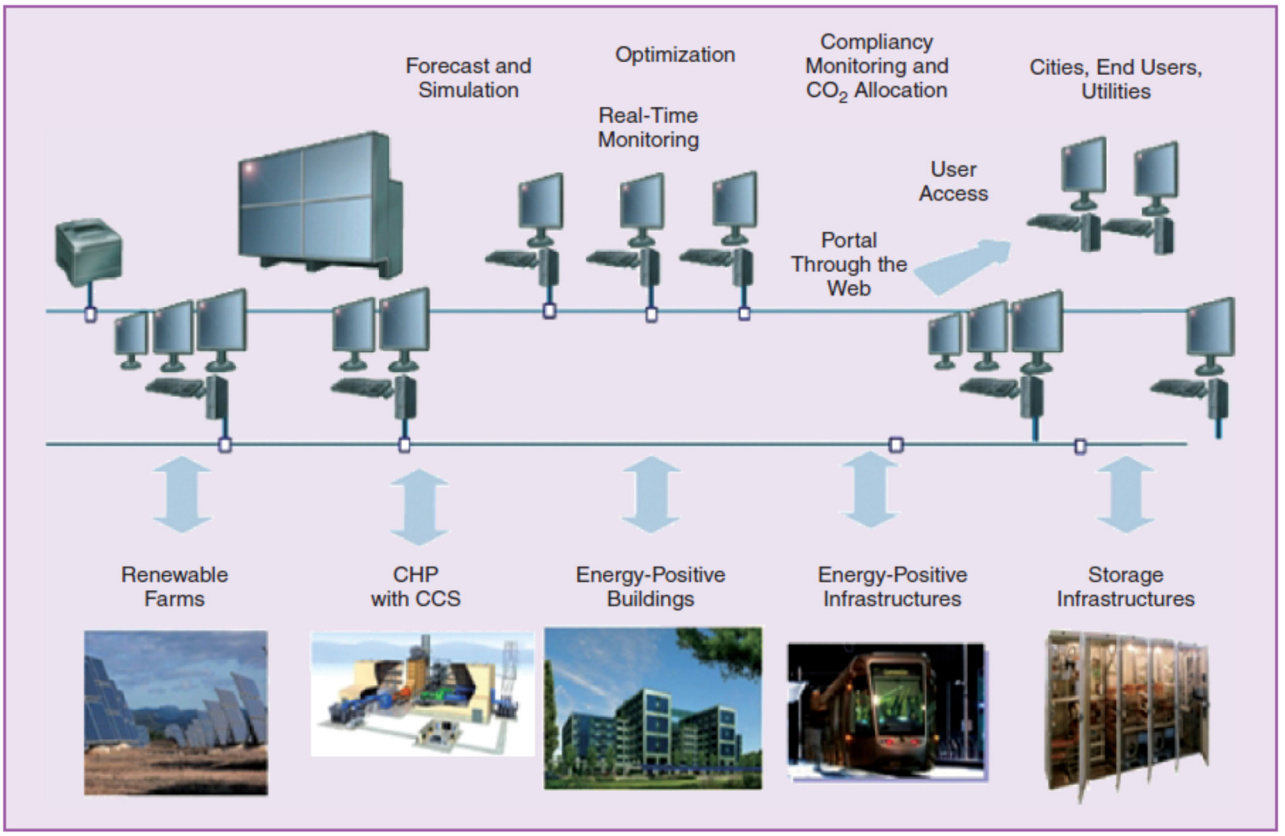

Fig.1.5. Réflexe VPP and microgrid schematic (source: Alstom Grid).

1.3. Conclusion

Microgrid penetration is currently growing across the globe, leading to various challenges and opportunities. This chapter attempted to provide a state of the art on micro-grids, hence paving the way for interested educators in gaining insight into this important and timely topic and understand a variety of microgrid-associated issues under investigation by the research community. The chapter comprised of an introduction to microgrids, their components, types of microgrids and associated benefits, and European project examples.

Chapter 02

2. Description and Modeling of the Active PV Generator

2.1. Introduction

An active generator is a hybrid power system combining the renewable energy sources and the storage units; it can provide the demanded power by the grid operator. Integrating long-term storage such us batteries with photovoltaic power sources, can lead to a long-term reliable energy source. To ensure a good power quality, the ultra-capacitors have fast dynamics; thus, can be used to smooth fast fluctuations of the photovoltaic power.

In this chapter, different forms of renewable energy and different kinds of electrical storage technologies will be presented. A hybrid system based on PV panels, lead acid batteries and ultra-capacitors will be proposed, and each source inside this hybrid generator is described and modeled.

2.2. Renewable Energy

Renewable energy is the energy generated from natural resources. As international Energy Agency describes: Renewable energy is derived from natural processes that are replenished constantly. In its various forms, it derives directly from the sun, or from heat generated deep within the earth. Included in the definition is electricity and heat generated from solar, wind, ocean, hydropower, biomass, geothermal resources, and biofuels and hydrogen derived from renewable resources [Iea03].

2.2.1. Importance of Renewable Energy

Accelerating the deployment of renewable energy will fuel economic growth, create new employment opportunities, enhance human welfare, and contribute to a climate safe future.

Advances in renewable energy technologies and growing cost-competitiveness have strengthened the business case of renewables and opened new opportunities for countries to transform their energy systems.

The study presented in [IRE16] demonstrates that the benefits of scaling up renewable energy surpass cost competitiveness. Increased deployment can meet the energy needs of a growing population, drive development and improve well-being, while reducing greenhouse gas emissions and increasing natural resource productivity. It provides empirical evidence that economic growth and environmental conservation are fully compatible, and that the conventional consideration of trade-offs between the two is outdated and erroneous.

2.2.2. Constraints

The development of the different renewable sources is limited by different constraints depending on their intrinsic characteristics. Hydropower and geothermal power are naturally limited because of the lack of geographic sites. Biomass requires large storage places for the natural resources. This is the reason why a large development of PV and wind turbines is waited. Unfortunately, these renewable energy sources are intermittent power sources (Fig.2.1). The production of electricity from solar sources depends on the amount of light energy in a given location. Solar output varies throughout the day and through the seasons, and is affected by cloud cover. Wind-generated power is a variable resource, and the amount of produced electricity will depend on wind speeds, air density and turbine characteristics (among other factors). If the wind speed is too low (less than about 2.5m/s) then the wind turbines will not be able to make electricity. If it is too high (more than about 25m/s) the turbines will have to be shut down to avoid damage. As this primary source is uncertain these kinds of renewable energy sources may produce a large amount of power when loads in the grid are very low. And they are not always available when it is necessary, such as solar in the night and wind power when the wind is not blowing. The addition of intermittent resources causes large amounts of variable power. Renewable energy based generations with intermittency decrease the reliability of a power system.

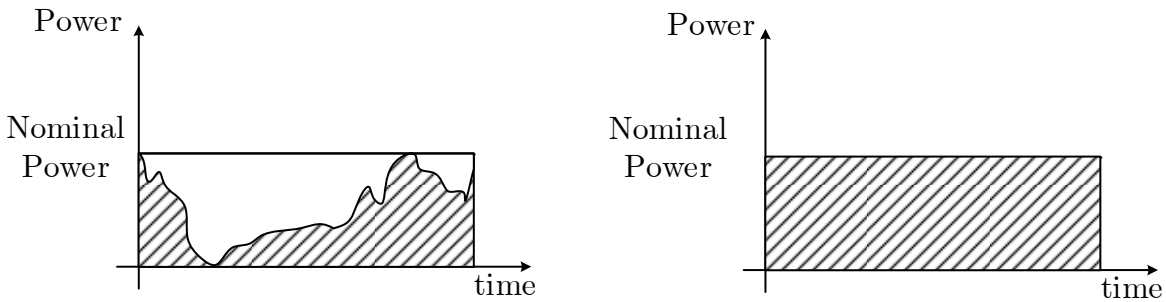

Fig.2.1. Difference between dispatchable and non-dispatchable energy sources.

2.2.3. Dispatchable and Non-Dispatchable Renewable Energy Based Generators

Dispatchable energy sources are those sources that can be ramped up or shut down in a relatively short amount of time. This could refer to time intervals of a few seconds up to a couple of hours. They are considered as active generators because they can usually provide some ancillary services to the grid, basically frequency regulation by active power control, voltage regulation by reactive power control, etc. Depending on the response speed of a form of dispatchable power, it may fulfill one of many distinct roles in the power grid. For

instance, hydroelectricity generally has very quick response times while coal and nuclear are relatively slow. While hydroelectricity might be used to match peaks in demand on a second to minute scale, the flexibility of some coal stations might be used to help follow the general trend of power usage during the day.

In contrast, many renewable energy sources are intermittent and **non-dispatchable**, such as wind power or solar power which can only generate electricity while their energy flow is input on them. They are not dispatched by a grid system operator because their output active and reactive powers are not controllable.

2.3. Energy Storage

In today's power systems, growing demand, as well as the increasing renewable energy portfolio, have amplified the need for utilities to find new ways to manage their system and improve reliability. One potential solution is what is commonly referred to as the "holy grail" of the industry "energy storage".

The utility industry does not have a common warehouse or inventory of the product they produce. When a customer turns on a light switch or starts a large industrial motor, the power is consumed immediately from on-line generation. Until now, it has not been economical to store this power. The increased attention on renewable energy makes energy storage a practical option, and increasing production of electric vehicles is driving cost improvements that make battery storage a solution that is finally viable [ABB11].

Electrical energy storages (EES) are considered as an effective solution counter the power intermittency, which is the major inconvenient of the renewable energy sources. The EES can handle the intermittency of power supply, which is caused by:

- The renewable energy sources;
- The operating error, unplanned outage, component failures and etc.

2.4. Distributed Energy Storage (DES)

NAATBatt broadly defines DES as a group of typically smaller energy storage units sited on the distribution-side of the electric grid system—either at a distribution substation, along the system feeders, or at an electric utility customer premise. DES units are usually two megawatts (MW) or less in size. However, DES units can also potentially be scaled in the tens-of-MWs range in certain grid applications. A new and emerging DES concept of community energy storage (CES) shows promise for wide-spread deployment. CES is a kilowatt (kW)-scale energy storage unit connected to secondary transformers along feeders

serving groups of houses or small commercial buildings. Fig.2.2. offers a visualization of the different scales and locations of grid-connected energy storage technologies [NAA12].

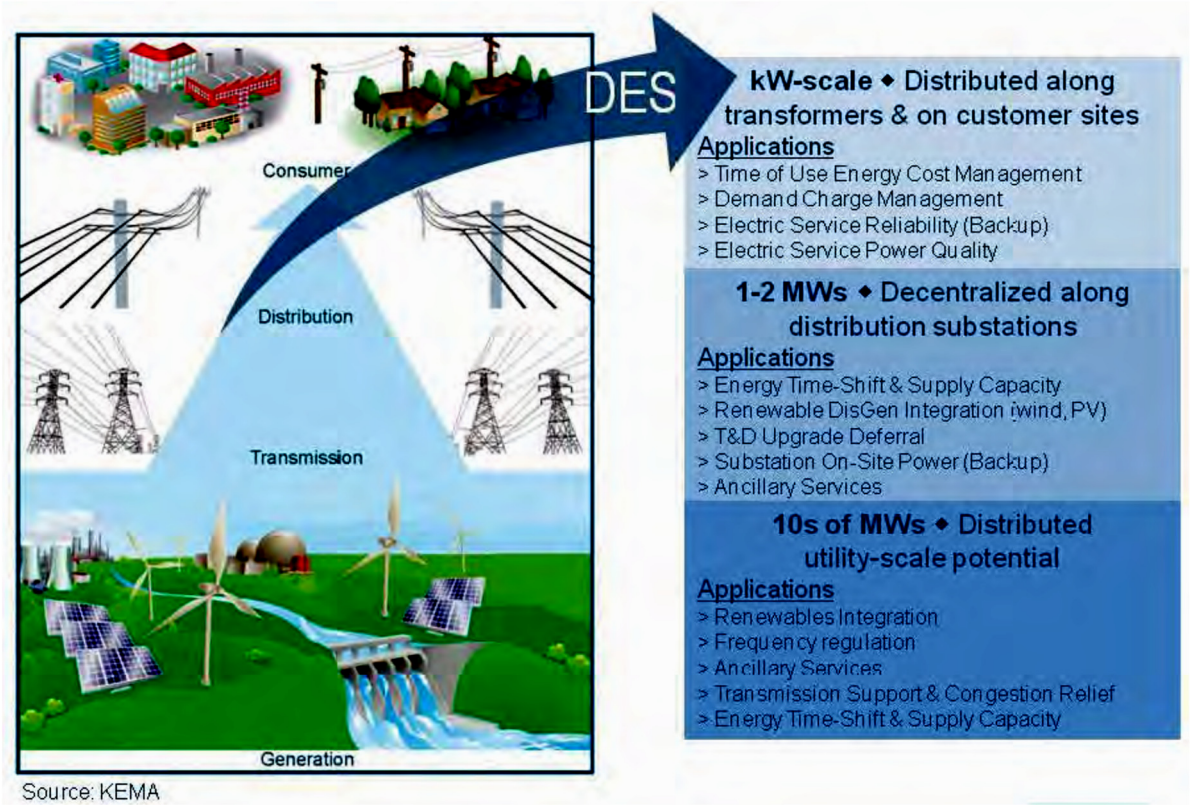

Fig.2.2. Different Scales & Locations of DES.

DES is a particularly valuable asset. Utilities across the world are already turning to DES as a cost-effective alternative to transmission and distribution upgrades, and as a way to avoid or defer construction and use of expensive, inefficient fossil-fueled peaker plants[1].

Small energy storage systems can be conveniently located behind the meter at the customer site, allowing for relief of grid congestion even in densely populated areas where space may be at a premium.

In addition to grid benefits, when combined with renewable generation, such as solar photovoltaic (PV) panels and islanding equipment, these systems can provide companies and communities with resilient power when the utility grid is unavailable due to equipment failure, natural disaster, or for other reasons.

2.4.1. Performance Requirements & Specifications

As summarized in Tab.2.1 and Tab.2.2, DES performance requirements can vary depending on system location, size and application needs. Performance requirements can also

[1] A supplemental power plant that operates only when demand for power is high. These plants often run on natural gas. The American Heritage® New Dictionary of Cultural Literacy, Third Edition

vary according to the primary end-user application. A DES is designed to meet specific system needs around cycle life, energy density, response time, rate of charge/discharge, and efficiency.

Tab.2. 1. Energy Storage Grid Applications & System Requirements.

Applications & Requirements	Group 1	Group 2	Group 3	Group 4
Storage Type	High-energy	High-power	High-energy	High-power
Discharge Duration	Hours	Minutes	Hours	Seconds
Frequency of Usage	Frequent	Frequent	Occasional	Occasional
Applications	1. Energy time shift 2. Electric supply capacity 3. Load Following 4. Time-of-use Energy Cost Management 5. Demand Charge Management 6. Renewables Time-shift 7. Renewables Capacity Firming 8. Wind integration(time shift)	9. Area Regulation 10. Voltage Support 11. Wind Integration (Intermittency) 12. PV Smoothing	13. Electric Supply Reserve Capacity 14. Transmission Congestion Relief 15. T&D Upgrade Deferral 16. Substation on-site Power (DC backup) 17. Electric Service Reliability (Backup)	18. Transmission Support 19. Electric Service Power Quality

A DES system can consist of different types of energy storage devices. Typically, an interconnected DES system is comprised of a distributed fleet of advanced battery technologies, each providing at least 15 kVA of active and reactive power and 25-75 kWh of energy at 240/120V AC. The DES fleet also requires a central dispatch control and communications (Chapter 04) to optimize the system operations and benefits.

Tab.2. 2. General DES System Performance Specification by End-User.

End-User	Key Parameter	Value
Residential	Power (active & reactive)	up to 100kVA
	Energy	up to 2 hours of discharge at rated power
	Voltage	120V/240V, single phase
Commercial & Light Industrial	Power (active & reactive)	Up to 500 kVA
	Energy	up to 2 hours of discharge at rated power
	Voltage	480V, three phase
Renewable	Power (active & reactive)	Application-specific
	Energy	Application-specific
	Voltage	Application-specific
Utility & System Operators	Power (active & reactive)	Larger than 1MVA
	Energy	Application-specific
	Voltage	Use Step-up transformers

2.4.2. Different kinds of energy storage

Energy can be stored in different forms:

- Chemical: Hydrogen, biofuels, liquid nitrogen, oxyhydrogen …
- Electrochemical: Batteries, flow batteries, fuel cells …
- Electrical: Capacitor, ultra-capacitor, superconducting magnetic energy storage, …
- Mechanical: Compressed air energy storage, flywheel energy storage, hydraulic accumulator…
- Thermal: Ice storage, air-conditioning…

For electrical applications, according to the different requirements, various kinds of storage technologies are used with specific characteristics such as the rated current /voltage, the capacity of electrical power/energy, the maximum current, the minimum voltage, the weight, the volume and etc.

Fig.2.3 shows the characteristics of the energy density and the power density for different electrical storage technologies.

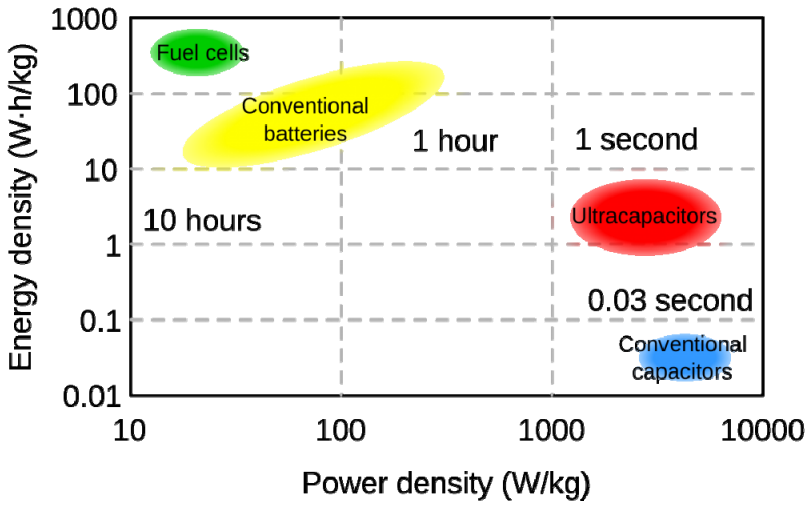

Fig.2.3. Energy Density & Power Density of Energy Storage Technologies [URL13]

2.4.3. Power Versus Energy Storage Systems

In general, electric energy storage is categorized based on function to provide power or to provide energy. Although certain storage technologies can be used for applications in both categories, most technologies are not practical and/or economical for both power and energy applications. For example, energy applications use storage to decouple the timing of generation and consumption of electric energy, while power applications use storage to ensure

continuity, quality, and proper frequency of delivered power in real time. In general, energy applications involve (relatively) long-duration discharge and power applications involve short duration discharge. Table 1.1 shows the suitability of some of the more common technologies (battery and others) for various applications.

Tab.2. 3. ESS applications by category (power or energy) [Ebk13].

Technology	Advantage	Disadvantage	Power applications	Energy applications
Flywheels	High power	Low energy density	Fully capable and reasonable	N/A
Electrochemical capacitors (ECs)	Long cycle life	Very low energy density	Fully capable and reasonable	N/A
Traditional Lead-acid	Low capital cost	Limited cycle life	Fully capable and reasonable	Feasible but not practical
Advanced lead-acid with carbon-enhanced electrodes	Low capital cost	Low energy density	Fully capable and reasonable	Fully capable and reasonable
Sodium sulfur (Na/S)	High power and energy density	High cost and restrictive operating parameters (high-temperature operation)	Fully capable and reasonable	Fully capable and reasonable
Lithium-ion (Li-ion)	High power and energy density	High cost and extensive control circuitry	Fully capable and reasonable	Reasonable
Zinc bromine (Zn/Br)	Independent power and energy	Medium energy density	Reasonable	Fully capable and reasonable
Vanadium redox	Independent power and energy	Medium energy density	Reasonable	Fully capable and reasonable
CAES	High energy, low cost	Special site requirements	N/A	Fully capable and reasonable
Pumped hydro	High energy, low cost	Special site requirements	N/A	Fully capable and reasonable

2.5. Hybrid Power Generator

2.5.1. Interest

Wind and solar energy based generators are passive generators since they cannot participate in the energy management of a grid. Their power production is not controllable. So, they cannot ensure a high reliability with a good efficiency for a power system.

In contrast, conventional power generators (fossil fuel generators, nuclear fuels…) are controllable and can supply the necessary power to satisfy the grid power requirements. Moreover, this controllable power can provide some ancillary services to the grid (frequency regulation, voltage regulation, etc…). However, conventional power generators must face to the fossil exhaustion and environmental challenge.

Since the PV power generation is intermittent, PV panels cannot be used directly as a power source because of the lack of the stability, reliability and controllability. Energy storage devices can be used to store or to release electrical power like an energy buffer, supporting the operation of sources, transmission, distribution and loads.

The combination of energy storage devices and a renewable energy based generator constitutes a hybrid power generator. It provides not only a clean energy but also a high

power quality. Moreover, this hybrid power system becomes an active generator, which can supply ancillary services to the grid as conventional generators.

2.5.2. Configuration and description

a. Improvement of reliability and erasing the intermittency

In the studied hybrid power generator, photovoltaic Arrays work as the main power source. A fleet of lead acid batteries is chosen as an energy storage device for shaving the PV peak power during the daytime and restoring it during sun unavailability. There sizing will depend on the desired reliability for the active power system. A bank of ultra-capacitors is used for the fast dynamic power compensator, in order to smooth the transient PV power fluctuations. A little description of the system components is now presented.

b. Photovoltaic Solar Cells

- *Energy conversion*

In the PV generator occurs the conversion of the incident radiation into electrical energy by means of the photoelectric effect. This occurs when doped semiconductors of main group IV of the periodic table of elements generate charge carriers when they are irradiated with light. The most used basic material is silicon, which is doped with elements of the main group III or V. The doping result is either an N-type or a P-type semiconductor. Between N-type and P-type semiconducting layers exist a P-N-junction which causes an electric field and generates a DC voltage. Contacts on the upper and lower side of the layers allow a current flow to an external electric circuit. These contacts are designed as metal fingers on the upper side and as metal film on the lower side of the PV cell (Fig.2.4). One PV cell delivers a no-load voltage in the range 0.5-0.7 V and a short-circuit current of 2.5 to almost 7 A. In PV modules the cells are connected in series for voltage increase.

Light of certain wavelengths are able to ionize the silicon atoms (causing atoms to either gain or lose electrons) and the internal field produced by the PN junction separates some of the positive charges ("holes") from the negative charges (electrons) within the photovoltaic device. The holes are swept into the positive or p-layer and the electrons are swept into the negative or n-layer. Although these opposite charges are attracted to each other, most of them can only recombine by passing through an external circuit outside the material because of the internal potential energy barrier. Therefore, if a circuit is made (Fig.2.4), power can be produced from the cells under light because the free electrons pass through the load to recombine with the positive holes.

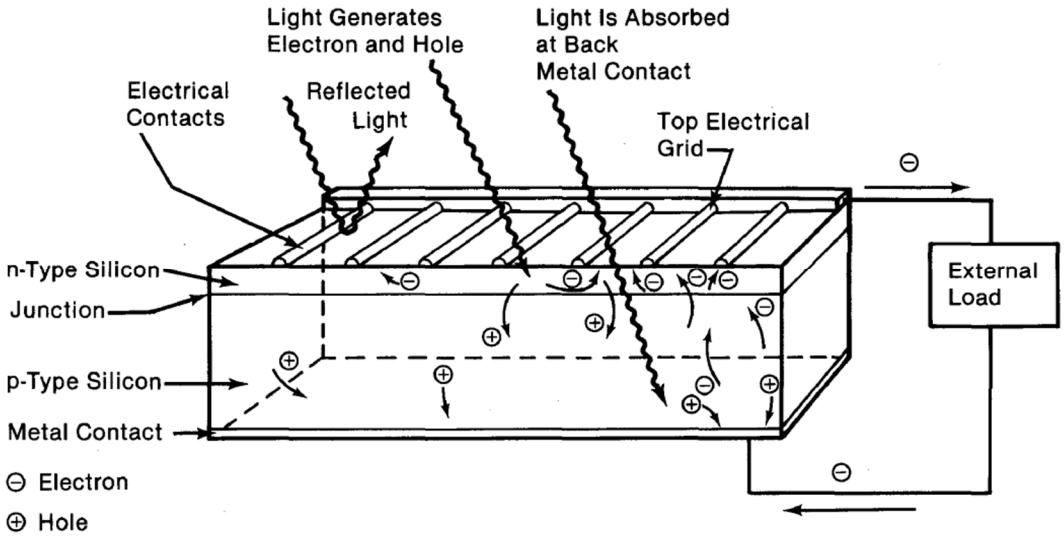

Fig.2.4. Photovoltaic effects in a solar cell [SERI82].

c. Lead-acid battery

Lead-acid batteries, invented in 1859 by the French physicist Gaston Planté, are the oldest type of rechargeable batteries. Despite having a low energy/weight density and a corresponding low energy/volume density, their ability to supply high surge currents means that the cells maintain a relatively large power/weight density. Batteries use a chemical reaction to do work on charge and to produce a voltage between their output terminals. A lead-acid battery uses lead and lead oxide for electrodes and sulfuric acid for the electrolyte solution (Fig.2.5). The reaction of lead and lead oxide with the sulfuric acid electrolyte produces a voltage. The supplying of energy to an external resistance discharges the battery. The discharge reaction can be reversed by applying a voltage from a charging source. With the energy for charging battery, the lead sulfate is broken down and with oxygen from ionized water, lead oxide is deposited on the positive electrode and lead is deposited on the negative electrode [Ebk01].

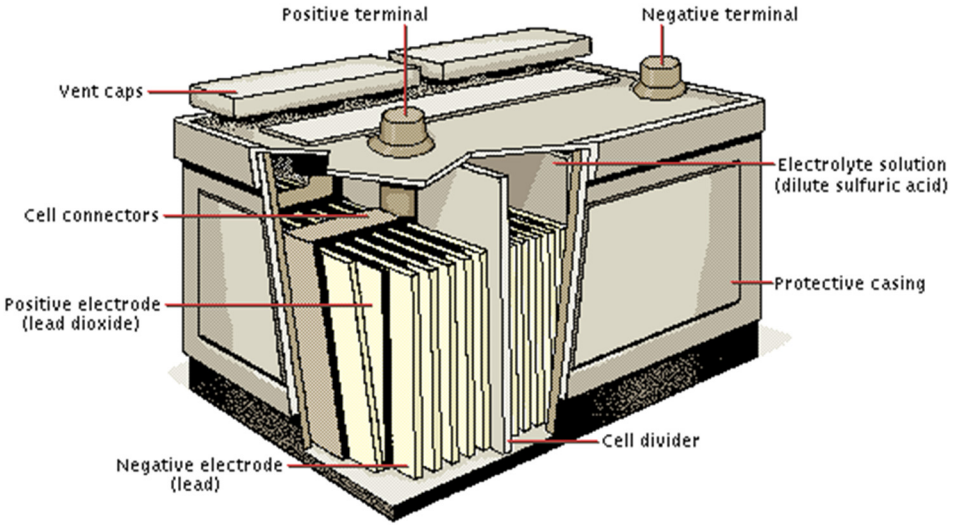

Fig.2.5. Lead acid battery constitution.

For PV applications, lead-acid batteries are yet used as an energy buffer Because of their low cost and also because lead recycling is a well-established industry we will consider this storage technology for our study [Url15].

d. Ultra-capacitor

Ultra-capacitors are electrochemical capacitors that have an unusually high energy density when compared to common capacitors. In an ultra-capacitor charges are stored at the interface of the solid electrodes ant the liquid electrolyte, forming a double layer [End01]. So the two monolayers form a capacitance. The distance between the charge layers is only a few atomic diameters; hence an improvement of about two or three orders of magnitude in capacitance is obtained, but usually at a lower working voltage. A double layer is formed at each electrode. Larger, commercial electric double-layer capacitors have capacities as high as 5,000 F. The highest energy density in production is 82.5Wh/kg at a power density of 930 W/kg [Yan16].

Fig.2.6. Variety of Maxwell Ultra-capacitors.

Ultra-capacitors have a variety of commercial applications, especially in "energy smoothing" and momentary-load devices. Some of the earliest uses were motor startup capacitors for large engines in tanks and submarines (Fig.2.6). As the cost has fallen, ultra-capacitors have started to appear on diesel trucks and railroad locomotives. Recently their ability to store energy quickly made them particularly suitable for regenerative braking applications, whereas batteries have difficulty in this application due to slow charging rates.

Due to the ultra-capacitor's high number of charge-discharge cycles (millions or more compared to 200–1000 for most commercially available rechargeable batteries) there are no limit parts during the whole operating life of the device, which makes the device environmentally friendly. Other advantages of ultra-capacitors are: the extremely low

internal resistor, the high efficiency (up to 97-98%), the high output power, extremely low heating levels and the improved safety.

In our study, the ultra-capacitors are used for implementing the fast dynamic power compensations thanks to their high power density.

2.6. Structure of the studied hybrid power generator

The structure that has been widely used for isolated power systems is based on the direct connection of a battery bank to the dc-bus of the grid-connected inverter (Fig.2.7). A PV controller is used to extract the maximum power from PV panels and send it to the battery bank. However, the stochastic nature of the PV power output and power demand, leads to a fast charge/discharge action of batteries and a fast battery ageing.

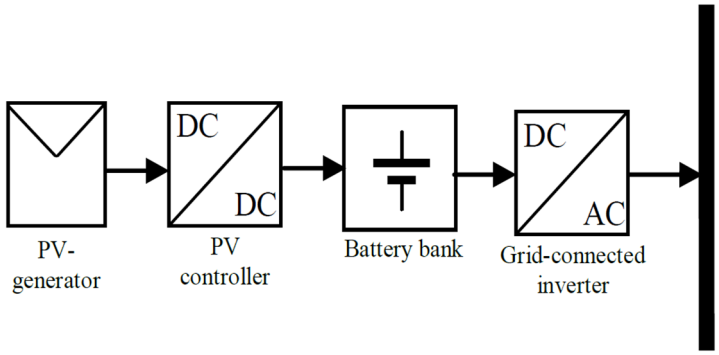

Fig.2.7. Cascade Coupled Structure.

To enable a more efficient use of batteries, AC-coupled and DC-coupled structures can be considered in order to have control abilities of the exchanged powers with the batteries.

In an AC-coupled hybrid power generators (HPG), all sources are connected to a main AC-bus (Fig.2.8.a) [Pen08]. This AC-bus can be the utility network. In AC coupled structure, different sources of HPG can be located anywhere in the grid with a long distance from each other. However, the voltage and the frequency of the main AC bus should be well controlled in order to ensure the stability of the distributed sources and the compatibility with the utility network.

In a DC-coupled HPG, all sources are connected to a main DC-bus before being connected to the grid through a main inverter (Fig.2.8.b) [Yu04]. In a DC-coupled structure, the voltage and the frequency of the grid are independent from those of each source. A first interest is that the battery bank is connected to the dc-bus via a DC/DC converter. This DC/DC converter can be used to implement an optimized charge/discharge operation mode. A second advantage is that an ultra-capacitor bank is added and is also connected to the dc-bus via another DC/DC converter. The PV array is connected to the dc-bus via a PV

converter. Apart from these two coupling structure, a mixed structure can be also used to build a HPG (Fig.2.8.c) with some advantages taken from both of DC and AC coupled structures.

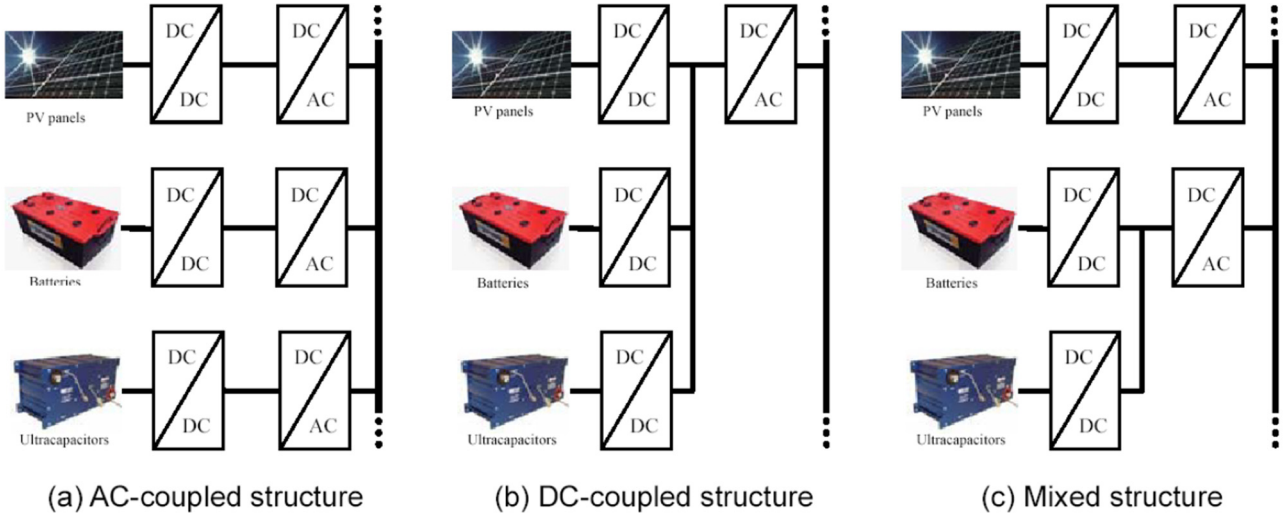

Fig.2.8. Different coupling structures of the hybrid power generator for distributed generation.

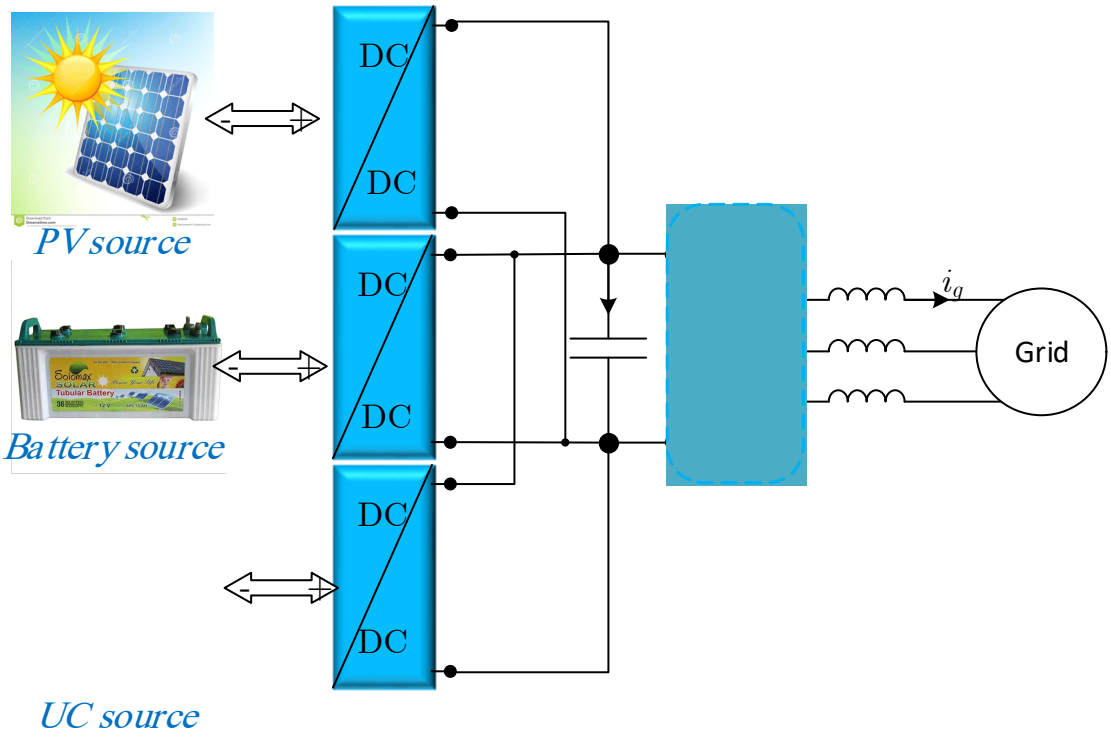

Fig.2.9. Grid-connected hybrid PV generator including batteries and ultra-capacitors.

In our study, a DC-coupled structure (Fig.2.9) is chosen because it is flexible and expandable since the number and the type of the energy sources can be freely chosen. Moreover, the grid frequency is independent from the sources through a DC bus. The grid voltage is also independent from the DC bus voltage and for each source's voltage through different power converters.

2.7. Modeling of the Studied Hybrid Power Generator

2.7.1. Description

The system considered in the present study consists of a PV generator of 100kW rated power, a lead acid battery bank as a long term storage system and an ultra-capacitor bank to deal with rapid power demand transitions as shown in Fig.2.9 The PV output power is processed by a MPPT based DC-DC converter while the powers of both battery and ultra-capacitor are handled by a dedicated bidirectional DC-DC converter to ensure the charge/discharge operations. The overall sources are gathered to the same DC-link given the merits that this configuration offers to the system, such as flexibility and expandability [Lu10, Fak11]. The connection to the grid utility is performed by a three phase inverter according to the grid restrictions. This configuration is known as an active generator where the excess of PV generation is stored in order to be restored when needed, whereas the energy stored in the ultra-capacitor is used to smooth the rapid changes in the demand side or in the PV generation side (Fig.2.9).

2.7.2. Silicon Solar Cells and Their Characteristics

2.7.2.1. P-N junction

Today, the most used photovoltaic cell consists of large-area P-N junctions, which are made from silicon. As a simplification, one can imagine bringing a layer of N-type silicon into direct contact with a layer of P-type silicon. In practice, P-N junctions of silicon solar cells are not made in this way, but rather, by diffusing a N-type dopant into one side of a P-type wafer.

In a P-N junction, the piece of P-type silicon and the piece of N-type silicon are intimately contacted. The electrons diffuse from the N-type side of the junction (high electron) into the P-type side of the junction (low electron concentration). When the electrons diffuse across the P-N junction, they recombine with holes on the P-type side. The diffusion of carriers does not happen indefinitely however, because of an electric field, which is created by the imbalance of charge immediately on either side of the junction. The electric field across the P-N junction creates a diode that promotes a charge flow, known as the drift current that opposes and eventually balances out the diffusion of electron and holes. This region where electrons and holes have diffused across the junction is called the depletion region because it no longer contains any mobile charge carriers. It is also known as the space charge region.

2.7.2.2. Equivalent circuit of a solar cell.

In order to analyze the electronic behavior of a solar cell, an electrical equivalent model is considered. An ideal PV cell may be considered as a current source in parallel with a diode. In practice a PV cell is not ideal, so a shunt resistance and a series resistance component are added to the model [Xia04]. The resulting equivalent circuit is shown on the Fig.2.10.

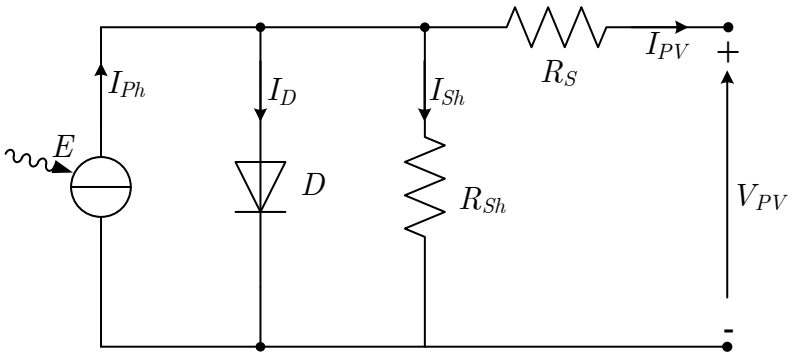

Fig.2.10. Equivalent circuit of a solar cell.

a. Characteristic equations

In this equivalent circuit, the PV cell is considered as a current source with the photovoltaic effect. The output current is expressed as:

$$I_{PV} = I_{Ph} - I_D - I_{Sh} \tag{2.1}$$

Where I_{PV}: Output current of the PV cell (amperes),

I_{Ph}: Photo-current (amperes),

I_D: Diode current (Amperes),

I_{Sh}: Shunt current (Amperes).

The current through these elements is governed by the voltage across them:

$$V_{Sh} = V_{PV} + R_S I_{PV} \tag{2.2}$$

Where V_{Sh}: Voltage across the diode and the resistor R_{Sh} (Volts),

V_{PV}: Voltage across the PV cell terminals (volts),

R_S: Series resistor (**Ω**).

With the Shockley diode equation, the current through the diode is expressed as:

$$I_D = I_0 \left(\exp\left(\frac{q V_{Sh}}{nkT} \right) - 1 \right) \tag{2.3}$$

Where I_0: Reverse saturation current (Amperes),

n: Diode ideality factor (1 for an ideal diode),

q: Elementary charge (1.6022×10^{-19} Coulomb),

k: Boltzmann's constant (1.3806×10^{-23} J/K),

T: Absolute temperature and ≈ 0.025 Volt at 25°C.

With the Ohm's law, the current through the shunt resistor is expressed as:

$$I_{Sh} = \frac{V_{Sh}}{R_{Sh}} \tag{2.4}$$

Where R_{Sh} : shunt resistor (**Ω**).

Substituting equations (2.4), (2.3) and (2.2) into the first equation gives the characteristic equation of a PV cell, which relates PV cell parameters to the output current and voltage:

$$I_{PV} = I_{Ph} - I_0 \left(\exp\left(\frac{q(V_{PV} + R_S I_{PV})}{nkT} \right) - 1 \right) - \frac{V_{PV} + R_S I_{PV}}{R_{Sh}} \tag{2.5}$$

For a given voltage V_{PV} the equation may be solved to determine the output current I_{PV}. Because the equation involves the current on both sides in a transcendental function the equation has no general analytical solution. However, it is easily solved by using numerical methods.

Since the parameters I_0, n, R_S, and R_{Sh} cannot be measured directly, a characteristic equation is generally used with a nonlinear regression to extract the values of these parameters on the basis of their combined effect on the PV cell behavior.

2.7.2.3. Origin of the Series and the Shunt Resistances

The series resistance arises from the bulk resistance of the silicon material, the resistance of the metal contacts of the front and back surfaces and further circuit resistances from connections and terminals.

The Shunt resistance is mainly caused by leakage currents due to P-N junction nonidealities and impurities near the junction, which cause partial shorting of the junction, particularly near the cell edges.

2.7.2.4. Determination of Resistances Values

- *Series Resistance*

For the determination of R_S, *I-V* curves at the same temperature but for two different intensities I_{SCA} and I_{SCB} are used (Fig.2.6). A point "*A*" is selected on the higher intensity curve corresponding to a voltage slightly greater than V_{MPP}. The corresponding current of the point A is named IA and the difference b is given as follow [GNT1O]:

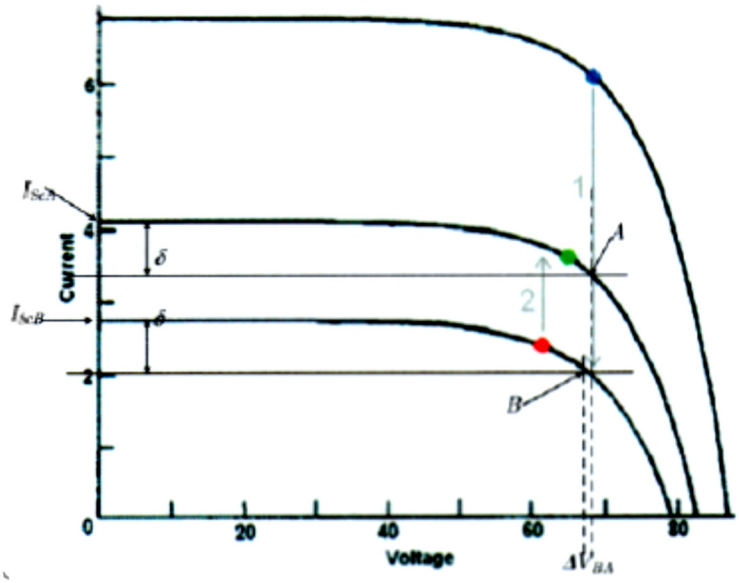

Fig.2.11. I-V curves for different intensities at the same temperature.

$$\delta = I_{SCA} - I_A \tag{2.6}$$

Next, a point B is selected on the lower intensity curve (B) such that,

$$I_B = I_{SCB} - \delta \tag{2.7}$$

The voltage difference corresponding to the voltages at A and B is,

$$\Delta V_{BA} = V_A - V_B \tag{2.8}$$

Hence, the series resistance of the PV cell is,

$$R_S = \frac{\Delta V_{BA}}{\delta} \tag{2.9}$$

This process can be repeated n times to obtain other values of R_S and the mean of these values gives R_S.

$$R_S = \frac{\sum_n R_n}{n} \tag{2.10}$$

- ***Shunt Resistance***

R_{Sh} can be determined from the slope of an *I-V* curve at the neighborhood of the short circuit point.

$$\frac{1}{R_{Sh}} = -\frac{\Delta I}{\Delta V}\bigg|_{V \to 0} \tag{2.11}$$

2.7.2.5. Photovoltaic Cell Model

When the cell is operated in short circuit ($V_{PV} = 0$), the current I_{PV} is defined as the short-circuit current I_{SC}. For a high-quality PV cell (low value of R_S and I_0, and high value of R_{Sh}), the short-circuit current I_{SC} is expressed as:

$$I_{SC} = I_{Ph} \tag{2.12}$$

By taking into account the effect of the irradiance and the temperature, the current I_{SC} is expressed as:

$$I_{SC} = I_{Ph} = I_{SCS}\frac{G}{G_S}[1 + \Delta I_{SC}(T - T_S)] \tag{2.13}$$

With G: Irradiance (W/m²);

T: Cell temperature (K);

I_{SCS}: Short circuit current measured in Standard Test Conditions (STC);

G_S: Standard illumination: 1000 W / m²;

T_S: Standard temperature: 298.15 K;

ΔI_{SC}: Temperature coefficient of short circuit current

When the cell is operated in open circuit (I_{PV}=0), the voltage V_{PV} is defined as the open-circuit voltage (V_{OC}). Assuming the shunt resistor (R_{Sh}) is high enough to neglect the final term of the characteristic equation (eq.1.5), the open-circuit voltage is expressed as:

$$V_{OC} \approx \frac{kT}{q}\ln(\frac{I_{PV}}{I_0} + 1) \tag{2.14}$$

In an open-circuit condition: $V_{PV} = V_{OC}$ and I_{PV}=0, the equation (eq.1.1) can be written as:

$$I_{Ph} = I_D + I_{Sh} = I_{Sat}[\exp(\frac{V_{OC}}{V_t}) - 1] + \frac{V_{OC}}{R_{Sh}} \tag{2.15}$$

With $V_t = \frac{AkT}{q}$ and A the ideality factor of the diode,

The saturation current is defined as:

$$I_{Sat} = \frac{I_{Ph} - \frac{V_{OC}}{R_{Sh}}}{\exp(\frac{V_{OC}}{V_t}) - 1} \tag{2.16}$$

The open-circuit voltage is expressed as:

$$V_{OC} = V_{OCS} + \Delta V_{OC}(T - T_S) \tag{2.17}$$

With V_{OCS}: open-circuit voltage in STC,

V_{OC}: temperature coefficient of open circuit voltage.

Note: The resistors and the ideality factor are influenced by the temperature [Sha04]. In order to simplify the model, these values are set in STC.

2.7.3. Lead-acid battery

a. Basic cell model

An equivalent electrical circuit of the CIEMAT battery model [Ger03] is shown in Fig.2.12.

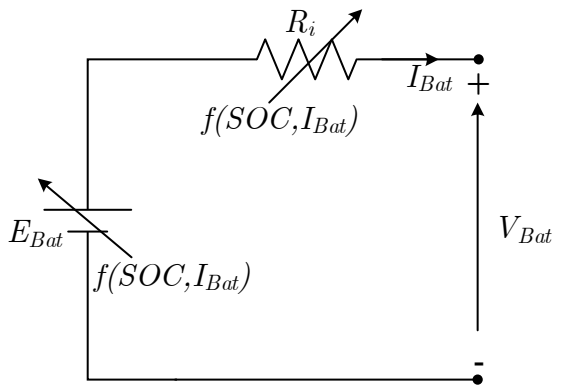

Fig.2.12. Equivalent electrical circuit of the CIEMAT battery model.

This model consists of a voltage source E_{Bat}, and an internal resistor R_i, it includes the main variables of the system: the state of charge (SOC); the battery current I_{Bat}; the temperature T and the number of cells in series n_b. The circuit equation is expressed as:

$$V_{Bat} = n_b(E_{Bat} + R_i I_{Bat}) \begin{cases} E_{Bat} = f(SOC) \\ R_i = f(I_{Bat}, SOC, T) \end{cases} \tag{2.18}$$

The voltage source E_{Bat} represents the voltage in open circuit across the battery terminals. This voltage is due to the stored energy into the battery through the electrochemical reactions. Obviously, this term depends directly on the stored energy. R_i is a resistor and represents the losses. This resistor value includes the effects of the working point (I, SOC, T) and the health of the battery. A damaged battery has a high value of resistor irrespective of its working point. Also, the resistor is inversely proportional to the state of charge. Furthermore, at the same time as the battery is discharging, the resistor value is increasing. Note that all physical effects are expressed into electrical equations and are modeled in these terms. The state of charge must be considered as an indicator of the electrical charge stored in the battery. The value range is $0<SOC<1$. The following equations describe the behavior of this indicator.

$$SOC(t) = \frac{1}{C(t)} \int_{-\infty}^{t} \eta_C I_{Bat}(t) dt \tag{2.19}$$

$$C(t) = \frac{C_{nom} C_{tcoef}}{\left(1 + A_{Cap} \left(\frac{\left| I_{Bat}(t) \right|}{I_{nom}} \right)^{B_{Cap}} \right) \left(1 + \alpha_C \Delta T(t) + \beta_C \Delta T(t)^2 \right)} \tag{2.20}$$

$$I_n = \frac{C_{nom}}{n} \tag{2.21}$$

Where $C(t)$ the battery capacity; η_C the charging efficiency; C_{nom} is the nominal battery capacity (at n hours); C_{tcoef}, A_{Cap} and B_{Cap} are model parameters; ΔT is the temperature variation from the reference value at 25°C; I_n the discharge current corresponding to the C_{nom}; n is the time in hours; α_C and β_C are the temperature parameters.

The SOC must be understood as the relation between the accepted energy and the available capacity at all times. The inner integral term models the accepted energy over the battery working life. Also, the outer integral term models the battery capacity due to the working point environment at any given time. Both terms are functions of time and are evolving continuously. When the SOC is unity the battery cannot accept more energy from

the system, because the stored energy fills all the battery capacity. And when the *SOC* is null the battery has no energy.

Fig.2.13 illustrates the voltage evolution of the battery with different working area. Thus, different possible working zones for a 2V element can be observed. For the first 16 hours the current is flowing inside the battery, and it evolves into different zones: charging, overcharging and saturation zones. From 16 hours to 27 hours the current is flowing outside the battery and it evolves into discharging, over discharging and exhaustion zones.

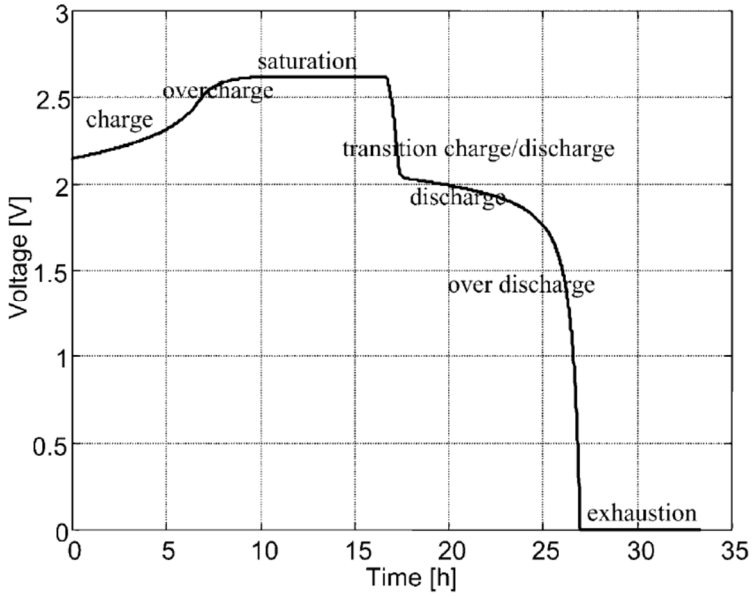

Fig.2.13. Working areas of a battery.

b. Simplified model

In the studied case, a simplified model is used by considering a constant internal resistor R_i. The resistor is supposed to be constant during the charge and the discharge cycles and does not vary with respect current. When this preset model is used in the SimPowerSystem software, a generic value is loaded, corresponding to the nominal voltage and the rated capacity of the battery. The battery voltage is expressed as:

$$E_{Bat} = E_0 - KQ\frac{1}{(Q - i_t)} + Ae^{-Bi_t} \tag{2.22}$$

$$i_t = \int_{t_0}^{t} i_{Bat}(t)dt \tag{2.23}$$

With E_0: Fully charged voltage (V); Q: Battery capacity (Ah); A: Exponential voltage (V); B: Exponential capacity (Ah); K: Polarization voltage (V).

All parameters of this equivalent circuit can be identified, by considering the discharge characteristics with a nominal current. A typical discharge curve is composed of three sections (Fig.2.14):

The first section represents the exponential voltage drop if the battery is initially fully charged. The width of this region depends on the battery type. The second section represents the charge that can be extracted from the battery until the voltage drops below the battery nominal voltage. Finally, the third section represents the total discharge of the battery, when the voltage drops quickly.

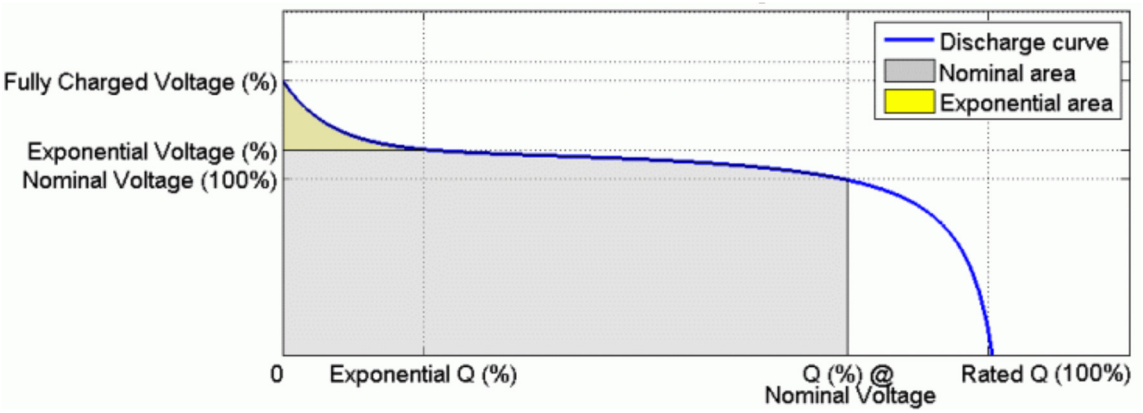

Fig.2.14. Discharge curve (Q-V) of a battery.

2.7.4. Ultra-capacitor

In our application, a simplified model is utilized (ssical equivalent circuit model Fig.2.14). It includes a final capacitor C_0 in series with a resistance R_S [Li08].

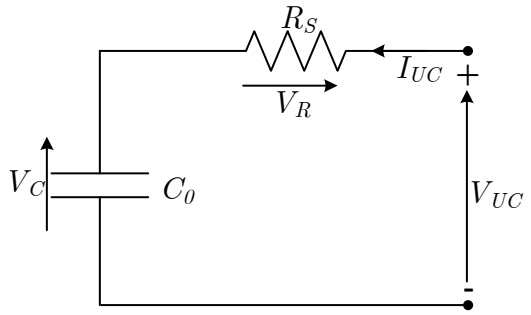

Fig.2.15. Simplified model of ultra-capacitor.

All internal electrical relations are expressed in the following equation:

$$\frac{dV_C}{dt} = \frac{1}{C_0} I_{UC}(t) \tag{2.24}$$

$$V_R(t) = R_S I_{UC}(t) \tag{2.25}$$

$$V_{UC}(t) = V_C(t) + V_R(t) \tag{2.26}$$

With the ultra-capacitor current I_{UC} and the output voltage V_{UC}.

2.8. Conclusion

In this chapter, the interests of renewable energy are shown in different aspects: energy security, environment protection and economic development. In the same time, the constraints about the use of renewable energy in an electrical power system are discussed. Facing to the problem of the power intermittency with the renewable energy sources, we propose to design a hybrid power generator with embedded energy storage units. The electrical energy storages can deal with not only the intermittency of power supply, but also they can help to provide the ancillary services in an electrical network. Several long term energy storage and fast dynamic power storage technologies are introduced in this chapter.

In order to transform PV panels in an active power system APS, a hybrid system is designed with PV panels, batteries and ultra-capacitors. The photovoltaic panels, the batteries and the ultra-capacitors are coupled to a common DC voltage bus by three DC/DC power electronic converters. The model description of each source is presented. From the different models, a simplified model is chosen. In the next chapter the modeling of this active generator will help to analysis its characteristics for the design of the control system.

Chapter 03

3. Modeling, Analysis and Automatic Control of the APG

3.1. Introduction

In order to have a local energy reserve and to filter fast PV power fluctuations, lead-acid batteries and ultra-capacitors are used to build a PV/batteries/ultra-capacitors hybrid power system in a DC coupled structure (Fig.3.1). This chapter consists of the modeling of the power converters with average values, the automatic control laws for all the dedicated power converters (DC-DC boost converter, DC-DC buck&boost bidirectional converter and grid inverter), and the switching control technics.

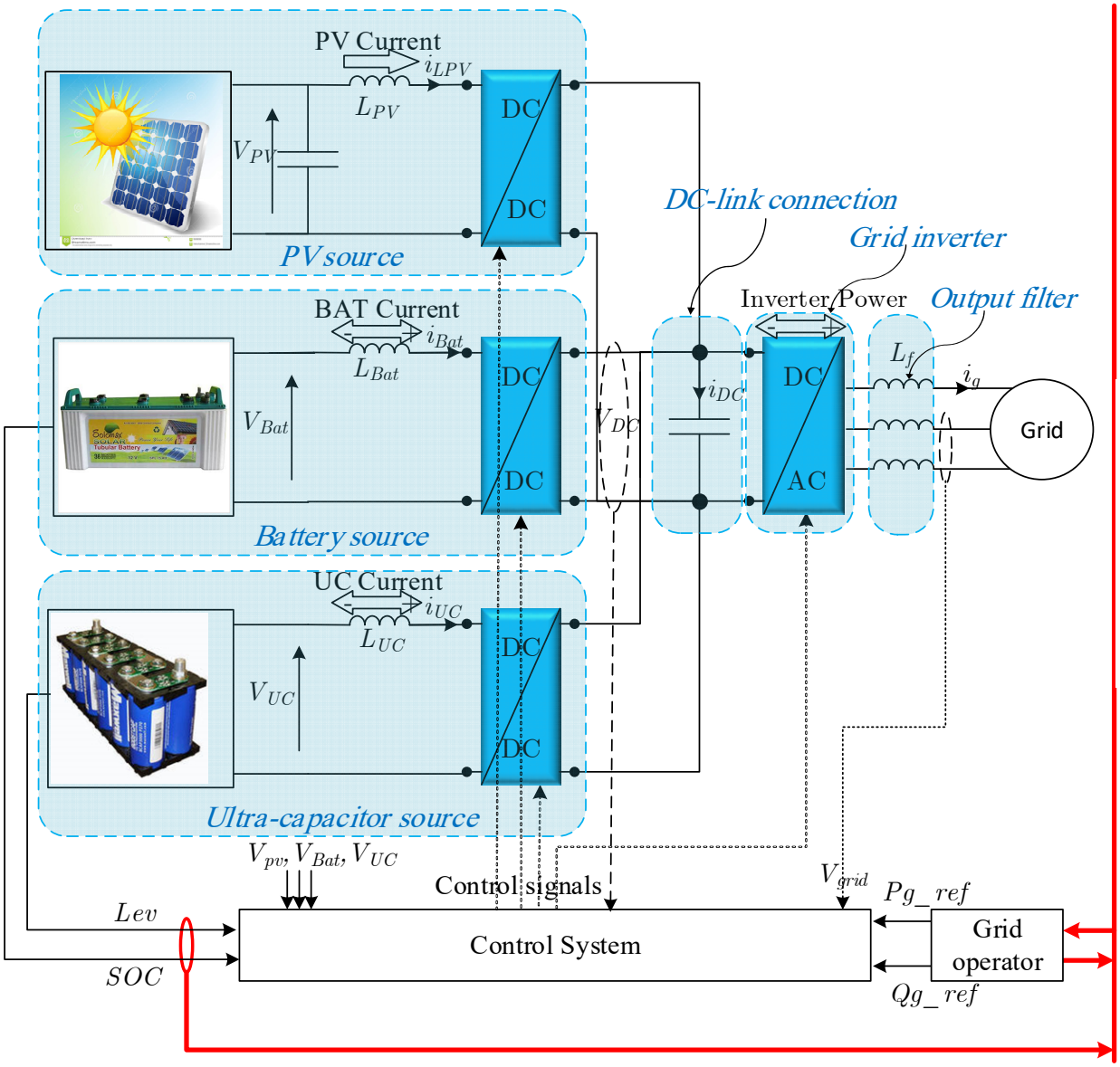

Fig.3.1. Grid-connected PV based active generator with the control system.

The electrical diagram shown in Fig.3.1 makes appear five parts corresponding to the PV conversion system, the batteries, the ultra-capacitors, the grid connection and the DC

bus. These four power converters are used to introduce control inputs for each power conversion system, in order to:

- Control the power generated by the PV panels;
- Maintain a constant DC bus voltage;
- Supply the required power exchange with the grid;
- Ensure the power buffering of each energy storage unit.

3.2. Steady State Analysis and Design of the Boost Converter

From the control point of view, the most important part of the control system is the boost converter, so, a detailed analysis for this converter is required. This section is devoted to the PWM boost DC-DC switching-mode converter [Mar16]. The converter is analyzed for continuous conduction mode (CCM.) Voltage and current waveforms, DC transfer functions stresses of the converter components are determined. Expressions for the inductance and the capacitance values are derived. Efficiency of the converter is estimated.

3.2.1. Circuit Description and Assumptions

The circuit of the PWM DC-DC boost converter is shown in Fig.3.2. Its output voltage V_0 is always higher than the input voltage V_I for steady-state operation. It boosts the voltage to a higher level. The converter consists of an inductor L, a power switch (IGBT, MOSFET), a diode D, a filter capacitor C, and an output current I_0 . The switch S is turned ON and OFF at the switching frequency fs=l/ T_S with the ON duty ratio D= T_{ON}/ T_S, where T_{ON} is the time interval when the switch S is ON.

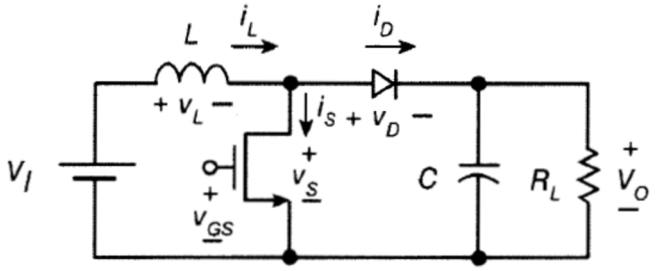

Fig.3. 2. Circuit of the PWM boost converter

The boost converter can operate in one of the two modes: a continuous conduction mode (CCM) or a discontinuous conduction mode (DCM), depending on the waveform of the inductor current.

Idealized waveforms of the currents and voltages that explain the principle of operation of the boost converter are depicted in Fig.3.3. For the time interval $0<t<DT_S$, the switch is

ON. Therefore, the voltage across the diode is $v_D = -V_0$, causing the diode to be reverse biased. The voltage across the inductor is $v_L = V_I$. As a result, the inductor current increases linearly with a slope of V_I / V_L, Consequently, the magnetic energy also increases. The switch current is equal to the inductor current. At $t = DT_S$, the switch is turned off by the gate-to source voltage. The inductor acts as a current source and turns the diode ON. The voltage across the inductor is $v_L = V_I - V_0 < 0$. Hence, the inductor current decreases with a slope of $(V_I - V_0)/L$. The diode current is equal to the inductor current. During this time interval, the energy is transferred from the inductor L to the filter capacitor C and the load resistance R_L. At time $t = T_S$, the switch is turned on again, terminating the cycle.

Remark

The boost converter has poor ability to prevent hazardous transients and failures. If a high positive voltage surge appears at the converter input, the input voltage exceeds the output voltage and the diode D is ON for many cycles due to cycle skip. This generates a large current spike through the diode, which may destroy the diode. A similar problem exists at the initial turn-on of the converter when the input voltage is high and the output voltage is initially zero and while the output voltage is lower than the input voltage until steady-state conditions are approached. One way to protect the converter is to add a diode whose anode is connected to the input source V_I and the cathode is connected to the output filter capacitor C. When the output voltage is lower than the input voltage, the additional diode and the filter capacitor form a peak rectifier and the energy flows from the input to the output of the converter through the additional diode. When the output voltage becomes higher than the input voltage, the additional diode is reverse biased and turns OFF and the boost converter begins normal operation.

Assumptions

The analysis of the boost PWM converter of Fig.3.2 begins with the following assumptions:

1) The power MOSFET and the diode are ideal switches.
2) The transistor output capacitance, the diode capacitance, and lead inductances (and thereby switching losses) are zero.
3) Passive components are linear, time invariant, and frequency independent.
4) The output impedance of the input voltage source Vi is zero for both DC and AC components.

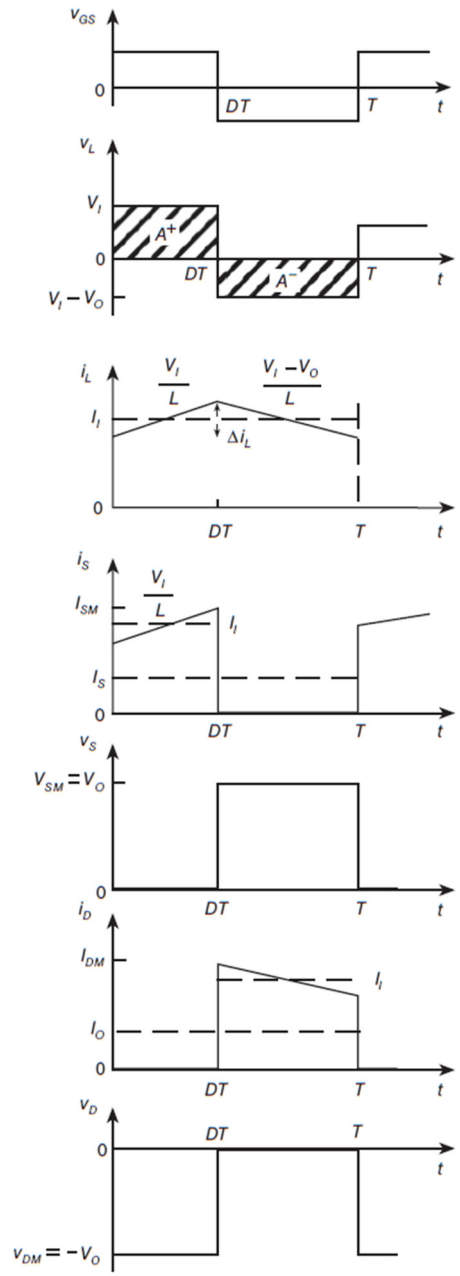

Fig.3.3. Idealized current and voltage waveforms in the PWM boost converter for CCM.

3.2.2. Voltage Conversion Ratio

The converter is operated in PWM, with a duty cycle D given by the following expression,

$$D = \frac{T_{ON}}{T_S} \tag{3.1}$$

The Volt-Sec principle in the inductor leads to the following equation,

$$\begin{aligned} v_L(ON)T_{ON} &= -v_L(OFF)T_{OFF} \\ V_I D T_S &= -(V_I - V_0)(1-D)T_S \end{aligned} \tag{3.2}$$

Finally, the voltage conversion ratio is given,

$$\frac{V_0}{V_I} = \frac{T_S}{T_{OFF}} = \frac{1}{1-D} \tag{3.3}$$

3.2.3. Current Conversion Ratio

The capacitor current is expressed as,

$$i_C = i_D - I_0 \tag{3.4}$$

The Amp-Sec principle in the capacitor leads to the following equation,

$$\begin{aligned} i_C(ON)T_{ON} &= -i_C(OFF)T_{OFF} \\ -I_0 D T_S &= -(I_I - I_0)(1-D)T_S \end{aligned} \tag{3.5}$$

Therefore,

$$\frac{I_0}{I_I} = 1 - D \tag{3.6}$$

3.2.4. Current Ripple Ratio

The peak to peak ripple is the difference between the mm1mum value (at t=0), and the maximum value (at t=DT_S) (Fig.3.3),

$$\Delta i_L = i_L(DT_S) - i_L(0) = \frac{V_I}{L} DT_S = \frac{(1-D)V_0}{L} DT_S \tag{3.7}$$

During the ON period, the inductor current can be expressed as,

$$i_L = I_I = \frac{I_0}{1-D} \tag{3.8}$$

Dividing eq.(37) by eq.(3.8) gives the current ripple ratio,

$$\frac{\Delta i_L}{i_L} = D(1-D)^2 \frac{V_0 T_S}{I_0 L} = D(1-D)^2 \frac{T_S}{(L\,/\,R)} \tag{3.9}$$

From eq.(3.9), the first design condition can be driven as follows:

To minimize the current ripple ratio, we should choose the switch period very much lesser than the time constant of the charging circuit.

$$T_S \ll \frac{L}{R} \tag{3.10}$$

3.2.5. Non-idealities and Efficiency

3.2.5.1. Switches Non-idealities

The Volt-Sec balance with the real switches non-idealities is applied,

$$(V_I - V_S)DT_S = -(V_I - V_D - V_0)(1-D)T_S \tag{3.11}$$

By rearranging eq.(3.11), the voltage conversion ratio is obtained,

$$\frac{V_0}{V_I} = \frac{1}{1-D}\left[\frac{(V_I - V_S)}{V_I}D + \frac{(V_I - V_D)}{V_I}(1-D)\right] \tag{3.12}$$

3.2.5.2. Inductor Non-ideality

The Volt-Sec balance on the real inductor (L,r_L) is applied,

$$V_I'D = -(V_I' - V_0)(1-D) \tag{3.13}$$

Where,

$$V_I' = V_I - r_L I_I = V_I - r_L\frac{I_0}{1-D} = V_I - \underbrace{\left(\frac{r_L}{R}\right)}_{\alpha}\frac{V_0}{1-D} \tag{3.14}$$

Substituting V_I' in eq.(3.13),

$$\frac{V_0}{V_I} = \frac{1}{1-D}\frac{1}{\left(1+\dfrac{\alpha}{(1-D)^2}\right)} \tag{3.15}$$

3.2.6. Efficiency

3.2.6.1. Efficiency with the Switches Non-idealities

Replacing the term (1/(1-D)) in the equation (3.12), by I_I / I_0 ,

$$\frac{V_0}{V_I} = \frac{I_I}{I_0}\left[\frac{(V_I - V_S)}{V_I}D + \frac{(V_I - V_D)}{V_I}(1-D)\right] \tag{3.16}$$

The efficiency of the converter is,

$$\eta = \frac{P_0}{P_I} = \frac{V_0 I_0}{V_I I_I} \tag{3.17}$$

From eq.(3.16) and eq.(3.17), we get the expression of the efficiency

$$\eta = \frac{(V_I - V_S)}{V_I} D + \frac{(V_I - V_D)}{V_I}(1 - D) \tag{3.18}$$

3.2.6.2. Efficiency with the Inductor Non-idealities

From the equation (3.15), we can get the efficiency with a real inductor,

$$\eta = \frac{1}{\left(1 + \frac{\alpha}{(1-D)^2}\right)} \tag{3.19}$$

For best understanding, Fig.3.4 shows the curves of the equations (eq.(3.3), eq.(3.12), and eq.(3.19)).

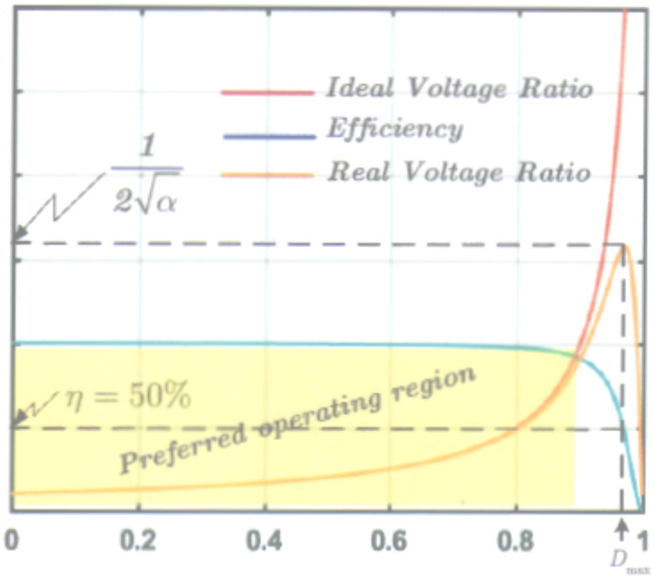

Fig.3.4. Voltage conversion ratio and efficiency of the lossy boost converter as a function of D for CCM.

3.2.7. Maximum real Voltage Gain

By differentiating the real voltage conversion ratio (eq. (3.15)) with respect to D,

$$\frac{d}{dD}\left(\frac{V_0}{V_I}\right) = 0 \tag{3.20}$$

We can obtain the optimal value of the duty cycle corresponding to the maximum voltage conversion ratio,

$$D_{\max} = 1 - \sqrt{\alpha} \tag{3.21}$$

Therefore,

$$\left.\frac{V_0}{V_I}\right|_{\max} = \frac{1}{2\sqrt{\alpha}} \tag{3.22}$$

Remark

When the voltage conversion ratio reach its maximum value, the efficiency becomes very low (50%) and therefore, the preferred operating region of the duty cycle should be such that D is lesser than D_{max}.

3.2.8. Voltage Ripple Ratio

The capacitor current is expressed by,

$$C\frac{dV_0(t)}{dt} = i_C \tag{3.23}$$

Then,

$$dV_0(t) = \frac{1}{C} i_C dt \tag{3.24}$$

Integrating the two sides,

$$\int_0^{DT_S} dV_0(t)dt = \frac{1}{C}\int_0^{DT_S} i_C(t)dt \tag{3.25}$$

During $t \in [0 - DT_S]$, the capacitor discharging current is given,

$$i_C = -I_0 \tag{3.26}$$

Substituting for i_C ,

$$V_0(DT_S) - V_0(0) = -\frac{I_0}{C}\int_0^{DT_S} dt \tag{3.27}$$

Finally, the voltage ripple ratio is obtained,

$$\frac{\Delta V_0}{V_0} = -D\frac{T_S}{RC} \tag{3.28}$$

From eq.(3.28), we can conclude the design guideline,

$$T_S \ll RC \tag{3.29}$$

In order to reduce the voltage ripple ratio, the switching period should be much lesser than the time constant of the discharging circuit.

3.2.9. Electrical Stresses on the Switches

a. During the Time Interval $0 < t < DT_S$

The diode voltage is

$$v_D = -V_0 \tag{3.30}$$

Therefore, the diode is OFF.

The average value of the inductor current I_L is equal to the DC input current I_I. Hence, one arrives at the peak value of the switch current

$$I_{SM} = I_I + \frac{\Delta i_L}{2} = \frac{I_0}{1-D} + \frac{\Delta i_L}{2} \tag{3.31}$$

Substituting for Δi_L (eq.(3.7)),

$$I_{SM} = \frac{I_0}{1-D} + \frac{1}{2}\frac{D(1-D)V_0}{L}T_S \tag{3.32}$$

The average value of the switch current is,

$$\overline{I}_S = I_I D = I_0 \frac{D}{1-D} \tag{3.33}$$

b. During the Time Interval $DT_S < t < T_S$

The voltage across the switch S is given by,

$$v_S = V_{SM} = V_0 \tag{3.34}$$

The peak diode current and the peak switch current are given by,

$$I_{DM} = I_{SM} = \frac{I_0}{1-D} + \frac{\Delta i_L}{2} \tag{3.35}$$

The diode current average value is,

$$\overline{I}_D = I_I(1-D) = I_0 \tag{3.36}$$

3.3. Modeling of the PV System with average values

The modeling of the PV panels has been introduced in the first chapter. In the whole PV power conversion chain, the photovoltaic panels are considered as a current source i_{PV} and it supplies a voltage source V_{PV}, which is the input of the DC-DC boost converter (Fig.3.5).

3.3.1. DC-DC Boost Converter (PV Converter)

The choke is modeled as a current source $i_{L,PV}$. This current depends on the PV voltage and the modulated voltage of the chopper $V_{m,PV}$ (Fig.3.5):

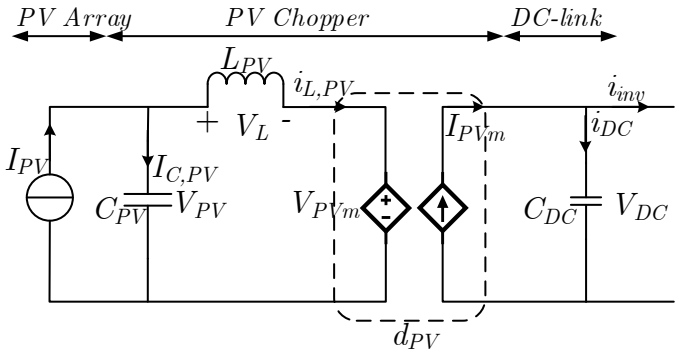

Fig.3.5. Equivalent electrical diagram of PV power conversion system in average mode.

$$\frac{d}{dt} i_{L,PV} = \frac{1}{L_{PV}} (\mathrm{V}_{PV} - \mathrm{V}_{m,PV}) \tag{3.37}$$

Losses in the filter and the capacitor are neglected. The capacitor C_{PV} can stabilize the voltage V_{PV} of the PV panels. This capacitor can be modeled by using the PV current i_{PV} and the filtered current $i_{L,PV}$:

$$\begin{cases} \dfrac{d}{dt} V_{PV} = \dfrac{1}{C_{PV}} i_{C,PV} \\ i_{C,PV} = i_{PV} - i_{L,PV} \end{cases} \tag{3.38}$$

$i_{C,PV}$ is the injected current in the capacitor. The voltage $V_{m,PV}$ of the chopper terminals is obtained from the DC-link voltage (V_{DC}) and the duty cycle ratio (d_{PV}):

$$\begin{cases} V_{m,PV} = d_{PV} V_{DC} \\ i_{m,PV} = d_{PV} i_{L,PV} \end{cases} \tag{3.39}$$

3.3.2. Batteries energy storage system

The modeling of lead acid batteries has been introduced in the first chapter. In the whole batteries energy storage system, the batteries are considered as a voltage source V_{Bat}, which is connected to a choke filter L_{Bat} (Fig.3.6).

By neglecting losses in the filter, the dynamic equation of the filtered current i_{Bat} is expressed with the battery voltage V_{Bat} and the modulated voltage $V_{m,Bat}$:

$$\frac{d}{dt} i_{Bat} = \frac{1}{L_{Bat}} (V_{Bat} - V_{m,Bat}) \tag{3.40}$$

where L_{Bat} is the inductor of the filter.

The average value of the voltage $V_{m,Bat}$ is obtained from the DC-link voltage and the duty cycle ratio of the battery converter d_{Bat}:

$$\begin{cases} V_{m,Bat} = d_{Bat} V_{DC} \\ i_{m,Bat} = d_{Bat} i_{Bat} \end{cases} \tag{3.41}$$

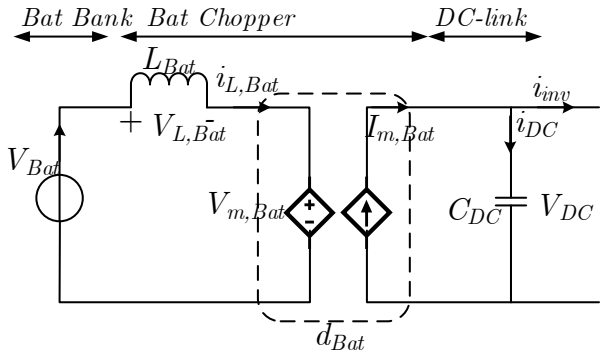

Fig.3.6. Equivalent electrical diagram of the batteries energy storage system.

In a same way, the filtered current i_{Bat} is modulated by the chopper, and then this modulated current $i_{m,Bat}$ is injected into the common DC-link.

3.3.3. Ultra-capacitors

The modeling of ultra-capacitors has been also introduced in the first chapter. In the whole ultra-capacitor power storage system, the ultra-capacitors are considered as an ideal voltage source V_{UC}, which is connected to a choke filter (L_{UC}) (Fig.3.7).

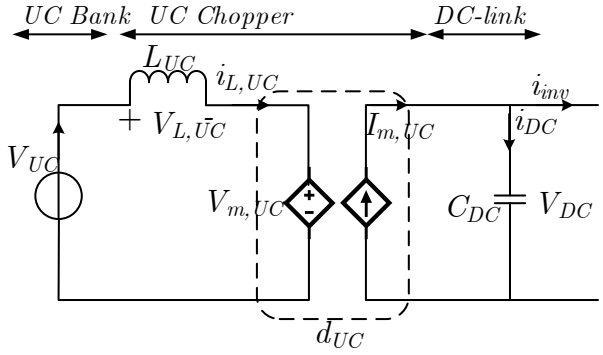

Fig.3. 7. Electrical diagram of the ultra-capacitor power storage system.

By neglecting losses, the filtered current i_{UC} is expressed with the following differential equation:

$$\frac{d}{dt} i_{UC} = \frac{1}{L_{UC}} (\mathrm{V}_{UC} - \mathrm{V}_{m,UC}) \tag{3.42}$$

The modulated voltage is obtained by the DC-link voltage V_{DC} and the duty cycle ratio d_{UC}:

$$\begin{cases} V_{m,UC} = d_{UC} V_{DC} \\ i_{m,UC} = d_{UC} i_{UC} \end{cases} \tag{3.43}$$

The current i_{UC} is modulated by the chopper, and then the resulting modulated current $i_{m,UC}$ is injected into the common DC-link.

3.3.4. Grid Connection

A three-phase inverter with an L filter is used for the grid connection (Fig.3.8)

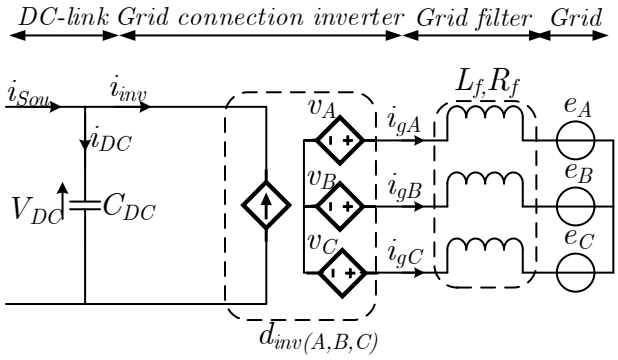

Fig.3.8. Electrical diagram of the grid connection.

The filter currents are deduced from following differential equations:

$$\begin{cases} \frac{d}{dt} i_{gA} = \frac{1}{L_f}(v_A - R_f i_{gA} - e_A) \\ \frac{d}{dt} i_{gB} = \frac{1}{L_f}(v_B - R_f i_{gB} - e_B) \\ \frac{d}{dt} i_{gC} = \frac{1}{L_f}(v_C - R_f i_{gC} - e_C) \end{cases} \quad (3.44)$$

Where,

v_A, v_B, and v_C are the polar voltages of the grid inverter;

i_{Sou}: The sum of all the available sources, including (PV source, battery sources, and ultra-capacitor source).

3.3.5. DC-link

In this hybrid generating system, four energy sources (PV panels, batteries, ultra-capacitors and the electrical grid) are all connected to the common DC-link via different power electronic converters (Fig.3.1). So, according to this DC-coupling, the capacitor current of the DC-link i_{DC} is expressed as:

$$i_{DC} = i_{Sou} - i_{Inv} \quad (3.45)$$

The current coming from both storage elements(i_{Sou}) is,

$$i_{sto} = i_{m,Bat} + i_{m,UC} \quad (3.46)$$

$$i_{sou} = i_{sto} + i_{m,PV} \quad (3.47)$$

With:

$i_{m,PV}$: the modulated current from the PV converter;
$i_{m,Bat}$: the modulated current from the Bat converter;
$i_{m,UC}$: the modulated current from the UC converter;
i_{Inv} : the inverter DC current.

The DC-link is governed by the following equation:

$$\frac{d}{dt} V_{DC} = \frac{1}{C_{DC}} i_{DC} \quad (3.48)$$

C_{DC} is the DC-link capacitor.

3.4. Automatic Control of the Active PV System

The automatic control level in the active PV system applies the control laws to get the suitable duty cycles or switching states of the power converters in order to meet the current or voltage references.

3.4.1. Control of the PV converter

It is well known that the boost converter is a non-linear system, so a non-linear controller is suitable if high performances are required. In this application, we'll use a simple PI control law. The reason is that the climatic conditions vary slowly (low dynamic parameters: sun light and ambient temperature), hence, the PV reference voltage doesn't vary suddenly, and therefore a simple PI controller is enough for this requirements.

The next figure, illustrates the scheme of the PV generator with its control system.

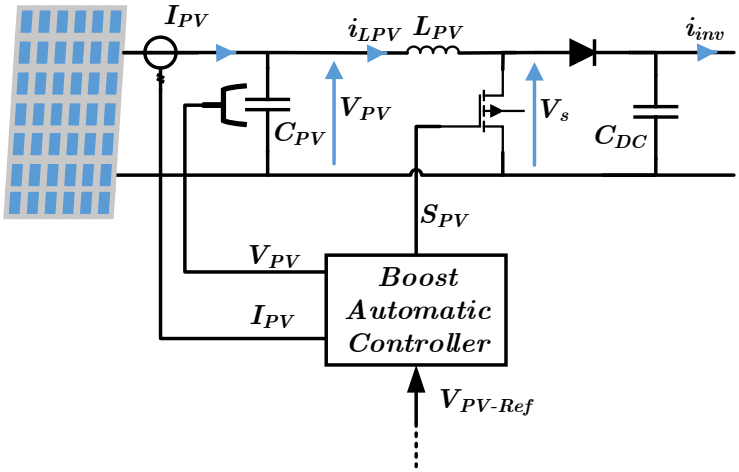

Fig.3.9. Global scheme of the PV generator.

Since the PV arrays is a voltage dependent current source (See Chapter 02), the role of the PV controller is to set the PV voltage value: to extract the maximum power from the PV array, or to extract a specified power value. To achieve that goal, a control loop must be closed and designed.

3.4.1.1. PI Control Law

We consider the PV current (I_{PV}) coming from the PV generator as a disturbance signal, and the power converter as two linear subsystems, with some disturbances signals. The first one is the PV capacitor, and the second is the PV inductor (Fig.3.10).

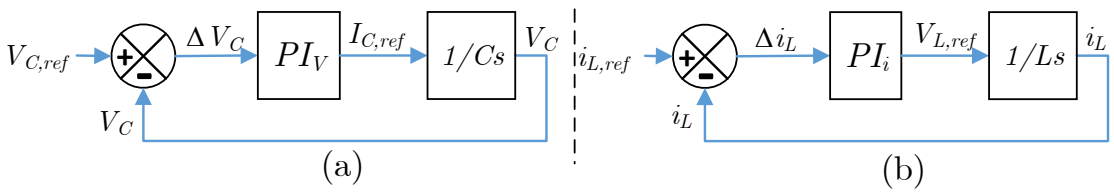

Fig.3.10. Two linear subsystems after the simplification.

The mathematical model of the first sub system is simply

$$\frac{d}{dt}V_{PV} = \frac{1}{C_{PV}}I_{C_{PV}} \tag{3.49}$$

The second is

$$\frac{d}{dt}i_{L,PV} = \frac{1}{L_{PV}}V_{L,PV} \tag{3.50}$$

3.4.1.2. Analysis of the Control Loops

As we can see in Fig.3.12, when the reference voltage comes from the PV algorithm (MPPT or limited Power algorithm), the output of the first PI_V controller gives the reference current that is required to charge/discharge the capacitor to the reference voltage. This reference current value is transmitted to the second PIi controller. The output of the current PIi controller gives the reference of the average applied voltage across the inductor terminals. By applying the KVL, we get the reference of the modulated PV voltage that relies the DC-link voltage with the reference duty cycle of the PV converter.

From Fig.3.9, we can construct the following equations:

$$i_C = i_{PV} - i_{L,PV} \tag{3.51}$$

$$V_{m,PV} = V_{PV} - V_{L,PV} \tag{3.52}$$

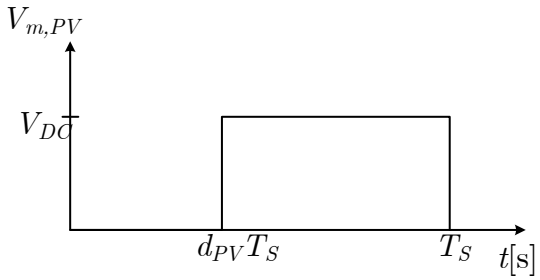

Fig.3.11. Waveform of the modulated PV voltage.

Fig.3.11 shows the waveform of the modulated PV Voltage, and gives the equation (3.53),

$$\bar{V}_{m,PV} = V_{m,PV,ref} = V_{DC}(1 - d_{PV}) \tag{3.53}$$

$$d_{PV} = 1 - \frac{\bar{V}_{m,PV}}{V_{DC}} \tag{3.54}$$

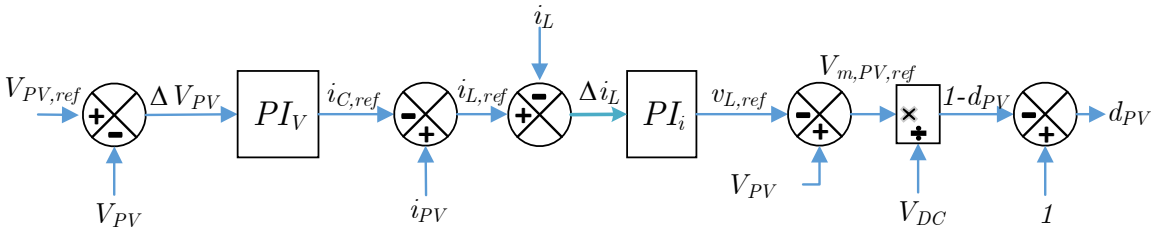

Fig.3.12. PI based control laws for the PV generator.

3.4.2. Control of the Storage Converter (Battery/Ultra-capacitor)

The storage converter must have the current bi-directionality option, in order to ensure the charge or discharge functions. In here, Buck&Boost DC-DC converter is used. This converter operates as a boost converter if we need to discharge the storage element and it operates as buck converter if we need to charge the storage element. So, two control laws must be included in the control system of the storage converter, the first one for the boost mode and the second for the buck mode.

Unlike the PV controller, there is no voltage controller; the current reference is obtained directly by dividing the required reference power over the actual storage voltage. Hence, the central role of the storage controller is to set the current at a desired value.

The Fig.3.11 illustrates the control scheme of the storage converter.

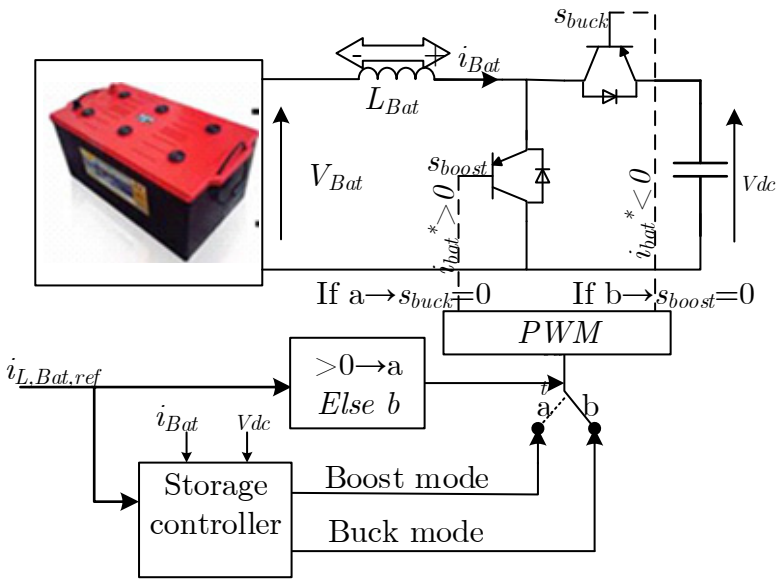

Fig.3.13. Control scheme of the storage converter.

3.4.2.1. PI Control Law

The PI control loop of the storage converter is very similar to the PV converter with the exception of the bi-directionality of the storage converter. When the switch s_{boost} operates a duration of (1-d) Ts the other complementary switch (s_{buck}) operates a duration of dTs (Fig.3.14).

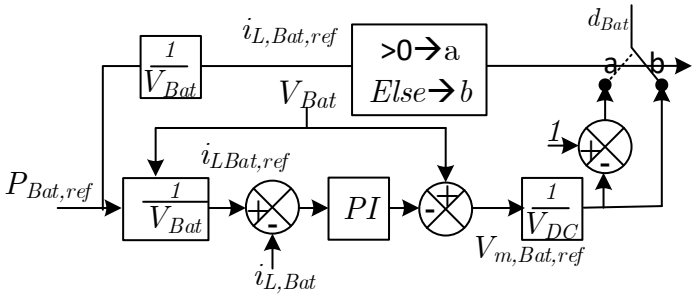

Fig.3.14. PI Control loop of the storage converter.

The design of the controller gains is presented in the appendix.

3.4.2.2. Nonlinear Controller

In the previous section, we have seen that there is no need to nonlinear controller. In the storage converters case, especially for the ultra-capacitor (UC) converter fast dynamic response is required, because the UC is used as a power compensator.

- ***Lyapunov Direct Method Based Controller***

Lyapunov's direct method has become the most important tool for nonlinear system analysis and design [Slo91]. In this section we use the results of the method directly, and we apply them in our case study.

The state variable of the model is the current throw the inductor *iL.Bat,* the non-linear average model of our subsystem can easily obtained from the electrical circuit presented in Fig.3.13.

- t∈[0-$d_{Bat}T_S$]:

the switch s_{boost} is ON: $$V_{Bat} - L_{Bat}\frac{d}{dt}i_{L,Bat} = 0 \quad (3.55)$$

- t∈[$d_{Bat}T_S$ -T_S]:

the switch s_{boost} is OFF: $$V_{Bat} - L_{Bat}\frac{d}{dt}i_{L,Bat} - V_{DC} = 0 \quad (3.56)$$

by combining equations (3.55) and (3.56),

$$V_{Bat} - L_{Bat}\frac{d}{dt}i_{L,Bat} - (1 - S_{Bat})V_{DC} = 0 \tag{3.57}$$

While S_{Bat}: is the state of the switch s_{boost}, it takes '1' for the on state and '0' for the off state.

By integrating the two sides of the equation (3.20) throw the switching period T_S, we get the averaged model,

$$V_{Bat} - L_{Bat}\frac{d}{dt}I_{L,Bat} - (1 - d_{Bat})V_{DC} = 0 \tag{3.58}$$

We note that: $\int_0^{T_S} S_{Bat}dt = \int_0^{d_{Bat}T_S} 1dt + \int_{d_{Bat}T_S}^{T_S} 0dt = d_{Bat}T_S$

The equation (3.58) can be rearranged as follows:

$$\frac{d}{dt}I_{L,Bat} = \frac{1}{L_{Bat}}\left(V_{Bat} - (1 - d_{Bat})V_{DC}\right) \tag{3.59}$$

We choose the quadratic error of the current as a candidate Lyapunov function,

$$F = \frac{1}{2}e^2 = \frac{1}{2}(I_{L,Bat,ref} - I_{L,Bat})^2 \tag{3.60}$$

first condition:

$$F\left(0\right) = \frac{1}{2}(0)^2 = 0 \tag{3.61}$$

The candidate function has no energy at the equilibrium.

Second condition:

We search of the control law that forces the scalar function F to decrease everywhere, except at the origin, this means that F tends to zero as t tends to infinity, therefore $(I_{L,Bat,ref} - I_{L,Bat})$ goes to zero and $I_{L,Bat}$ will reach its reference value.

The derivative of F with respect to time is,

$$\frac{d}{dt}F = \frac{1}{2}\frac{d}{dt}e^2 = \frac{1}{2}\frac{de}{dt}\frac{d}{de}e^2 = \dot{e}e = (\dot{I}_{L,Bat,ref} - \dot{I}_{L,Bat})e \tag{3.62}$$

As the reference current $\dot{I}_{L,Bat,ref}$ is a constant value, eq.(3.62) can be simplified to,

$$\frac{d}{dt}F = -\dot{I}_{L,Bat}e \tag{3.63}$$

Substituting eq.(3.59) in eq.(3.63),

$$\frac{d}{dt}F = \underbrace{-\frac{1}{L_{Bat}}\left(V_{Bat} - (1-d_{Bat})V_{DC}\right)}_{Q}e \tag{3.64}$$

If we choose the control signal d_{Bat} such that the term Q of the equation (3.64) satisfies the relation,

$$Q = ke \tag{3.65}$$

The derivative of the Lyapunov function becomes ***negative definite function***,

$$\frac{d}{dt}F = -ke^2 \tag{3.66}$$

With K: a positive constant (how fast the energy function decreasing).

From the previous synthesis, the proposed candidate function is a ***Lyapunov function*** and, this will guarantee the ***asymptotic stability*** of the equilibrium point $e = 0$.

Where,

$$Q = ke = \frac{1}{L_{Bat}}\left(V_{Bat} - V_{DC} + d_{Bat}V_{DC}\right)$$

The control signal is obtained,

$$d_{Bat} = \frac{L_{Bat}ke + V_{DC} - V_{Bat}}{V_{DC}} = 1 - \frac{V_{Bat}}{V_{DC}} + Ke$$

We take,

$$L_{Bat}k = K$$

$$d_{Bat} = 1 - \frac{V_{Bat}}{V_{DC}} + \frac{K}{V_{DC}}e \tag{3.67}$$

From the equation (3.67), we can divide the control signal into two parts, steady state, and transient part:

- When the error goes to zero, the relationship between the input and the output voltages of the boost converter is satisfied.

$$d_{Bat} = d_{Bat,boost} = 1 - \frac{V_{Bat}}{V_{DC}} + \underbrace{\frac{K}{V_{DC}} e}_{Tends\ to\ zero} \Rightarrow \frac{V_{DC}}{V_{Bat}} = \frac{1}{1 - d_{Bat}} \tag{3.68}$$

- The delivered duty cycle (eq.(3.68)) is for the boost operating mode ($I_{L,Bat,ref} \geq 0$);
- If ($I_{L,Bat,ref} \leq 0$), the control signal of the buck operating mode is obtained simply as follows;

$$d_{Bat,buck} = 1 - d_{Bat,boost} \tag{3.69}$$

- When the error deviates from the origin, the transient part plays the role of a proportional corrector with an adjustable gain (K/V_{DC}).
- In order to minimize the steady state error, an integral action of the error must be added to the control law, as shown in Fig.3.15.

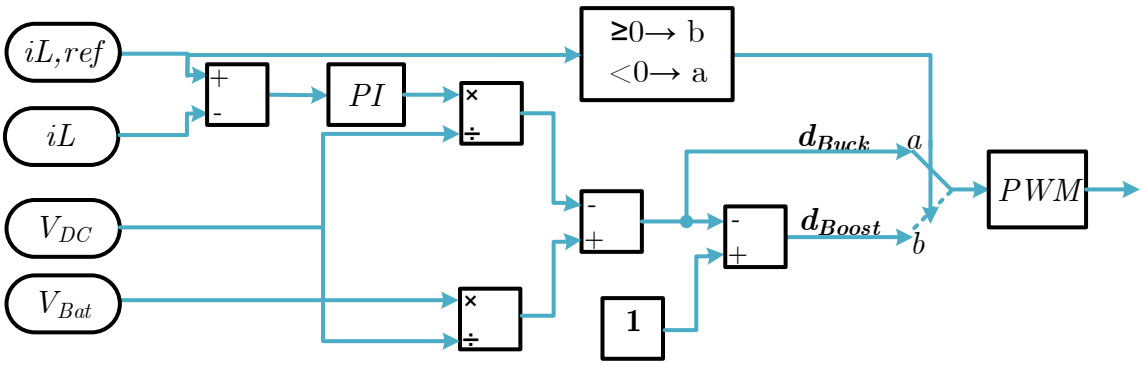

Fig.3.15. Lyapunov based nonlinear controller.

3.4.2.3. Simulation Results and Discussion

The global scheme of the storage system with the dedicated converter is shown in Fig.3.16.

The Presented simulation curves (Fig.3.15) are obtained from the execution of the previous system with Matlab/Simulink software.

When the reference current is positive (discharging mode), the boost mode is activated by the controller, and the control loop gives the proper duty cycle to the parallel switch, while the series switch still open during the boost mode.

When the reference current comes negative (charging mode), the controller will activate the buck mode, and the control loop gives the proper duty cycle to the series switch, while the parallel switch is open during the buck mode.

We observe clearly from the simulation results that the Lyapunov direct method controller gives more performances to the control system (higher dynamic, less overshoot) than the PI controller either in buck or boost mode.

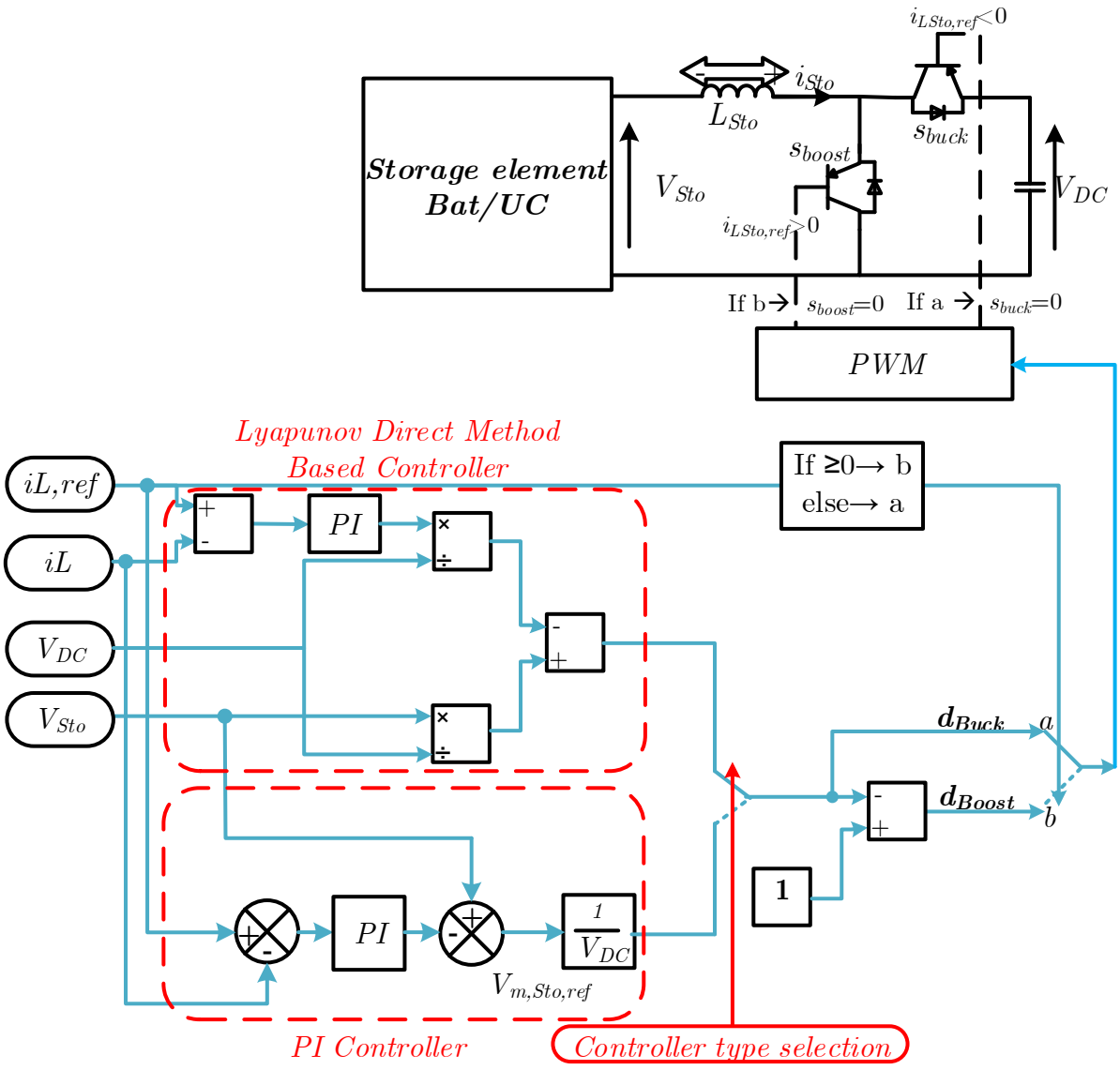

Fig.3.16. Global scheme of the storage system

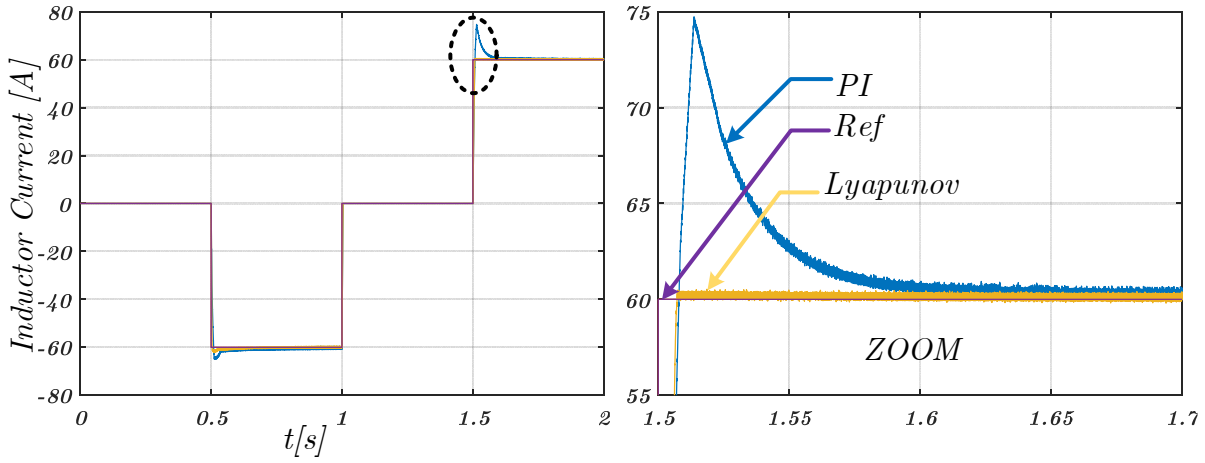

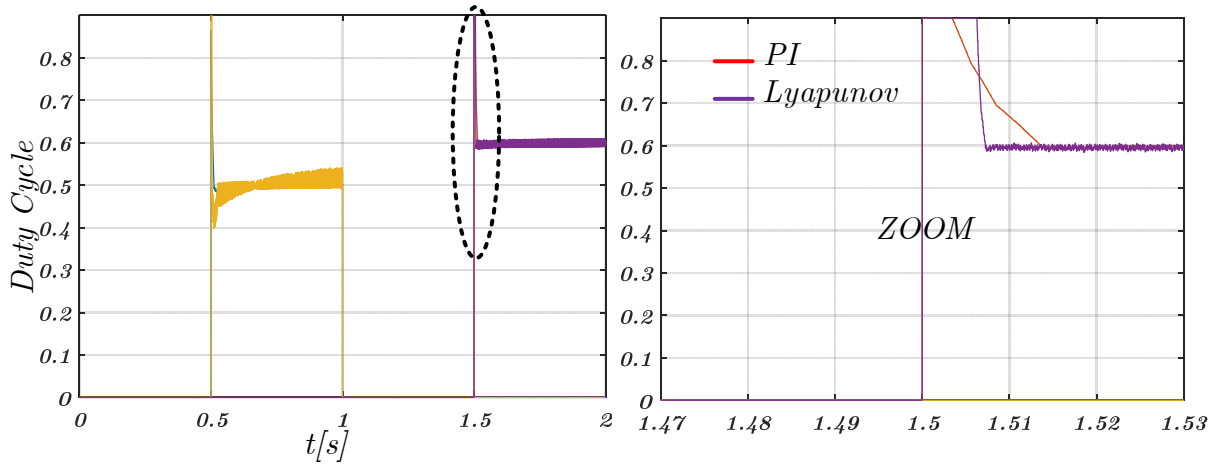

Fig.3.17. Simulation results of the Lyapunov based current controller in the two operating modes (buck&boost).

3.4.3. Control of the DC-link Voltage

The decomposition into the different subsystems relies on the assumption that the DC-bus voltage V_{DC} is constant, this is realized by a PI control loop as explained in Fig.3.18.

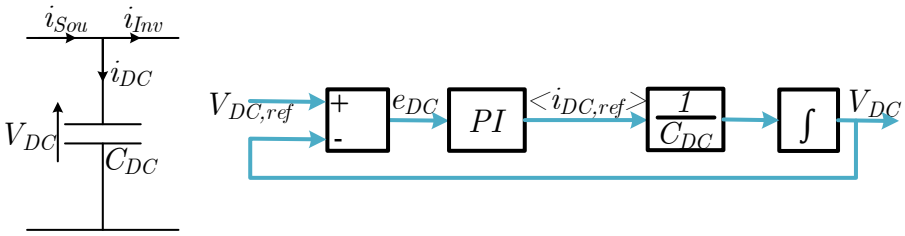

Fig.3.18. DC-link voltage control loop.

The DC-link is considered as a linear system governed by the following differential equation:

$$C_{DC}\frac{d}{dt}V_{DC} = i_{DC} \tag{3.70}$$

If we convert the instantaneous equation (3.70) to an average discretized equation (integrating the two sides from zero to T_S), we get:

$$\frac{\Delta V_{DC}}{T_S} = \frac{1}{C_{DC}}\left\langle i_{DC}\right\rangle \tag{3.71}$$

The control law can be easily derived from eq.(3.71) as follows:

$$\left\langle i_{DC,ref}\right\rangle = C_{DC}\frac{\left(\Delta V_{DC}\right)_{ref}}{T_S} = \underbrace{\frac{C_{DC}}{T_S}}_{P}\left(V_{DC,ref} - V_{DC}\right) \tag{3.72}$$

Note: The term C_{DC}/T_S represent a proportional action to the error, in some cases, when the system contains an integral action, this proportional action is enough for the error compensation. Generally, we add an integral action to the error path in order to optimize the transient response of the system.

The controller parameters are designed in the appendix.

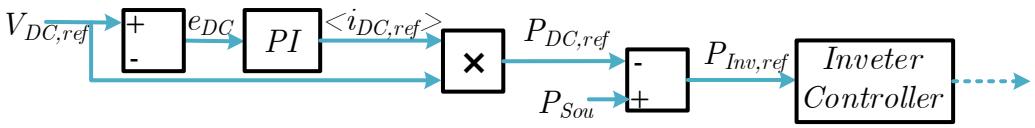

Fig.3.19. Control chain of the DC-link sub-system.

The current reference can be used to compute the power reference that is extracted/delivered from/to the DC-link capacitor in order to keep its voltage constant, this is accomplished by passing the task to the grid inverter:

$$P_{Inv,ref} = P_{Sou} - P_{DC,ref} \tag{3.73}$$

While,

$$P_{Sou} = P_{PV} + P_{Bat} + P_{UC} \tag{3.74}$$

3.4.4. Control of the Grid Inverter

The objective of the grid connection control is to regulate the exchanged active and reactive power to the grid. In our case, the power control is based on the Direct Power Control (DPC).

3.4.4.1. Principles of DPC

A. System Configuration

DPC is based on the instantaneous active and reactive power control loops. In DPC scheme, the converter switching states are selected by a switching table based on the instantaneous errors between the actual power and the reference power values of active and reactive powers. Fig.3.20 shows the configuration of the direct instantaneous active and reactive power control for three-phase PWM converter.

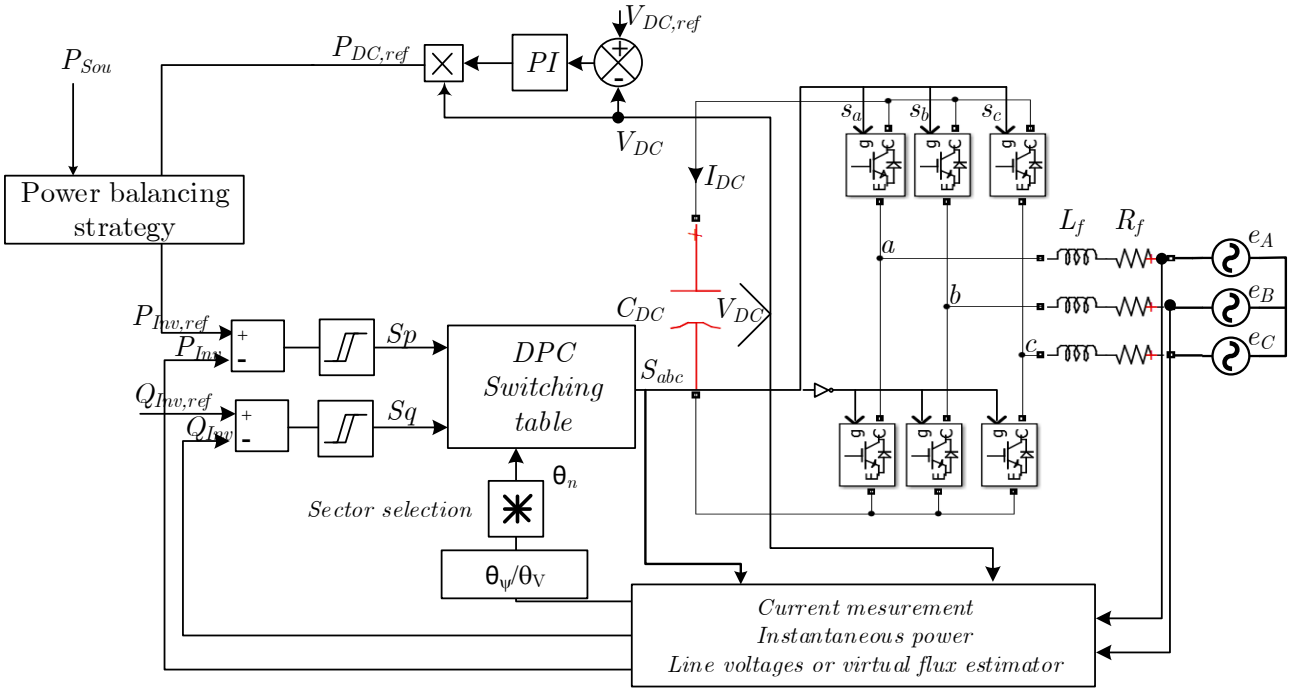

Fig.3.20. Configuration of DPC for three-phase PWM converter

In DPC scheme, the DC-link voltage is regulated by adjusting the active power. As shown in Fig.3.20, the active power command, $P_{Inv,ref}$, is provided from the power balancing strategy. The reactive power command, $Q_{Inv,ref}$, is provided directly from the grid operator. Errors between the commands and the actual feedback powers are input to the hysteresis comparators and digitized to the signals S_p and S_q. Also, the phase of the power-source voltage vector is converted to the digitized signal θ_n. For this purpose, the stationary reference frame is divided into 12 sectors, as shown in Fig.3.21.

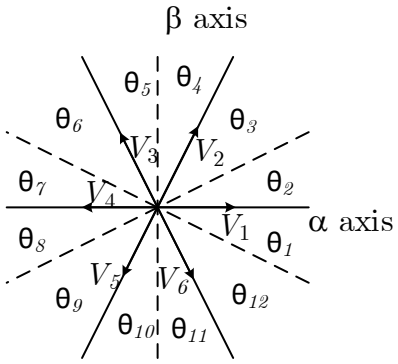

Fig.3.21. Sectors in stationary coordinates and convertor voltage vectors.

The digitized error signals S_p and S_q and digitized voltage phase θ_n are input to the switching table in which the switching states, Sa, Sb, and Sc, of the converter are stored. By using this switching table, the optimum switching states of the converter can be selected uniquely in every specific moment according to the combination of the input signals.

3.4.4.2. New Switching Table Synthesis

In the stationary reference frame α-β and for a balanced three-phase system, the line currents equation can be represented as follows:

$$\begin{cases} \frac{d}{dt} i_{\alpha} = \frac{1}{L}(e_{\alpha} - V_{\alpha} - R_f i_{\alpha}) \\ \frac{d}{dt} i_{\beta} = \frac{1}{L}(e_{\beta} - V_{\beta} - R_f i_{\beta}) \end{cases} \tag{3.75}$$

From eq.(3.75), line current vector $[i_{\alpha}\ i_{\beta}]^T$ can be controlled by selecting the proper rectifier voltage vector. The change in line current depends on the actual grid voltage vector $e_{\alpha\beta}$, on the selected rectifier voltage vector $V_{\alpha\beta}$, and in low factor on the actual line current. The parameter R_f can be practically neglected and a discrete first order approximation of eq.(3.75) can be adopted. Therefore, the change in line current vector for the next control period is given by:

$$\begin{cases} \Delta i_{\alpha} = i_{\alpha}(k+1) - i_{\alpha}(k) = \frac{T_S}{L}(e_{\alpha}(k) - V_{\alpha}(k)) \\ \Delta i_{\beta} = i_{\beta}(k+1) - i_{\beta}(k) = \frac{T_S}{L}(e_{\beta}(k) - V_{\beta}(k)) \end{cases} \tag{3.76}$$

The instantaneous active and reactive power can be represented as follows:

$$\begin{bmatrix} P \\ Q \end{bmatrix} = \begin{bmatrix} e_{\alpha} & e_{\beta} \\ e_{\beta} & -e_{\alpha} \end{bmatrix} \begin{bmatrix} i_{\alpha} \\ i_{\beta} \end{bmatrix} \tag{3.77}$$

As first approximation, and if the switching frequency is high enough, the change in grid voltage can be neglected. The change in the active and reactive power can be estimated for the next control cycle as follows:

$$\begin{cases} \Delta P = e_{\alpha}(k)\Delta i_{\alpha} + e_{\beta}(k)\Delta i_{\beta} \\ \Delta Q = e_{\beta}(k)\Delta i_{\alpha} - e_{\alpha}(k)\Delta i_{\beta} \end{cases} \tag{3.78}$$

Substituting (3.76) in (A.3.78) leads to:

$$\begin{cases} \Delta P = \frac{T_S}{L}(e_{\alpha}^2(k) + e_{\beta}^2(k)) - \frac{T_S}{L}(e_{\alpha}(k)V_{\alpha}(k) + e_{\beta}(k)V_{\beta}(k)) \\ \Delta Q = \frac{T_S}{L}(e_{\alpha}(k)V_{\beta}(k) - e_{\beta}(k)V_{\alpha}(k)) \end{cases} \tag{3.79}$$

To control the instantaneous active and reactive power there are six basic none zero converter voltage vectors and two zero converter voltage vectors available as shown in Fig.3.21. For each possible voltage vector there exist one possible value for the change in the active and reactive powers. As a result, there are different possibilities to select the corresponding switching state that controls the evolution in active and reactive power. With i=(0,1,2,…,6) the changes in the active and reactive powers are given by the following expressions:

$$\begin{cases} \Delta P = \dfrac{T_S}{L}(e_\alpha^2(k) + e_\beta^2(k)) - \dfrac{T_S}{L}(e_\alpha(k)V_{\alpha i}(k) + e_\beta(k)V_{\beta i}(k)) \\ \Delta Q = \dfrac{T_S}{L}(e_\alpha(k)V_{\beta i}(k) - e_\beta(k)V_{\alpha i}(k)) \end{cases} \quad i = 0,...,6 \tag{3.80}$$

In the stationary reference frame α-β, the power-source voltage vector is given by the following transformation:

$$e_{\alpha\beta} = \begin{bmatrix} e_\alpha \\ e_\beta \end{bmatrix} = \frac{2}{3}\begin{bmatrix} 1 & -1/2 & -1/2 \\ 0 & \sqrt{3}/2 & -\sqrt{3}/2 \end{bmatrix}\begin{bmatrix} e_a \\ e_b \\ e_c \end{bmatrix} \tag{3.81}$$

This vector can be represented in (α,β) plane as:

$$e_\alpha = E\cos(\theta), e_\beta = E\sin(\theta),\ E = \left\| e_{\alpha,\beta} \right\| \tag{3.82}$$

Where: E is the RMS value of the line-to-line grid voltage and θ is the angular position of the power-source voltage vector in α-β coordinates defined as follows:

$$\theta = \arctan(e_\beta / e_\alpha), -\pi/6 \le \theta \le 11\pi/6 \tag{3.83}$$

V_α and V_β components values are shown in Tab.3.1.

Tab.3.1. Voltage space vectors of the PWM converter.

Vi	Va	Vb	Vc	Vαi	Vβi
V0	0	0	0	0	0
V1	$2/3V_{DC}$	$-1/3V_{DC}$	$-1/3V_{DC}$	$\sqrt{2/3}V_{DC}$	0
V2	$1/3V_{DC}$	$1/3V_{DC}$	$-2/3V_{DC}$	$\sqrt{1/6}V_{DC}$	$\sqrt{1/2}V_{DC}$
V3	$-1/3V_{DC}$	$2/3V_{DC}$	$-1/3V_{DC}$	$-\sqrt{1/6}V_{DC}$	$\sqrt{1/2}V_{DC}$
V4	$-2/3V_{DC}$	$1/3V_{DC}$	$1/3V_{DC}$	$-\sqrt{2/3}V_{DC}$	0
V5	$-1/3V_{DC}$	$-1/3V_{DC}$	$2/3V_{DC}$	$-\sqrt{1/6}V_{DC}$	$-\sqrt{1/2}V_{DC}$
V6	$1/3V_{DC}$	$-2/3V_{DC}$	$1/3V_{DC}$	$\sqrt{1/6}V_{DC}$	$-\sqrt{1/2}V_{DC}$

The converter voltage vector in (α, β) plane is given by:

$$V_{\alpha\beta} = [V_a \; V_\beta]^T, \left\|V_{\alpha\beta}\right\| = \sqrt{2/3}V_{DC} \tag{3.84}$$

The normalized value of the change in active power and reactive power can be deduced from (3.80) as follows:

$$\begin{cases} \overline{\Delta P_i} = \dfrac{\Delta P_i}{\dfrac{T_S}{L}\left\|e_{\alpha\beta}\right\|\left\|V_{\alpha\beta}\right\|} = \dfrac{\left\|e_{\alpha\beta}\right\|}{\left\|V_{\alpha\beta}\right\|} - (\bar{V}_{\alpha i}(k)\cos\theta + \bar{V}_{\beta i}(k)\sin\theta) \\ \overline{\Delta Q_i} = \dfrac{\Delta Q_i}{\dfrac{T_S}{L}\left\|e_{\alpha\beta}\right\|\left\|V_{\alpha\beta}\right\|} = (\bar{V}_{\beta i}(k)\cos\theta - \bar{V}_{\alpha i}(k)\sin\theta) \end{cases} / \begin{cases} \bar{V}_{\alpha i}(k) = \dfrac{V_{\alpha i}(k)}{\left\|V_{\alpha\beta}\right\|} \\ \bar{V}_{\beta i}(k) = \dfrac{V_{\beta i}(k)}{\left\|V_{\alpha\beta}\right\|} \end{cases} \tag{3.85}$$

It can be seen from eq.(3.85) that the change in reactive power during all sectors has a sinusoidal waveform for all PWM converter voltage vectors *Vi*. The change in active power has a shifted sinusoidal waveform as shown in Fig.3.22 and Fig.3.23, respectively.

The basic idea of this DPC is to choose the best converter voltage vector among the seven possible vectors in order to ensure smooth control of instantaneous active and reactive power during each sector. The active power is controlled to be constant and equal to its reference value; the reactive power should be maintained zero for all sectors. For this reason, the switching table synthesis is based on the sign and magnitude of the change in active and reactive power for each sector, as shown in Fig.3.22 and Fig.3.23.

For example, for sector one the sign of the change in active and reactive power is shown in Tab.3.2.

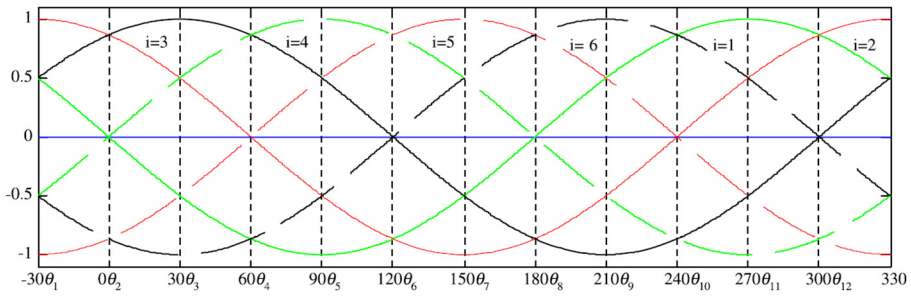

Fig.3. 22. Normalized Change in reactive power.

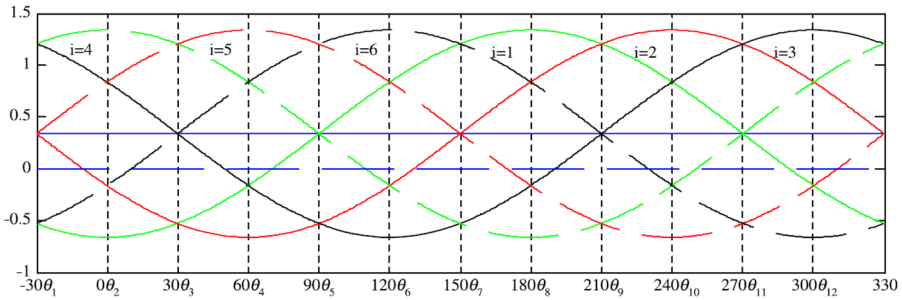

Fig.3. 23. Normalized Change in active power.

Tab.3.2. sign of change in active and reactive powers for sector 1.

$\overline{\Delta P_i}$		$\overline{\Delta Q_i}$		
>0	<0	>0	$=0$	<0
$V_0,\ V_3,\ V_4,\ V_5$	$V_1,\ V_6$	$V_1,\ V_2,\ V_3$	V_0	$V_4,\ V_5,\ V_6$

For each combination of hysteresis output signals, Sp and Sq, converter voltage vectors are selected for sector one as shown in the following table:

Tab.3.3. Selected converter voltage vectors for sector 1.

Sector 1		$\overline{\Delta Q_i}$	
		$>0\ /Sq=1$	$<0\ /Sq=0$
$\overline{\Delta P_i}$	$>0\ /Sp=1$	V_3	$V_4,\ V_5$
	$<0\ /Sp=0$	V_1	V_6

For all sectors, the switching table is represented in Tab.3.4.

Tab.3.4.Switching table for the DPC based controller [Bou08].

$\mathbf{S_P}$	$\mathbf{S_Q}$	θ_1	θ_2	θ_3	θ_4	θ_5	θ_6	θ_7	θ_8	θ_9	θ_{10}	θ_{11}	θ_{12}
1	**0**	V_5	V_6	V_6	V_1	V_1	V_2	V_2	V_3	V_3	V_4	V_4	V_5
	1	V_3	V_4	V_4	V_5	V_5	V_6	V_6	V_1	V_1	V_2	V_2	V_3
0	**0**	V_6	V_1	V_1	V_2	V_2	V_3	V_3	V_4	V_4	V_5	V_5	V_6
	1	V_1	V_2	V_2	V_3	V_3	V_4	V_4	V_5	V_5	V_6	V_6	V_1

V1(100), V2(110), V3(010), V4(011), V5(001), V6(101), V0(000), V7(111).

Where $Vi(S_a,S_b,S_c)$ are the switching variables of the inverter's legs.

3.4.4.3. Steady-state Properties and Limitations

For proper operation of PWM converter, a minimum DC-link voltage is required. Generally, it can be determined by the peak of line-to-line supply voltage [Mar0l]:

$$V_{DC,\min} > \sqrt{3}\sqrt{2}e_{LN,rms} \tag{3.86}$$

It is true definition but does not concerns all situations. It depends on many parameters. As an example, we will introduce the design procedure for the hysteresis based current controller.

As shown in Fig.3.24, In order to control the current throw the inductor L_f, we should control the voltage across its terminals (A_1 and A_2).

The inductor current evolution is governed by the following differential equation,

$$L_f \frac{d}{dt} i_{g,a} = v_{Lf,a} = v_{A1}(S_a, S_b, S_c) - v_{A2} \tag{3.87}$$

The point A_2 is uncontrolled; it depends on the line voltage source. While polar voltages (V_a, V_b, V_c) of the PWM converter control the point A_1, which is depends on the state of the switches S_a, S_b, S_c.

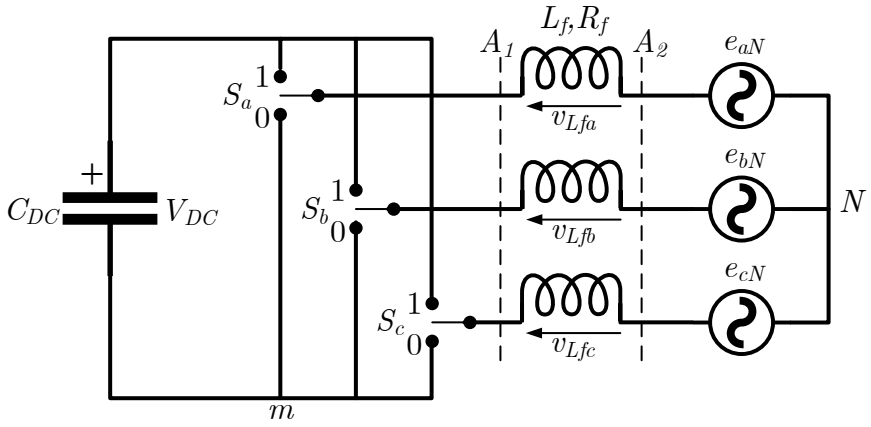

Fig.3. 24. Hysteresis current control principle on a three-phase PWM converter.

By means of a hysteresis controller, there exist two possible state for every switch;

"1": to increase the switch current;

"0": to decrease the switch current.

But, there is an important condition that guarantees the controllability of the inductor current.

When the state is "1", v_{A1} always must be greater than V_{A2}, it means that,

$$\min\left(v_{A1} = V_a\right) > \max\left(V_{A2} = e_{aN}\right) \tag{3.88}$$

In order to compare these two voltages, they must have the same reference (the neutral point N).

From Fig.3.24 we get,

$$\begin{cases} V_{aN} = V_{am} + V_{mn} \ (a) \\ V_{bN} = V_{bm} + V_{mn} \ (b) \\ V_{cN} = V_{cm} + V_{mn} \ (c) \end{cases} \tag{3.89}$$

The sum of (a), (b), and (c) in eq.(3.89) gives,

$$V_{aN} + V_{bN} + V_{cN} = V_{am} + V_{bm} + V_{cm} + 3V_{mn}$$

In balanced three-phase system,

$$V_{aN} + V_{bN} + V_{cN} = 0$$

and

$$\begin{aligned} V_{am} &= S_a V_{DC} \\ V_{bm} &= S_b V_{DC} \\ V_{cm} &= S_d V_{DC} \end{aligned} \tag{3.90}$$

The arrive to the following equation,

$$V_{mN} = -\frac{V_{DC}}{3}(S_a + S_b + S_c) \tag{3.91}$$

Substituting for eq.(3.90) and eq.(3.91) in eq.(3.89),

$$\underline{V}_{Inv} = \begin{bmatrix} V_{aN} \\ V_{bN} \\ V_{cN} \end{bmatrix} = \begin{bmatrix} \frac{V_{DC}}{3}(2S_a - S_b - S_c) \\ \frac{V_{DC}}{3}(-S_a + 2S_b - S_c) \\ \frac{V_{DC}}{3}(-S_a - S_b + 2S_c) \end{bmatrix} \tag{3.92}$$

Eq.(3.92) leads to Tab.3.5,

Tab.3.5. Polar voltages according to the switches states.

(S_a,S_b,S_c)	V_{aN}	V_{bN}	V_{cN}
100	$2V_{DC}/3$	$-V_{DC}/3$	$-V_{DC}/3$
110	$V_{DC}/3$	$V_{DC}/3$	$-2V_{DC}/3$
101	$V_{DC}/3$	$-2V_{DC}/3$	$V_{DC}/3$
111	0	0	0
000	0	0	0
010	$-V_{DC}/3$	$2V_{DC}/3$	$-V_{DC}/3$
001	$-V_{DC}/3$	$-V_{DC}/3$	$2V_{DC}/3$
011	$-2V_{DC}/3$	$V_{DC}/3$	$V_{DC}/3$

From Tab.3.5, when the switch S_a is ON,

$$\min(V_{aN}) = \frac{V_{DC}}{3} \tag{3.93}$$

Substituting for eq.(3.93) in eq.(3.88),

$$\begin{aligned} &\frac{V_{DC}}{3} > (e_{aN,\max} = \sqrt{2} e_{aN,rms}) \\ &V_{DC} > \sqrt{3}\sqrt{2} U_{L-L,rms} \end{aligned} \tag{3.94}$$

When the state is "0" $V_a(t)$ must be always lesser than $e_{aN}(t)$, it means that,

$$\max(V_{aN}) < \min(e_{aN}) \tag{3.95}$$

From Tab.3.5, when the switch S_a is OFF,

$$\max(V_{aN}) = -\frac{V_{DC}}{3} \tag{3.96}$$

From eq.(3.95),

$$\begin{aligned} &-\frac{V_{DC}}{3} < -e_{aN,\max} \\ &V_{DC} > \sqrt{3}\sqrt{2} U_{L-L,rms} \end{aligned} \tag{3.97}$$

Same result as obtained in eq.(3.94).

3.4.4.4. Voltage and Virtual Flux Estimation [Mar0l]

Line Voltage Estimator

It is possible to calculate the voltage across the inductance by differentiating the current. The line voltage can then be estimated by adding the converter polar voltage to the calculated voltage drop across the inductor. However, this approach has the disadvantage that the current is differentiated and noise in the current signal is gained through the differentiation. To prevent this, a voltage estimator based on the power estimator can be applied. The current is sampled and the power is estimated several times in every switching state.

In conventional space vector modulation (SVM) for three-phase voltage source converters, the AC currents are sampled during the zero-vector states because no switching noise is present and a filter in the current feedback for the current control loops can be

avoided [Mar0l]. Using the two following equations, the estimated active and reactive power of the filter in this special case (zero states) can be expressed as:

$$P_{Lf} = L_f i_{g,a} \frac{di_{g,a}}{dt} + L_f i_{g,b} \frac{di_{g,b}}{dt} + L_f i_{g,c} \frac{di_{g,c}}{dt} = 0 \tag{3.98}$$

$$Q_{Lf} = \frac{3}{\sqrt{3}} L_f \left(i_{g,a} \frac{di_{g,c}}{dt} - i_{g,c} \frac{di_{g,a}}{dt} \right) \tag{3.99}$$

Since powers are DC-values it is possible to prevent the noise of the differentiated current by use of a simple (digital) low pass filter. This ensures a robust and noise insensitive performance of the voltage estimator.

Based on instantaneous power theory, the estimated voltages across the inductance are:

$$\underline{v}_{Lf,est} = \begin{bmatrix} v_{Lf\alpha,est} \\ v_{Lf\beta,est} \end{bmatrix} = \frac{1}{i_{g\alpha}^2 + i_{g\beta}^2} \begin{bmatrix} i_{g\alpha} & -i_{g\beta} \\ i_{g\beta} & i_{g\alpha} \end{bmatrix} \begin{bmatrix} 0 \\ Q_{Lf} \end{bmatrix} \tag{3.100}$$

Where:

$v_{Lf\alpha,est}$, $v_{Lf\beta,est}$ are the estimated values of the three-phase voltages across the inductance L, in the fixed (α, β) coordinates.

The estimated line voltage $\underline{e}_{g,est}$, can now be found by adding the voltage reference of the PWM converter to the estimated inductor voltage.

$$\underline{e}_{g,est} = \underline{v}_{Lf,est} + \underline{V}_{Inv} \tag{3.101}$$

Where:

$\underline{V}_{Inv}$: is the vector of the three phase polar voltages of the converter (eq.(3.92)).

$$\underline{e}_g = \begin{bmatrix} e_{aN} \\ e_{bN} \\ e_{cN} \end{bmatrix} \tag{3.102}$$

Virtual Flux Estimator

The voltage imposed by the line power in combination with the AC side inductors are assumed to be quantities related to a virtual AC motor as shown in Fig. 3.25.

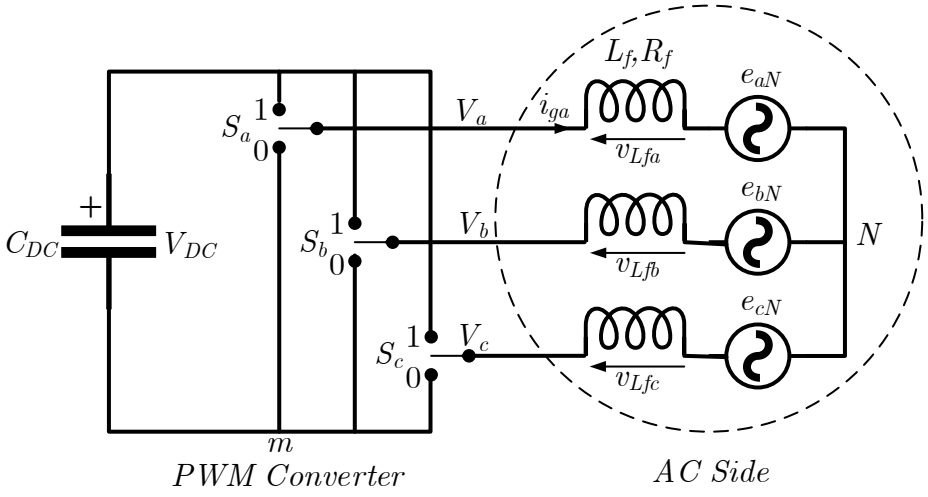

Fig.3.25. Three-phase PWM converter with AC-side presented as virtual AC motor

Thus, R_f and L_f represent the stator resistance and the stator leakage inductance of the virtual motor and phase-to-phase line voltages: U_{ab}, U_{bc}, U_{ca}, would be induced by a virtual air gap flux. In other words, the integration of the voltages leads to a virtual line flux vector $\underline{\Psi}$, in stationary (α, β) coordinates (Fig. 3.26).

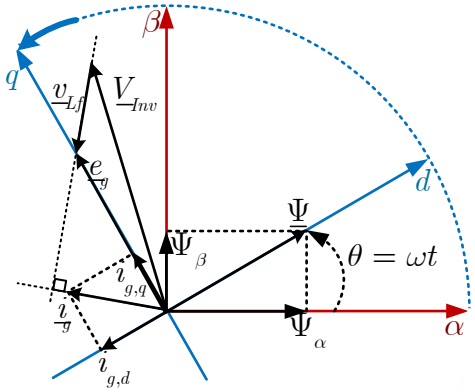

Fig.3.26. Vectors representation in $\alpha\beta$ and dq reference frames.

Where:

$\underline{\Psi}$: is the virtual grid flux vector;

$\underline{e}_g$: is the grid voltage vector;

$\underline{i}_g$: is the grid voltage vector;

$\underline{V}_{Inv}$: is the inverter voltage vector;

$\underline{v}_{Lf}$: is the filter voltage vector.

By similarity with eq.(3.101), a virtual flux equation can be presented as:

$$\underline{\Psi}_{est} = \underline{\Psi}_{Lf,est} + \underline{\Psi}_{Inv} \tag{3.103}$$

Based on the measured DC-link voltage V_{DC}, and the converter switch states S_a, S_b, S_c, the converter input voltages are estimated as follows,

$$\begin{aligned} V_{Inv,\alpha} &= \sqrt{\frac{1}{6}} V_{DC}(2S_a - S_b - S_c) \\ V_{Inv,\beta} &= \sqrt{\frac{1}{2}} V_{DC}(S_b - S_c) \end{aligned} \tag{3.104}$$

Then, the virtual flux $\underline{\Psi}$ components are calculated in stationary (α,β) reference frame,

$$\begin{cases} \Psi_{\alpha,est} = \int \underline{e}_{g,\alpha,est} dt = \int \left(v_{Lf,\alpha} + V_{Inv,\alpha}\right) dt = L_f i_{Lf,\alpha} + \int V_{Inv,\alpha} dt \\ \Psi_{\beta,est} = \int \underline{e}_{g,\beta,est} dt = \int \left(v_{Lf,\beta} + V_{Inv,\beta}\right) dt = L_f i_{Lf,\beta} + \int V_{Inv,\beta} dt \end{cases} \tag{3.105}$$

It is not necessary to implement PLL's to achieve robustness in the flux-oriented scheme, since $\underline{\Psi}$ rotates much more smoothly than $\underline{e}_g$. The angular displacement of virtual flux vector $\underline{\Psi}$ in (α,β) frame is defined as:

$$\tan(\theta) = \frac{\Psi_\beta}{\Psi_\alpha} \tag{3.106}$$

3.4.4.5. Simulation Results

The main objective of the following simulations is to present the dynamic behavior under a step change of the delivered active and reactive power, Fig. 3.27.

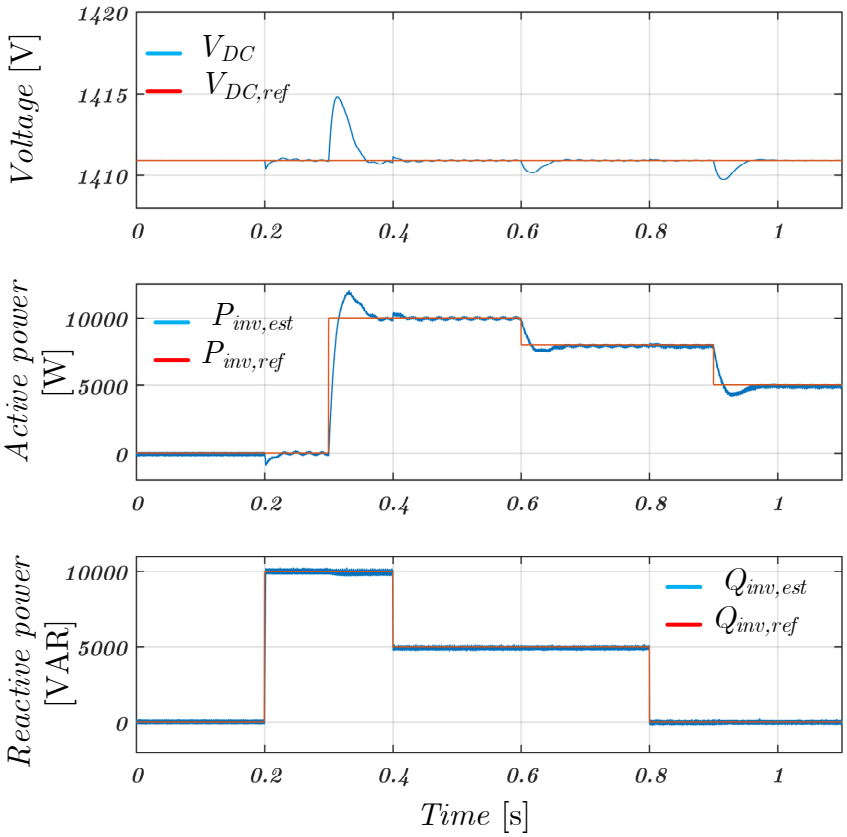

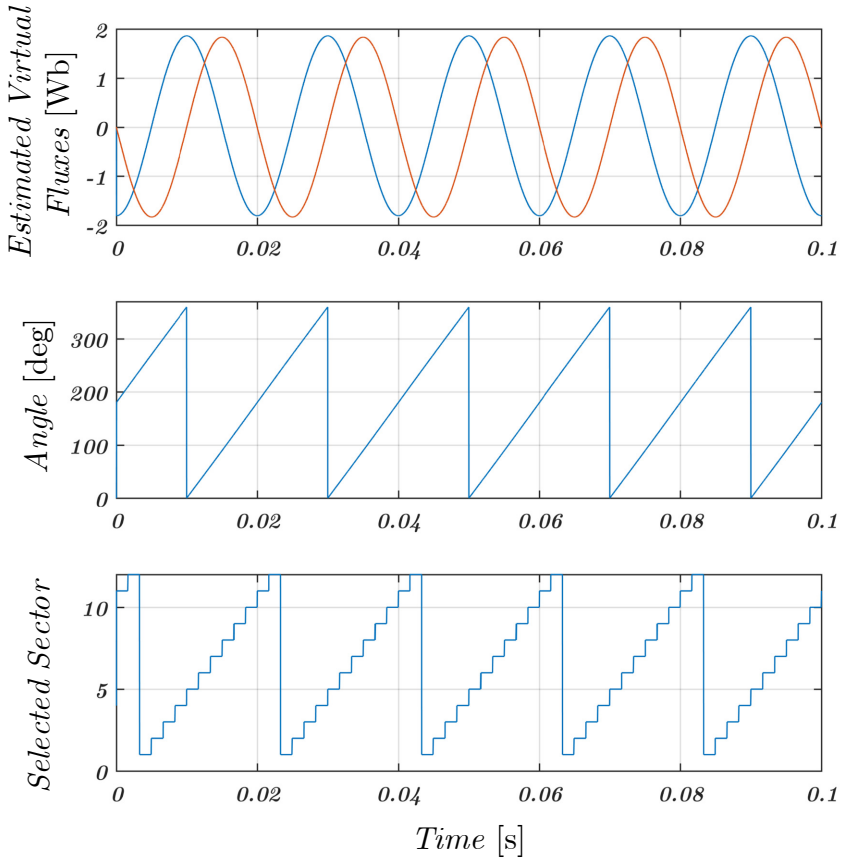

Fig.3.27. Simulated basic signal waveforms under a Virtual-Flux based DPC.

We note a good dynamic and steady state behaviors under an estimated virtual flux based DPC:

✓ The DC-link voltage is regulated.

✓ After an acceptable transient (overshoot), both reactive and active powers returns to their references in a decoupling manner.

3.4.5. Automatic Control Unit for the Whole APG

The presented scheme (Fig.3.19) shows the automatic control unit (ACU) for the APG.

The global control scheme of the entire active PV generator is obtained by combining all control schemes, which have been presented in the previous parts. A block diagram of all control functions inside the automatic control units (ACU) is presented on Fig.3.28. four references ($V_{DC,ref}$, $i_{LUC,ref}$, $i_{LBat,ref}$, $V_{PV,ref}$) must be set based on the grid operator power demand ($P_{g,ref}$, $Q_{g,ref}$).

3.5. Basic Maximum Power Point Tracking Algorithms

The operating point at maximum power in systems based on PV modules depends on solar-radiation level, operating temperature and load current (Fig.3.29 and Fig.3.30).

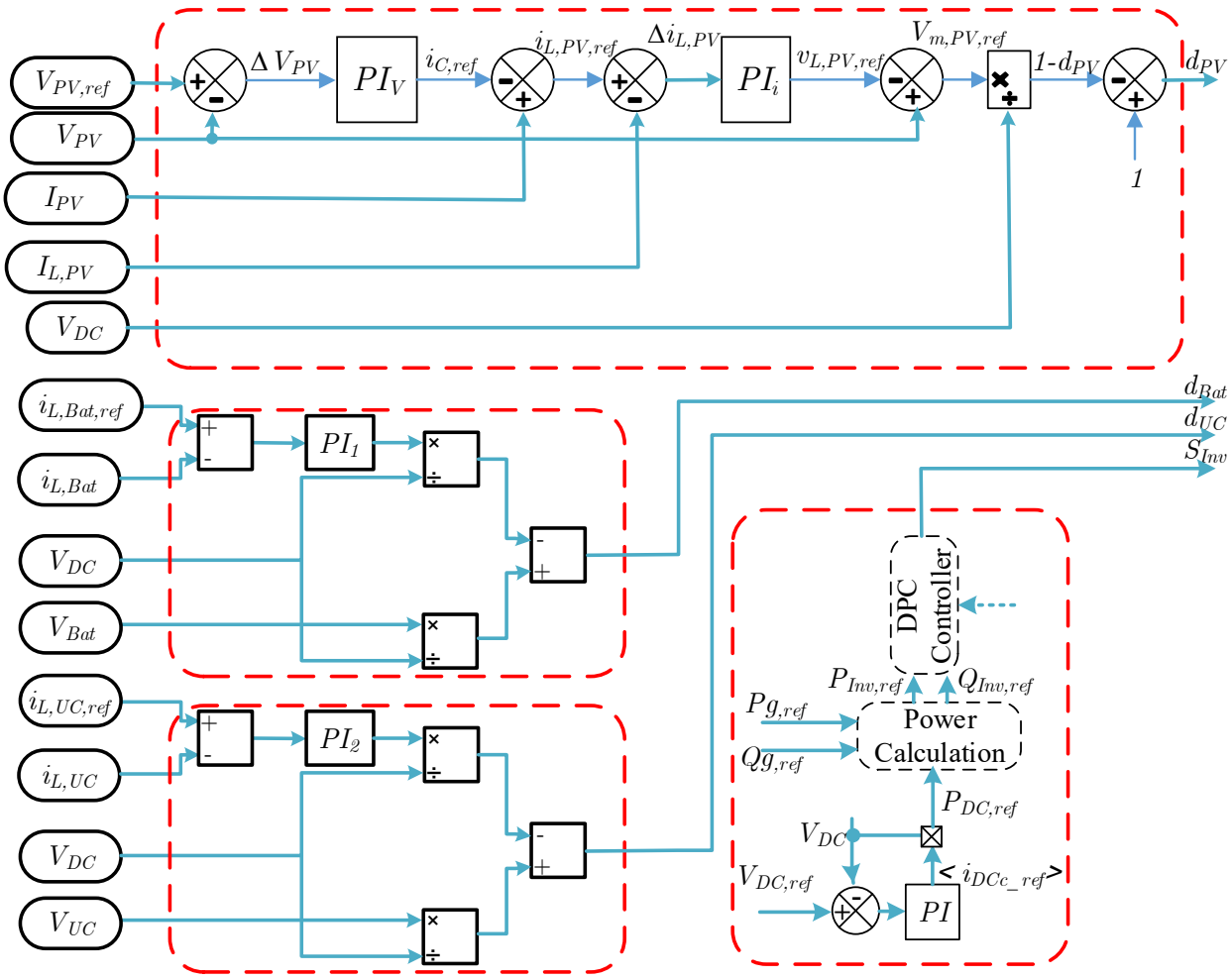

Fig.3.28. Global control scheme of the ACU for the APG.

Fig.3.29 shows both characteristics, power - voltage and current - voltage of a PV module BPSX3200B, for different solar radiation levels at 25 °C of cell temperature. Fig.3.30 present the same characteristics for different temperatures at 1000W /m^2 of radiation level.

To ensure maximum power operating point, we must develop control technics and algorithms. Main techniques mostly used are:

- MPPT based on voltage or current control (V_{MPPT} and C_{MPPT});
- Hill climbing (HC);
- Perturbation and Observation (P&O)
- Incremental conductance method (IncCon).

Some other methods have appeared as a modification or combination of those basic techniques.

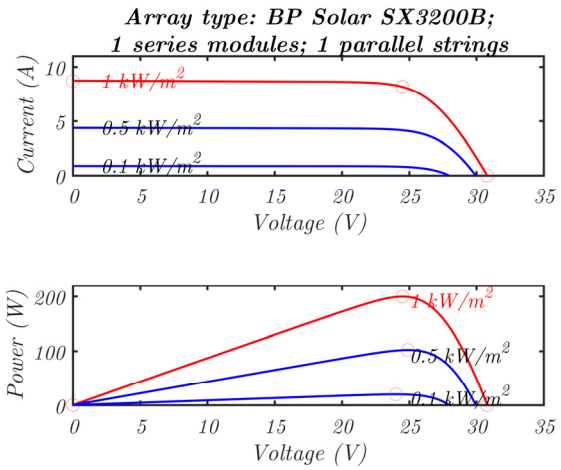

Fig.3.29. P-V and I-V characteristics BPSX3200B for different radiation levels at T=25°C

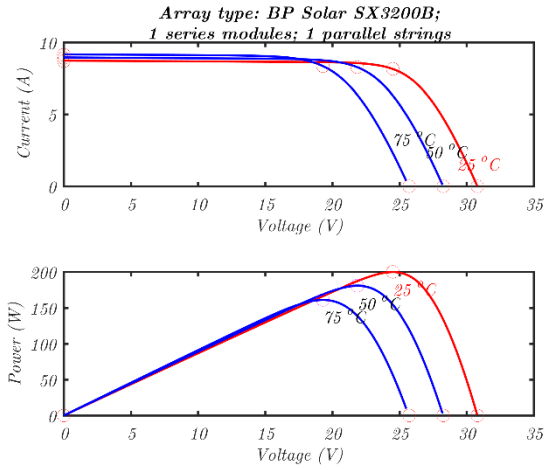

Fig.3.30. P-V and I-V characteristics BPSX3200B for different temperature levels at 1000W/m2

3.5.1. MPPT Based on Voltage or Current Control (V_{MPPT} and C_{MPPT})

In order to achieve the operating point according to maximum power for different radiation levels, the partial derivative of power with respect to current yields to a linear relationship between cells-short circuit current and maximum power point current. This is the basis of C_{MPPT} technique. A similar procedure shows that maximum power voltage and open circuit voltage have a linear dependence for different solar radiation and operating temperatures. Then, this is the key to develop V_{MPPT} technique.

To implement C_{MPPT} method, a shunt switch, placed in between PV cell, and switching converter (DC/DC or DC/ AC), allowing online measurements of the short-circuit current.

To implement V_{MPPT} method, a series switch also placed in between PV cell, and switching converter, allowing online measurement of the open circuit voltage.

In both cases, the system is completed with a PWM switching converter and a microcontroller that controls the shunt switch or the series switch and drives firing command to drive converter switches. The main drawback of that technique is, because the relationship between the short circuit current and the maximum power current (maximum power voltage and open circuit voltage) is strongly dependent of the PV characteristics.

3.5.2. Hill Climbing Technique (HC)

This is one of the so-called power feedback method. It is based on the relationship of the switching converter duty cycle (*d)* and PV array power (*P).* The plot of this function shows a hill shape. Maximum power point can be achieved if the expression *dP/ dd* is forced to zero by means of the control. The algorithm compares periodically the current power level P_k with the value calculated in the previous sample P_{k-1}. According to the result of comparison, the value of d is increased or decreased. Therefore, the duty cycle changes until the working point is around the MPP. The main advantage of this method is its simplicity. Its drawback is the deviation from the optimal operating point in case of quickly changing weather conditions. In this situation controller can be confused and lead the working point in the wrong direction. Another inconvenience is the dependence between good performances in both dynamic and steady state responses and the adopted value of incremental step of the duty cycle.

3.5.3. Perturb and Observe

This is a technique similar to HC and is based on the regulation of PV cells array voltage to follow an optimal set point, which is the voltage of maximum power working point. This point is periodically tracked and updated in order to achieve a simple mathematical condition, that is $dP/\ dV = 0$, where P and V are PV output power and output voltage respectively. Due to the power-voltage relationship of a typical PV array, the maximum power point can always be followed if the condition $dP/\ dV = 0$ is satisfied for any solar radiation or temperature. This is possible because all maximum power points have the same mathematical attribute. This technique as well as HC technique could present oscillations about the MPP and control problems when the system works under strong changes on solar radiation.

3.5.4. Incremental Conductance Method (IncCon)

The incremental conductance (IncCon) technique is based again on the fact that the derivative of function *p=F(V)* is zero at the MPP, in any case of PV solar radiation, it is positive on the left of the MPP and it is negative on the right (Fig.3.31).

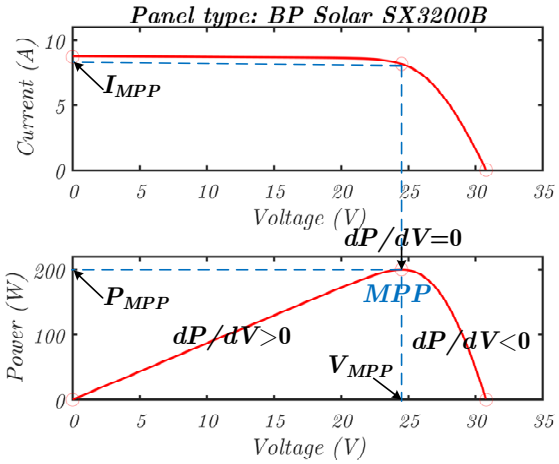

Fig.3. 31. Signs of the power derivative with respect to voltage around the maximum power point.

These conditions are summarized in the following equations eq.(3.107 and 3.108).

$$\frac{dP}{dV} = \frac{d(VI)}{dV} = I + V\frac{dI}{dV} \tag{3.107}$$

$$\begin{cases} \dfrac{\Delta I}{\Delta V} = -\dfrac{I}{V}, \text{ at } MPP \\ \dfrac{\Delta I}{\Delta V} > \dfrac{I}{V}, \text{ at the left of the } MPP \\ \dfrac{\Delta I}{\Delta V} < \dfrac{I}{V}, \text{ at the right of the } MPP \end{cases} \tag{3.108}$$

Therefore, MPP can be achieved by doing a comparison between the negative instantaneous conductance ($-I/V$) and the incremental conductance ($\Delta I/\Delta V$) and force both to get the same value. $V_{PV,ref}$ is the voltage reference at which the PV module is obligated to work. When the MPP is achieved, the operation of the PV module is hold at that point ($V_{PV,ref} = V_{MPP}$), unless, a change in ΔI is detected. This will mean, there is a change in weather conditions and then in the MPP.

The flowcharts of the P&O and IncCon algorithms are presented in Fig.3.32 and 33 respectively.

3.6. Limited Power Point Tracking (LPPT) Algorithm

At certain conditions, when the storage units are fully charged and the PV production is greater than the grid demand or the load demand in the case of standalone PV system, the PLA must be applied (Fig.3.37). From the P-V curve of the PV panel (Fig.3.34), we can observe that, there exist two set points for the same power value. Hence, two possible ways exist to reduce the PV power generation from the MPP to the set point:

✓ The first one is to shift the operating voltage from the V_{MPP} into the right side of the MPP, by increasing V_{PV}.

✓ The second one is to shift the operating voltage from V_{MPP} into the left side of the MPP, by decreasing V_{PV}.

✓ In the present work, shifting V_{PV} to the right side has been adopted since a great current diminution will occur (see I-V curve, Fig.3.35), especially when the set point is so far from the MPP (small power reference).

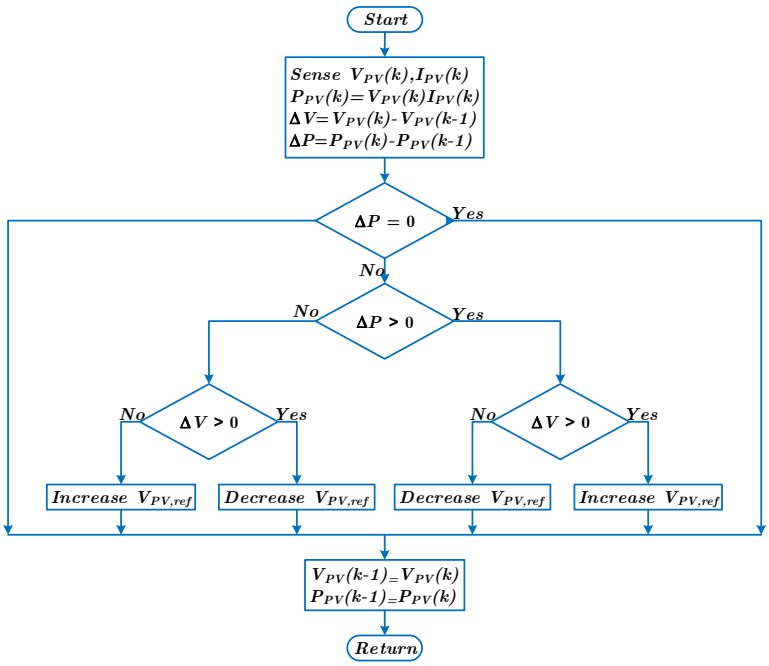

Fig.3.32. Flowchart of the P&O MPPT algorithm.

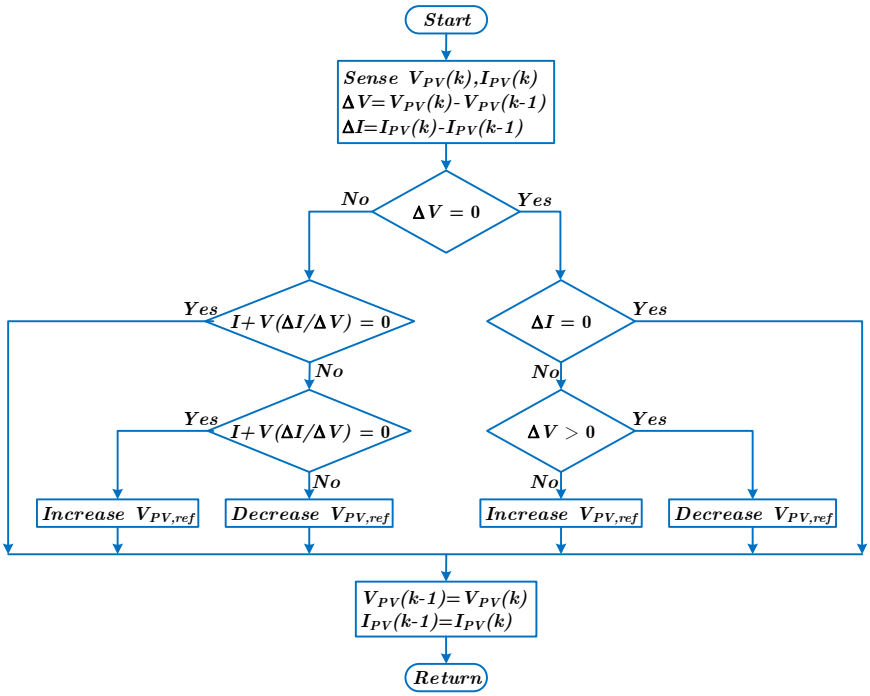

Fig.3. 33. Flowchart of the IncCon MPPT algorithm.

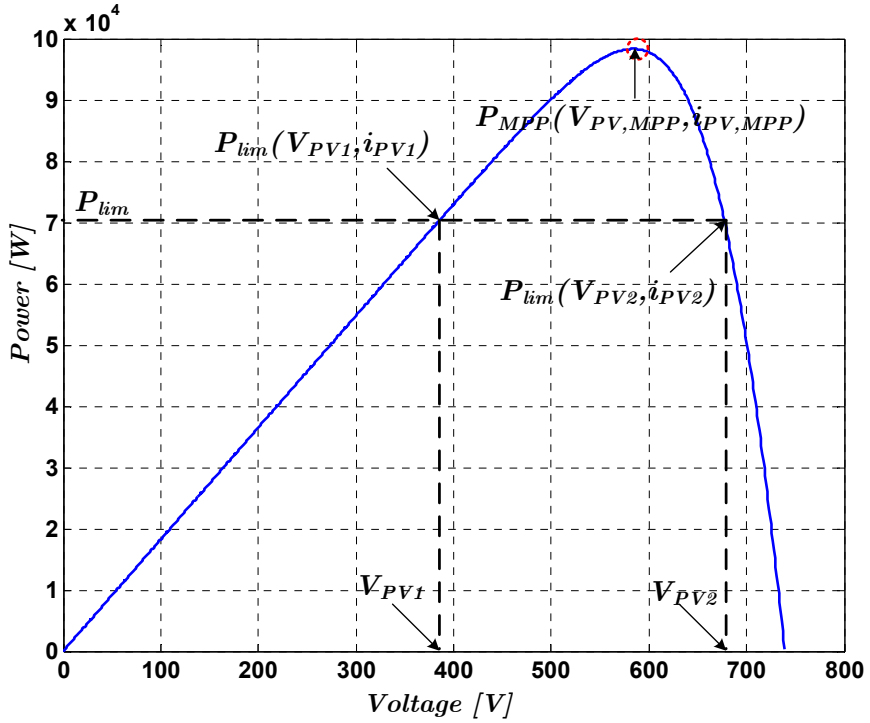

Fig.3. 34. P-V curve of a 100 kW PV array at 1000w/m2.

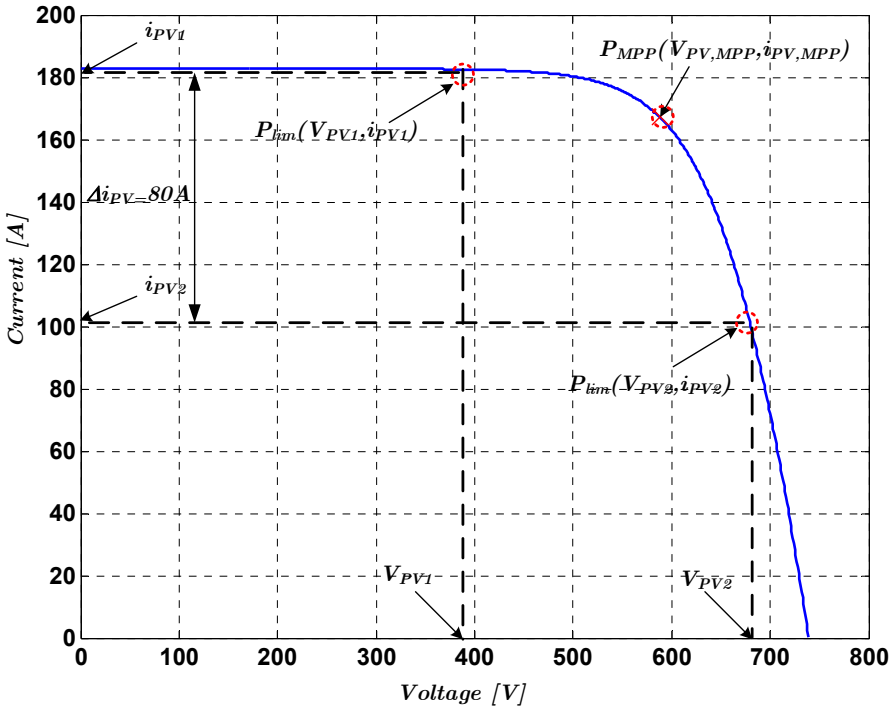

Fig.3. 35. I-V curve of a 100 kW PV array at 1000w/m2.

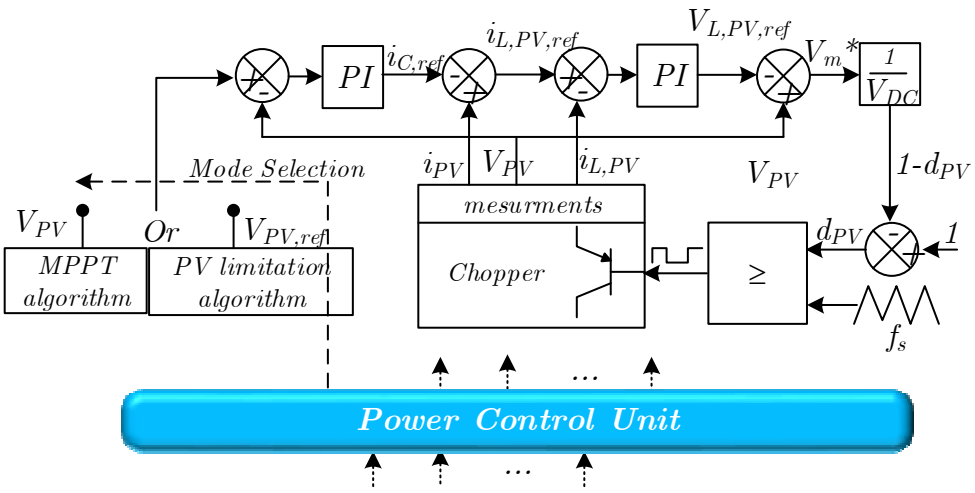

Fig.3.36. Control unit present MPPT and PV limitation of the PV array.

The control algorithm allowing the LPP operating mode is depicted in the flowchart given in Fig.3.37.

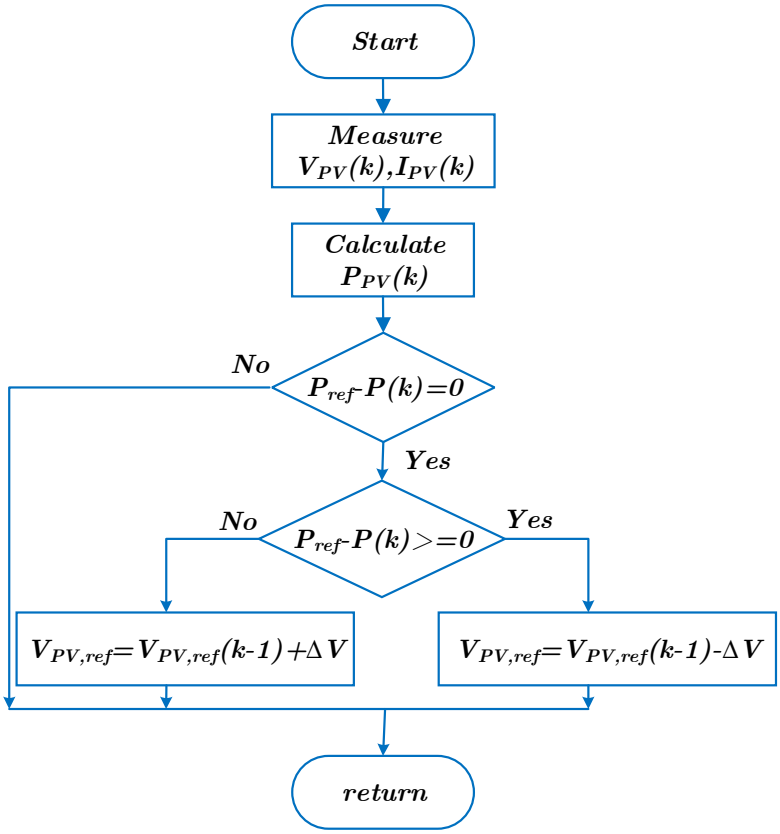

Fig.3. 37. Limited power point tracking algorithm.

3.7. Conclusion

In this chapter, a steady state analysis of the switching DC-DC boost converter is presented. This analysis, leads to good design of all the converter components. After that,

an average model of a PV based active generator in a DC-coupled structure has been detailed. The modelling of this generation system is led by considering each source with the dedicated power electronic converter. The objective is to control the different sources in order to satisfy the microgrid power requirements, in spite of the PV power fluctuations.

Control algorithms are obtained by the inversion principle, which helps to find all control equations of the different variables in the automatic control unit.

For the PV converter, where we don't need much dynamic performance, a simple two PI controllers have been used. While a Lyapunov direct method based controller have been used for both storage converters, in this case we have seen a comparison between this nonlinear control law and the PI control law. The obtained simulation results show that the nonlinear controller is better than the PI controller in terms of dynamical performances.

An overview of the classic MPPT algorithms is presented, and the important of a power limitation algorithm is clarified.

Chapter 04

4. Energy Management and Coordinated Control of the Active PV Generator

4.1. Introduction

The power flows between the different sources must be controlled in order to supply the real and reactive power required by the grid operator ($P_{go,ref}$, $Q_{go,ref}$). This is performed by a coordinated control of the different power electronic converters (Fig.3.1). Different control strategies have been presented to design the energy management of hybrid power systems and for various applications [Aya07], [Haj07], [Mor06]. In order to achieve the previous objectives, several specific problems have to be overcome, e.g. the fast and exact power control of each source with the power electronic converters; power dispatching of storage units according to their different technological characteristics for ensuring their optimal use of each storage device (life of the batteries, energy limit of the ultra-capacitor).

In this chapter, a hierarchical control structure is used and the design of the control system, including the power balancing and energy management strategies are detailed. The objective is to set up an active PV generator, which can work like a classical power plant; e.g. it must supply the power references coming from a grid operator.

4.2. System Description

The considered system in the present study consists of a PV generator, a lead acid battery as a long term storage system and an ultra-capacitor to deal with rapid power demand transitions as shown in Fig.1.1. The PV output power is processed by a MPPT based DC-DC converter while the powers of both battery and ultra-capacitor are handled by a dedicated bidirectional DC-DC converter (Buck&Boost converter) to ensure both charge and discharge operation modes. The overall sources are interconnected to the same DC-link, given the merits that this configuration offers to the system more flexibility and expandability [Lu10], [Fak11]. The connection to the grid utility is performed by a three-phase inverter, according to the grid restrictions [Lu10]. This configuration is known as an active generator where the excess of PV generation is stored in order to be restored when needed, whereas the energy stored in the ultra-capacitor is used to smooth the rapid changes in the power demand or in the PV generation (Fig.3.1).

4.3. Control of the Active PV Generator

4.3.1. Layout of the Control Structure

Since the first constraint of the control system is coming from a grid operator by giving a prescribed set point to the APG, on the other hand, the limited power generation of the APG sources, then a hierarchical control structure becomes the better solution for the control of the APG operation.

The schematic diagram shown in Fig.4.1 depicts the concept of this hierarchical control structure. The top level of the control structure is the Power Control Unit (PCU), which is the main task of the presented work, it consists of two sub-units namely: Control of the Operating Mode (COM) and Calculation of the Control Variables (CCV).

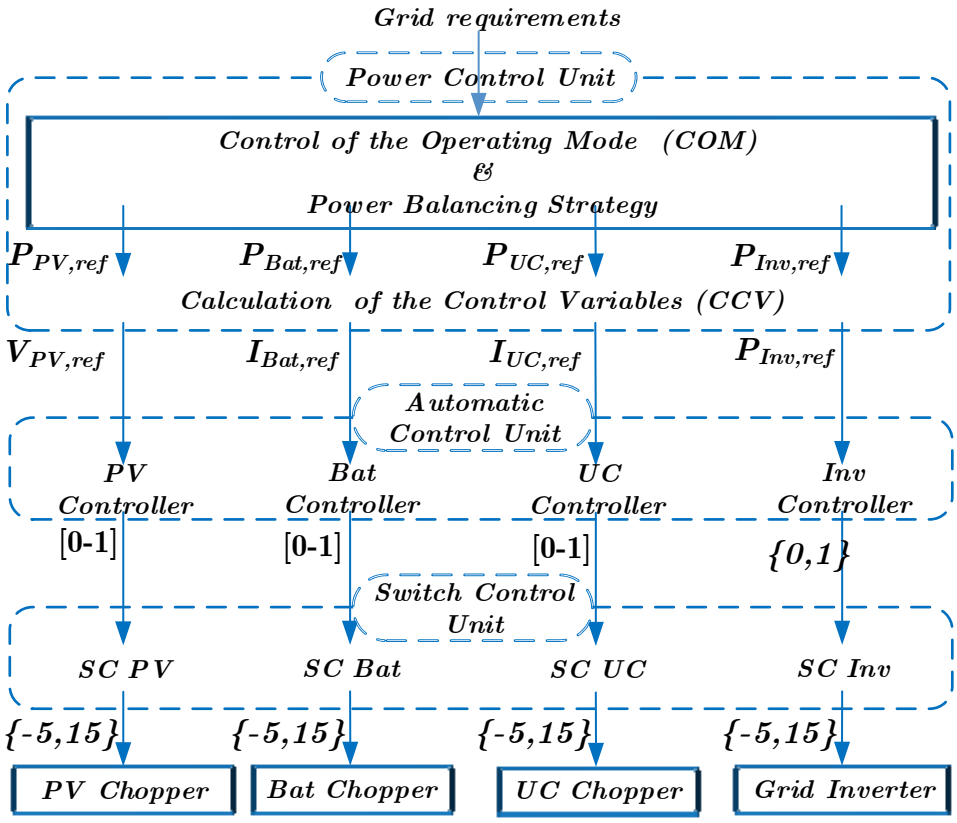

Fig.4. 1. Hierarchical control structure of the APG.

According to the prescribed power references, the PV power availability, and the state of charge of the storage units, the COM is responsible of generating the expected power references involved hereafter in the local control of the APG's sources. While the CCV receive the references coming from the COM and calculates the corresponding control variables (voltages or currents).

Tab.4.1 summarizes the equations used to calculate actual powers and reference control variables.

Tab.4.1. Power calculation for the active PV generator.

Power source	Power calculation	Power control
DC-link	$P_{DC} = V_{DC} i_{DC}$	$P_{DC,ref} = V_{DC} i_{DC,ref}$
Inverter	$\begin{bmatrix} Pg \\ Qg \end{bmatrix} = \begin{bmatrix} vg_d & vg_q \\ -vg_q & vg_d \end{bmatrix} \begin{bmatrix} i \\ i \end{bmatrix}$	$\begin{bmatrix} ig_{d,ref} \\ ig_{q,ref} \end{bmatrix} = \begin{bmatrix} vg_d & vg_q \\ -vg_q & vg_d \end{bmatrix}^{-1} \begin{bmatrix} Pg,ref \\ Qg,ref \end{bmatrix}$
PV panels	$P_{PV} = V_{PV} i_{PV}$	$V_{\mathrm{PV},ref} \leftarrow MPPT\ or\ LPPT$
Batteries	$P_{Bat} = V_{Bat} i_{Bat}$	$i_{Bat,ref} = P_{\mathrm{Bat},ref} / V_{\mathrm{Bat}}$
Ultra-capacitors	$P_{UC} = V_{UC} i_{UC}$	$i_{UC,ref} = P_{UC,ref} / V_{UC}$

The second unit is, called Automatic Control Unit (ACU). It allows the local controllers to generate the required duty cycles to set the output electrical quantities to their calculated references.

The last stage is the Switch Control Unit (SCU), responsible of generating the switching patterns determined by the integrated modulation technique.

In Fig.4.2, an explicit explanation of different stages is given.

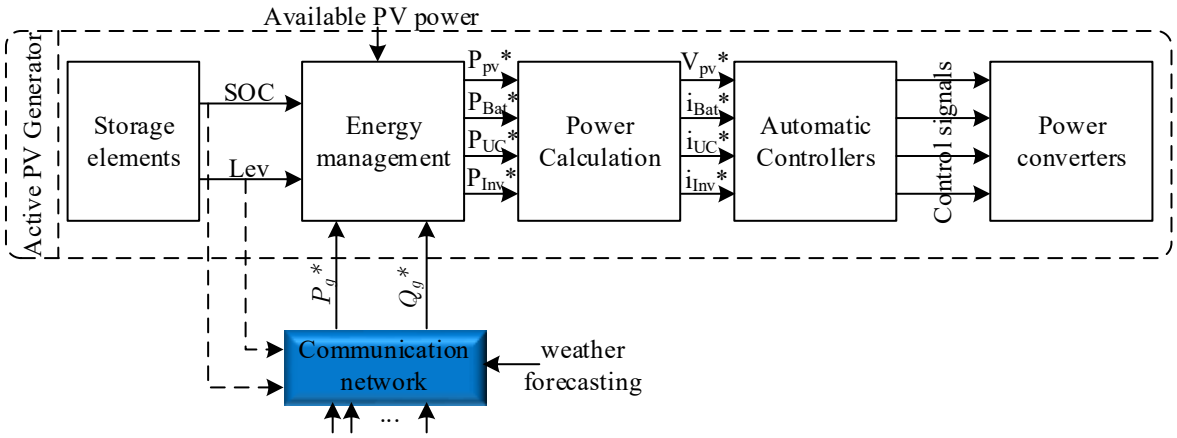

Fig.4.2. Control action of the APG.

4.3.2. Power Flow Modeling

The power flow between *APG*'s elements and the grid is described in (Fig.4.3).

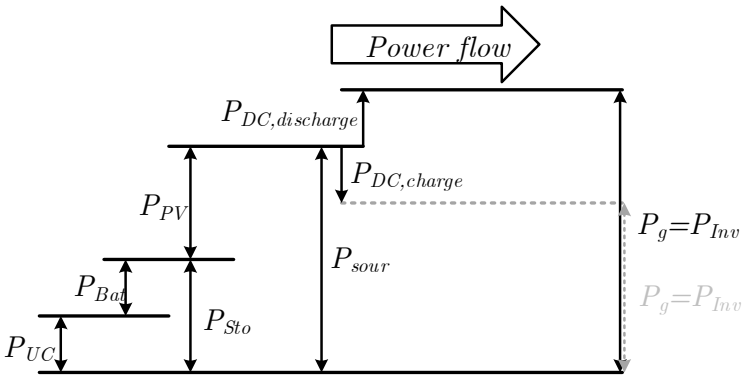

Fig.4.3. Power flow in a normal operating mode.

P_{Bat} and P_{UC} constitute P_{Sto}.

$$P_{Sto} = P_{Bat} + P_{UC} \tag{4.1}$$

P_{Sto} is used to complement P_{PV}, forming P_{Sour}.

$$P_{Sour} = P_{Sto} + P_{PV} \tag{4.2}$$

To obtain P_g, we finally reduce P_{DC}:

$$P_g = P_{Sour} - P_{DC,ref} \tag{4.3}$$

P_g must be supplied as a reference to the grid inverter, it must be equal to $P_{go,ref}$ asked by the grid operator at steady state.

$$P_{Inv} \cong P_{Inv,ref} = P_g \cong P_{go,ref} \tag{4.4}$$

4.3.3. Power Balancing Strategies

There exist two balancing strategies in the literature, which are the grid following strategy and the power dispatching strategy [Zho09]:

a- Grid Following Strategy (GFS)

In this strategy, the line control loops regulate the DC-link voltage (V_{DC}), where the control unit dispatches P_{Sour}. This strategy is used in classical "passive" PV generators.

When the normal operating mode happens, V_{DC} is regulated by adjusting the exchanged power with the grid, while the PV generator works in MPPT strategy.

$$P_{PV,ref} = P_{PV,mppt} \tag{4.5}$$

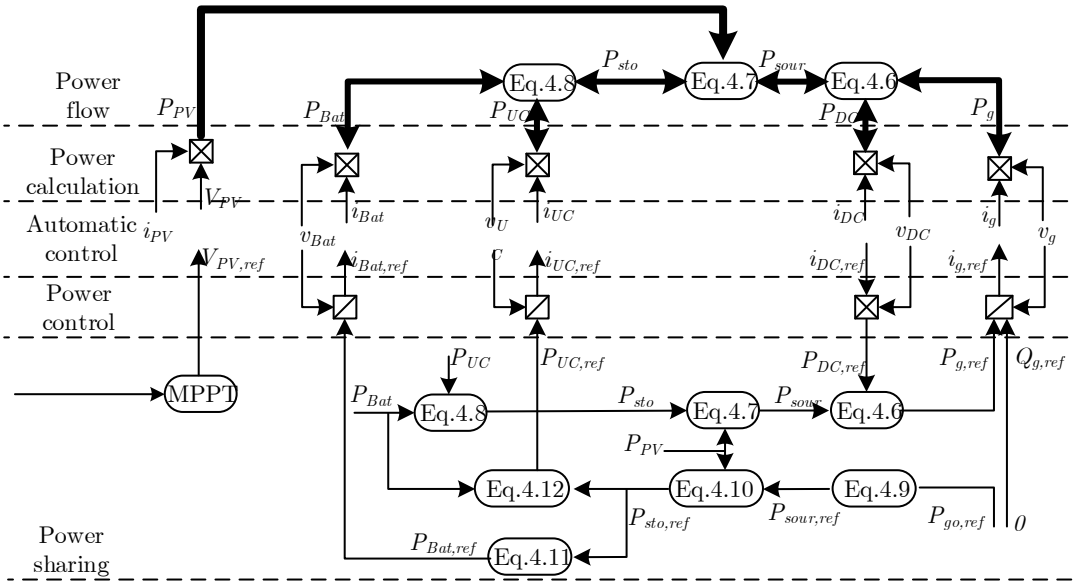

Fig.4. 4.Presentation of the power flow in the grid following strategy.

$P_{DC,ref}$ is used to calculate $P_{g,ref}$,

$$P_{g,ref} = P_{Sour} - P_{DC,ref} \tag{4.6}$$

The source power is,

$$P_{Sour} = P_{PV} + P_{Sto} \tag{4.7}$$

$$P_{Sto} = P_{Bat} + P_{UC} \tag{4.8}$$

The storage elements complement the PV generator to satisfy the asked power. In steady state, $P_{DC,ref}$ is zero, therefore,

$$P_{Sour,ref} = P_{g,ref} = P_{Inv,ref} = P_{go,ref} \tag{4.9}$$

The storage elements should supply or absorb the difference between the required power and the available PV power as shown in (Fig.4.6),

$$P_{Sto,ref} = P_{Sour,ref} - P_{PV} \tag{4.10}$$

However, $P_{Sto,ref}$ is a fast varying quantity due to the fluctuant PV power and the varying grid power. Moreover, the batteries have relatively slow power dynamics, and fast varying power reference is not suitable for their operating lifetime. To dispatch the power between batteries and ultra-capacitors, a Low-Pass filter is used:

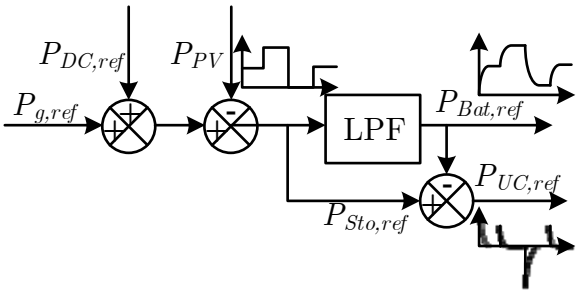

Fig.4. 5. Power references for storage units in the normal mode.

$$P_{Bat\_ref} = \frac{1}{1+\tau s} P_{Sto\_ref} \tag{4.11}$$

$$P_{UC,ref} = P_{Sto,ref} - P_{Bat} \tag{4.12}$$

Where the time constant of the LPF should be set by taking into account the dynamic of the batteries as well as the size of the ultra-capacitors.

The ultra-capacitors have a short energy storage capacity. However, they have a fast power dynamics and can supply power peaks. They can be used to fill the power gaps during the batteries transients.

b- Power Dispatching Strategy

In this strategy, the PV generator and storage units regulate the DC-link voltage, where the asked power can be controlled by the line control loops. This strategy is useful for islanding operation. In this work, according to the selected operating mode we use both grid following and power dispatching strategies.

If the PV generator is disconnected from the grid, the local control objectives change. Moreover, the DC-link cannot be controlled by adjusting the exchanged power with the grid, so the grid following strategy cannot be used. The only way to control the DC-link voltage is a combined use of powers of both PV array and storage units (Fig.4.6).

$$P_{Sour,ref} = P_{DC,ref} \tag{4.13}$$

The stored reference power is given by,

$$P_{Sto,ref} = P_{Sour,ref} - P_{PV} \tag{4.14}$$

4.3.4. Power Control Unit

4.3.4.1. Control of the Operating Mode (COM)

According to the state of charge and availability of each source (P_{PV}, Lev, SOC, grid requirements); several operating modes of the APG can be selected. In the present work, three main operating mode are explained giving a particular importance to the power limitation strategy (PLA), and additional operating modes are taken into account with details.

- ***Normal Operating Mode***

In this mode, the PV panels work always in MPPT. All storage units are in the normal range (available to enable a charge or discharge of power).

- ***PV Limitation Mode***

When the PV power is greater than the required power reference from the grid operator and the storage units are fully charged, the limitation mode should be applied [Cho15]. Therefore, we must limit the produced PV power.

- ***Islanding Mode***

When the primary source has low power and the storage units are empty, the produced power is not supplied to the grid, because it is not enough, so the APG must be disconnected from the grid and the PV panels work in MPPT to recharge batteries and ultra-capacitors as soon as possible.

- ***Short Duration Recovering Modes***

a. Full ultra-capacitor mode,

When the ultra-capacitors level increases above Lev_{max} and the SOC of the batteries still in a good range, the APG begins to work in the "full ultra-capacitors mode". The management strategy should be performed to recover the Lev as soon as possible. We do not use batteries in generating mode. As a result, the ultra-capacitors start to discharge and to return to the normal state rapidly.

b. Empty Ultra-capacitor Mode

When the level of the ultra-capacitors is too low ($Lev<Lev_{min}$), and the SOC of the batteries still in a good range, the APG begins to work in the "empty ultra-capacitors mode". The management strategy should be performed to recover the Lev as soon as possible. We do not use the batteries to store the extra power from the PV array, hence, ultra-capacitors start to recharge.

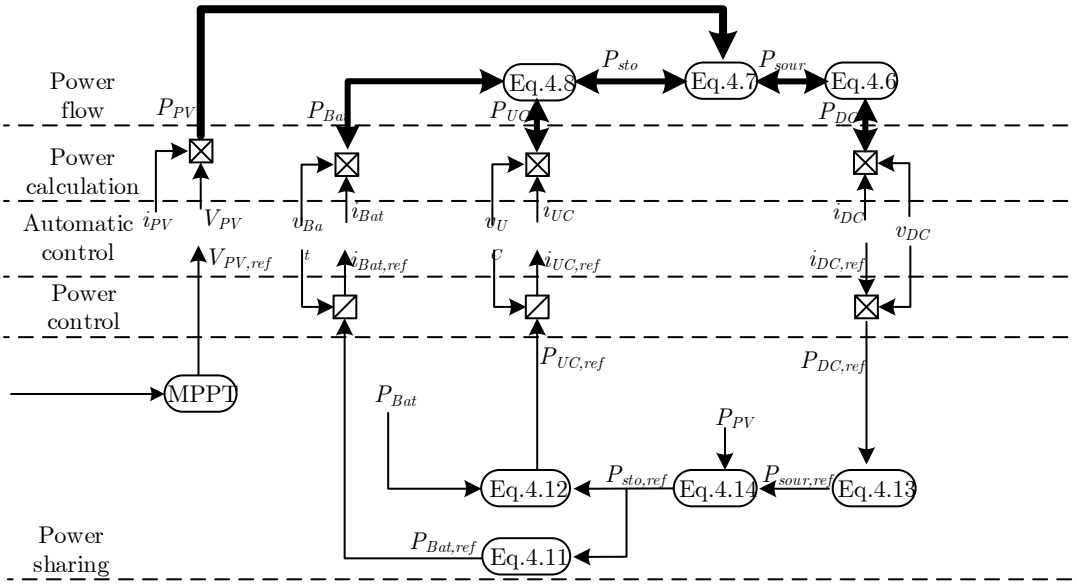

Fig.4. 6. Presentation of the power flow in the power dispatching strategy.

c. Full battery mode

When the SOC of the battery is full, the Lev of the ultra-capacitor is not full and the PV power is greater than the asked power, we do not switch directly to the PV limitation mode, but we use ultra-capacitor to store the extra power. When the ultra-capacitors become full, the PV limitation mode will be activated.

The flowchart presented in Fig.4.8. summarizes how to select the appropriate operating mode [Cho15].

4.4. Simulation Results and Interpretation

In order to validate the control design, and the performance of the energy management strategy, many simulations of the active PV generator are implemented with the *Matlab/Simulink* software (Fig. 4.8), the simulation parameters are presented in Tab.4.2,

the power converters are modelled with *SimPowerSystem* and the controllers are programmed in Embedded Matlab function blocs.

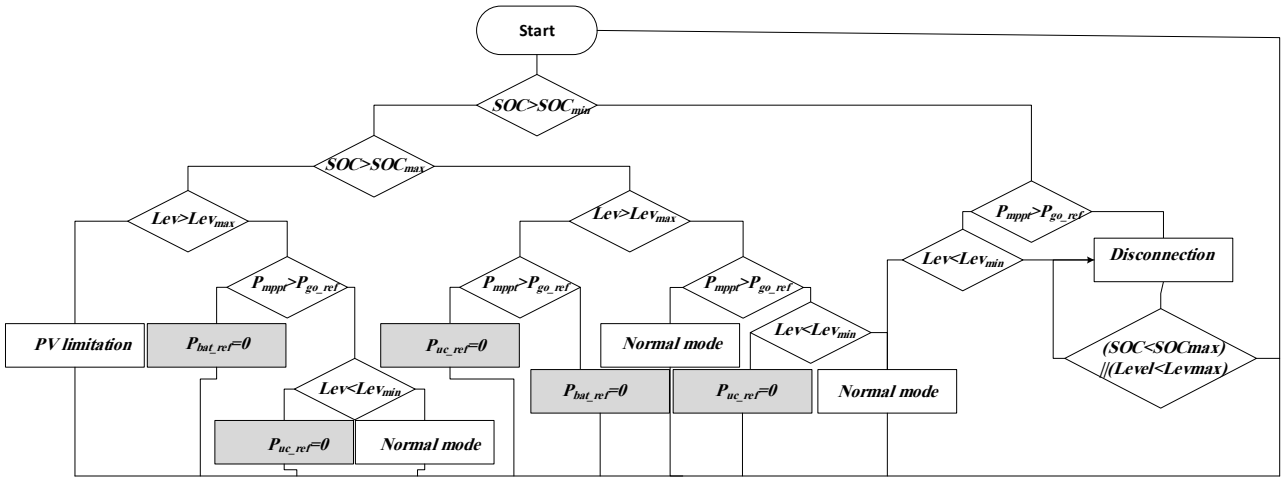

Fig.4.7. Flowchart showing the selection of the suitable operating mode.

Figures (4.9–4.12) show the variation of the storage power (P_{UC}, P_{Bat}) as a function of the (climatic conditions, state of charge and the grid requirements). They also, show the DC-link voltage, the inverter current and state of charge of both storage units. Here we considered a change every 10s in order to view the behavior of the system on electrical waveforms during the transient as well as the steady states.

4.4.1. Normal Operating Mode

In (Fig.4.9), from 0 to the 10th second, the grid power reference is equal to the maximum available PV power ($P_{PV,mppt}$=$P_{go,ref}$=70kW), before the PV power reaches the maximum power point, the missed grid power is delivered from the storage units, hence, the generated power (P_{Inv}) meet the requested reference ($P_{go,ref}$) very quickly.

At 10th second, according to the power production plan, the asked power from the grid changes very quickly to 100kW, the PV power (P_{PV}) is about 70kW and is not sufficient. The batteries cannot provide the missing power because of their low dynamic, where the ultra-capacitors are well used to compensate the power gap between the PV production and the grid demand. A good organization and tasks commutation between both storage units are reached.

Tab.4. 2. Simulation parameters.

	PV converter	Storage converters	Grid converter
Converter Topology	Boost converter	Buck & boost bidirectional converter	PWM inverter
Control technic	Two cascade PI Controllers	Two cascade PI Controllers or Two non-linear Controllers	Direct Power Controller (DPC) improved table
Control parameters (kp,ki)	Voltage: (0.164, 3.3) Current: (11.67, 1170)	Voltage : / Current_bat: (40, 2000) Current_uc: (15, 1000)	DC-link: (1.11, 61.68) DPC: /
Sample times: System: (discrete, Ts=$5e^{-6}$s)	MPPT algorithm: Ts,mppt=$0.5e^{-4}$s Controllers: Tc,*PV*=$0.5e^{-4}$s	Controllers: Tc,stor=$0.5e^{-4}$s	DC-link Controller: Tc,dc=$0.5e^{-4}$s. DPC: T_{DPC}=$0.5e^{-4}$s.

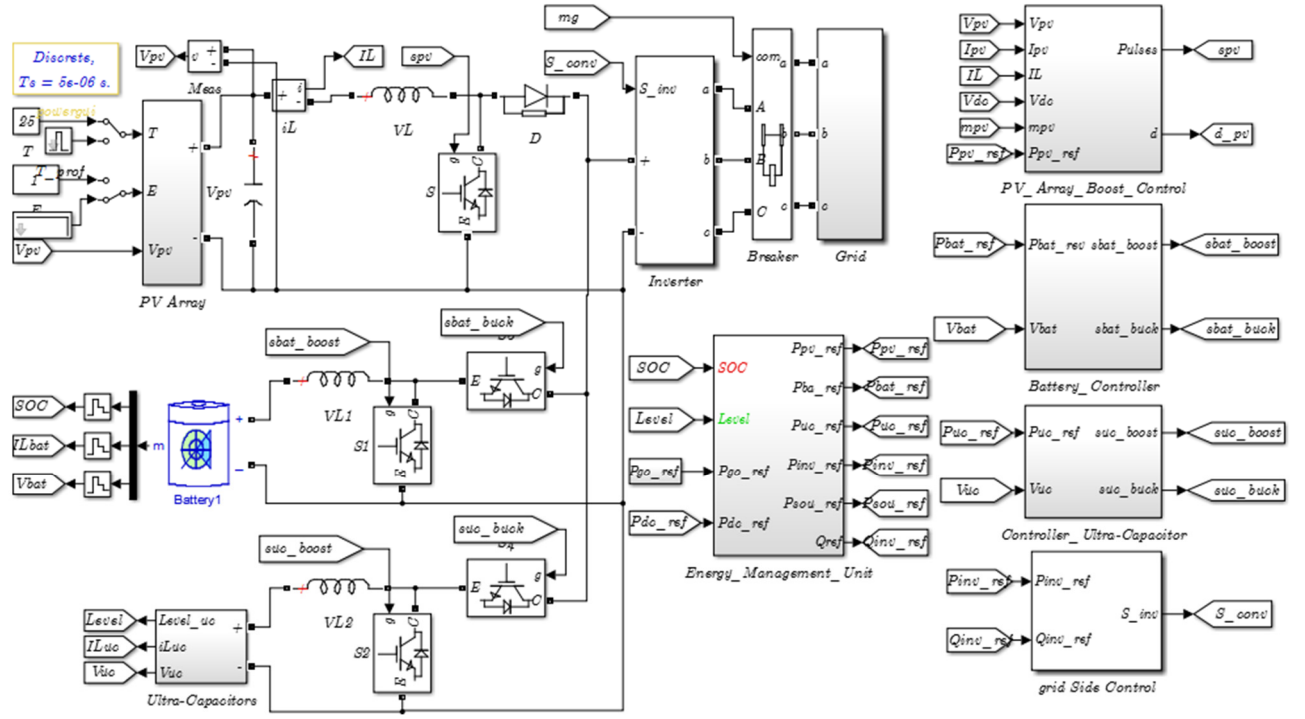

Fig.4.8. Presentation of the APG's models in Matlab/Simulink.

4.4.2. PV Limitation Mode

In this operating mode, when the day is sunny, the *SOC* of the batteries reach its maximum SOC_{max} and the voltage level of the ultra-capacitors reach also the Lev_{max}. Hence, the *PV* power must be limited at a certain set point, this is what called *PV limitation* mode.

In Fig. 4.11, during the time interval [0s-8s], we see that the generated *PV* power (100kW) is divided into 80kW to the grid and 20kW to the storage units. When the storage units reach the fully charged state (t=8s), the excess *PV* power cannot be injected into the storage units. Thus, the exchanged power with batteries and ultra-capacitors is null, and we can see that the generated power by the *PV* panels can strictly follow the grid reference (P_{PV}=$P_{inv,ref}$=$P_{go,ref}$). At t=20s, when the asked grid power changes to 90kW, the *PV*

limitation point changes to 90kW, therefore, we can observe that the PV panels are controlled in a dynamic set point of the PV limitation mode. At t=30s, the solar irradiation decreases from 1000 W/m^2 to 800W/m^2, here, the PV power is less than the grid reference, hence, the storage units will compensate the power gap between the PV production and the grid demand. First time, the ultra-capacitors support the batteries, after the transient, the ultra-capacitors will come back, and the batteries take the task of the permanent power.

We can observe: firstly, oscillations on the PV power waveform, due to the nature of the panel's I-V curve, when we move away from the MPP point to the right side, the sensitivity of the PV current versus the voltage perturbation will increase $(\Delta V_{pv} / \Delta i_{pv})_1 > (\Delta V_{pv} / \Delta i_{pv})_2$ this implies $\Delta P_1 > \Delta P_2$ (Fig.4.10.a). Secondly, these oscillations do not appear in the grid power, because they are absorbed by the ultra-capacitors. Therefore, the ultra-capacitors played their role perfectly.

4.4.3. Islanded mode (disconnection from the grid)

In this test (Fig.4.11), the generated PV power is less than the grid demand. The storage units still compensating the missed power until the SOC of batteries reach the SOC_{min}, at this time (t=5s), we can see that the active generator is disconnected from the grid, the injected power (P_{inv}) is null, and the batteries are charged with the available PV power. Ultra-capacitors are used to limit the batteries current during the transient, to regulate the DC-link voltage and to filter the PV power fluctuations. We observe that the DC-link voltage is well regulated with the power dispatching strategy (without the grid inverter) (Fig.4.12. -d-).

4.4.4. Recovering modes

As an example, we take the empty ultra-capacitors mode. In this test, the level of the ultra-capacitors is less than the minimum value, in other hand, the SOC of the batteries is normal; hence, we want to recover the Lev to its normal value. The suitable instant is t_1 (Fig.4.13.a), when both previous conditions occur and P_{PV} is greater than $P_{go,ref}$. Then, we do not use batteries to store the extra PV power. Hence, ultra-capacitors start to recharge. When the level of the ultra-capacitors becomes at the normal range (Fig.4.13.a. at $t=t_2$), we return to the original operating mode.

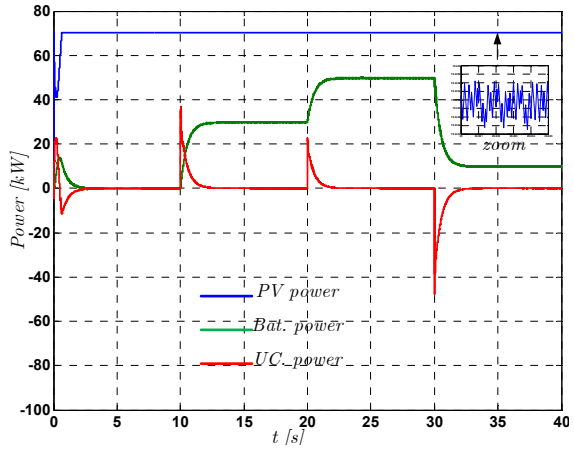

-a-

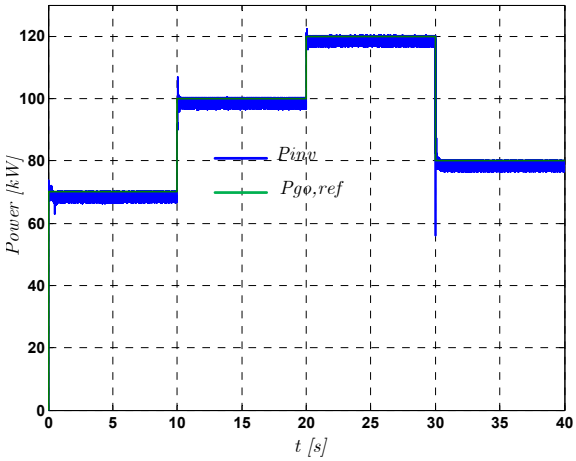

-b-

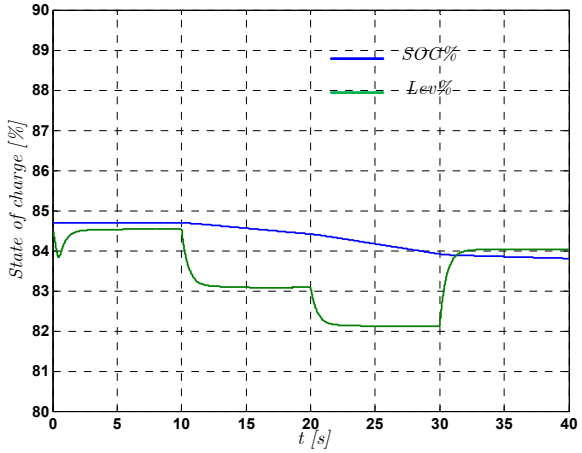

-c-

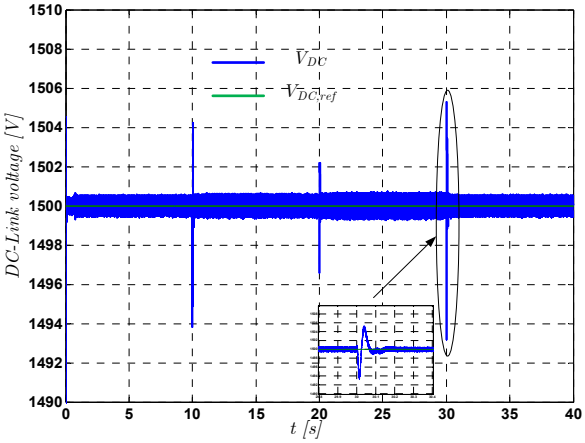

-d-

Fig.4. 9.Waveforms of the electrical quantities in a normal operating mode.

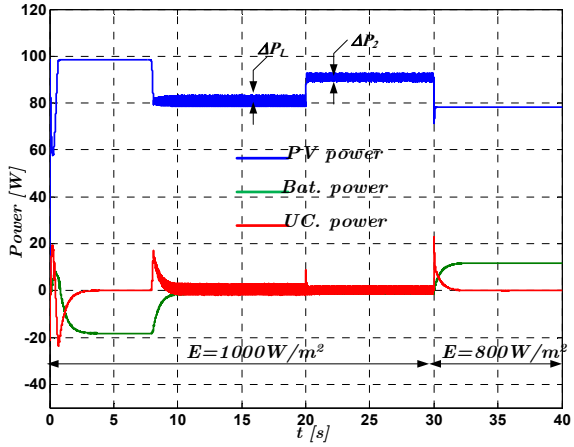

-a-

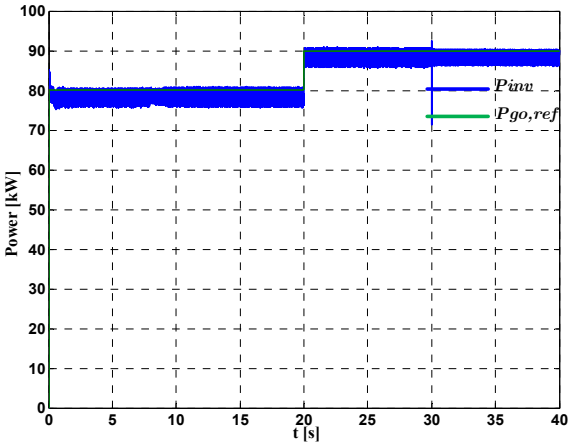

-b-

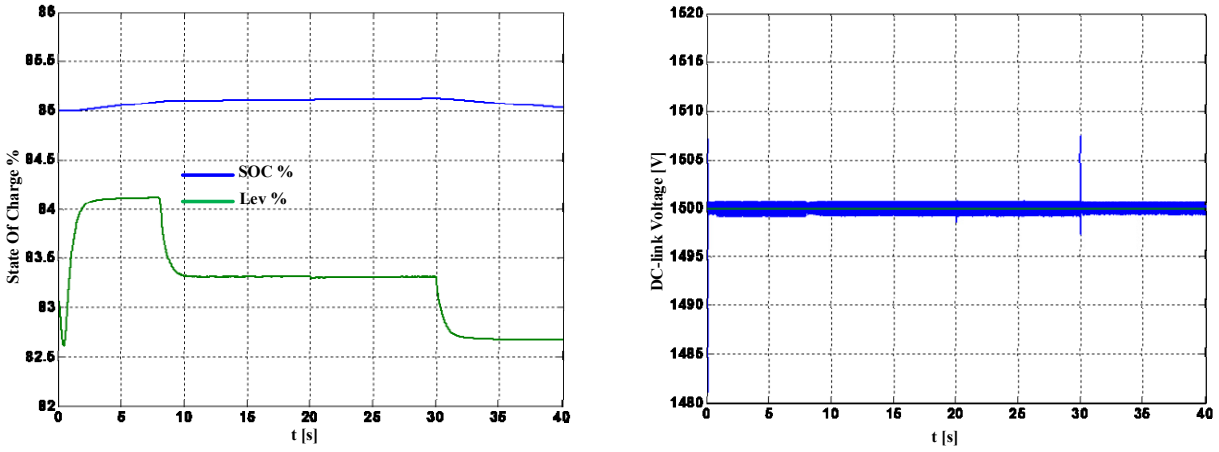

-c- -d-

Fig.4.10. Waveforms of the electrical quantities at PV limitation mode.

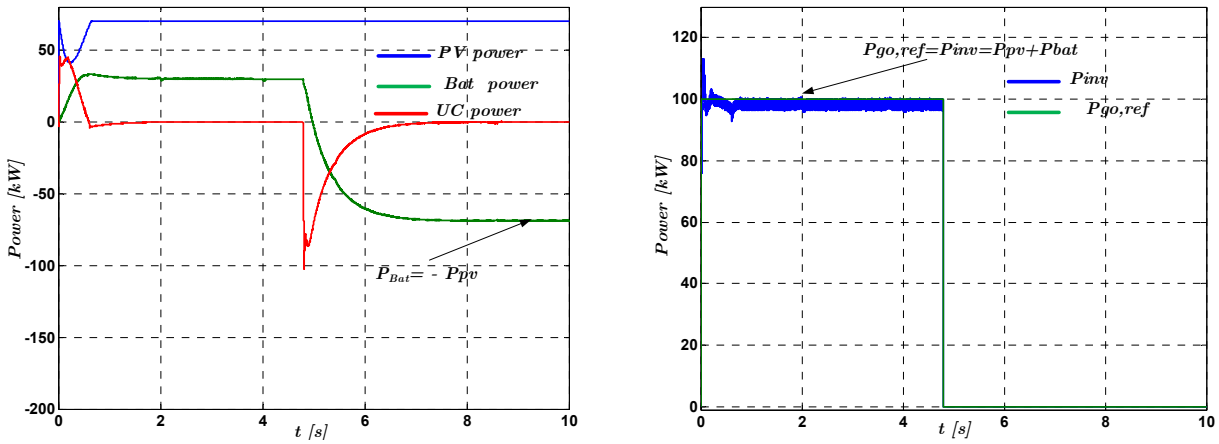

-a- -b-

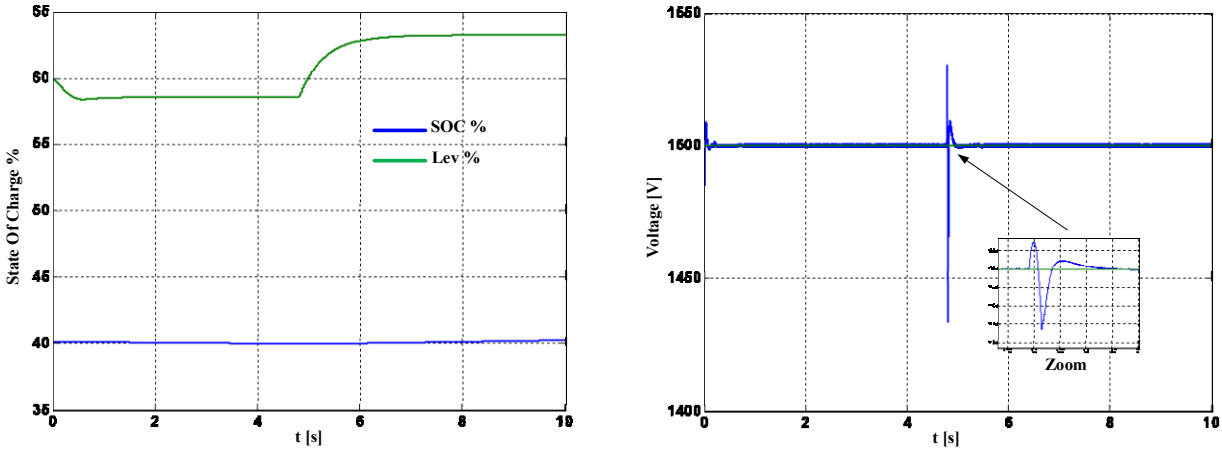

-c- -d-

Fig.4. 11. Waveforms of the electrical quantities in islanding (disconnected) mode.

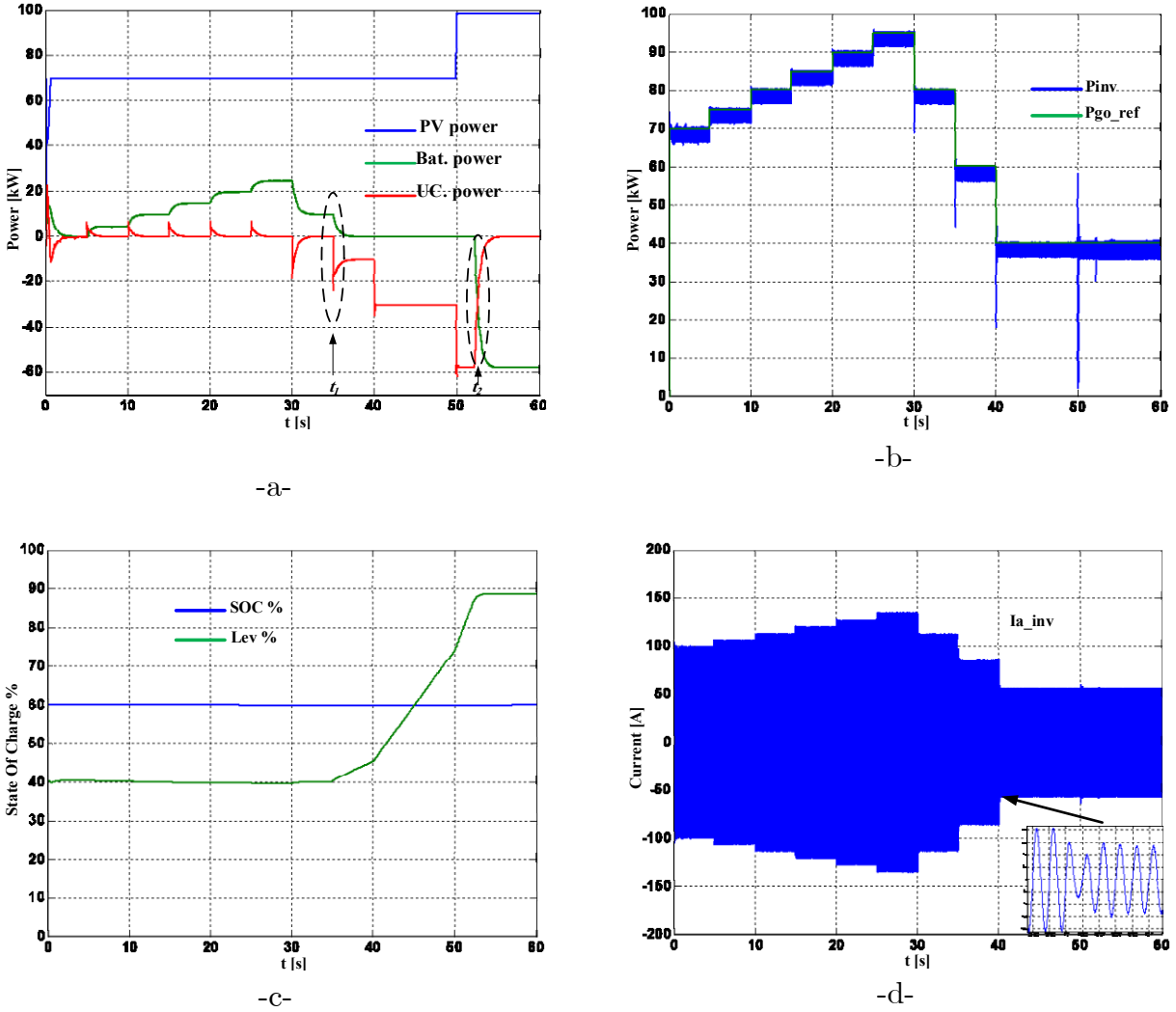

Fig.4. 12. Waveforms of the electrical quantities including some recovering modes.

4.5. Conclusion

In this chapter, a local energy management strategy of an active *PV* generator for a smart microgrid application is presented. Based on the weather prediction and the load forecasting, the power references is given by the grid operator. The real time power exchange of the *APG* with the microgrid is detailed. Different levels of the control system are studied and organized in a hierarchical control structure. Three main operating modes, other recovering modes that correspond to some faulty conditions, are highlighted and analyzed.

According to the state of the three sources, the energy management strategy chooses the corresponding operating mode and calculates the power reference for each source. Before passing the task to the batteries, the ultra-capacitors should undertake it; it is controlled to

supply the required transient power from storage units. From the calculated power references, the electrical references (voltages, currents) are realized by various control strategies. The regulation scheme of the DC-link depends on the chosen operating strategy, the grid following strategy is used when the APG is connected to the microgrid and the power dispatching strategy is used when the APG is disconnected, where the ultra-capacitors take up the task. Finally, the simulation results show that the energy management strategy works very well with good performances of the APG, such as smooth power, fast dynamic compensation, optimum utilization of storage elements.

General Conclusion

General Conclusion

Facing to the challenges of the energy and the environmental crisis, the development of renewable energies is encouraged. But their intermittent and fluctuant characteristics restrict the use of PV power as a main source of an electrical system. In this thesis, the concept of the PV based active generator is presented. Indeed, it consists in coupling on a common DC-link, energy storage systems in order to smooth the PV power fluctuations and to constitute an available energy reserve.

In the first chapter, the concept of smart microgrid and its related important parts and concepts are briefly clarified. A state of the art about microgrids and some EU examples are presented.

In the second chapter, a PV based active generator including lead acid batteries and ultra-capacitors was presented, and each source inside this hybrid generator was described and modeled. PV panels are modeled as a DC current source with the current output dependent on the terminal voltage, the temperature and the solar irradiation.

In the third chapter, average-values based models of all the sources in a DC-coupled structure are detailed. The modelling of this complex generation system is led by considering each source with the dedicated power electronic converter. The objective is to control the different sources in order to satisfy the microgrid power requirements, in spite of the PV power fluctuations. Control algorithms are obtained by the inversion principle, which helps to find all control equations of the different variables in the Automatic Control Unit. For the PV converter, where we don't need much dynamic performance, a simple two PI controllers have been used. While a Lyapunov direct method based controller have been used for both storage converters. In this case we have seen a comparison between this nonlinear control law and the PI control law, where the simulation results have shown that the nonlinear controller is better than the PI controller.

In the last chapter, a local energy management strategy of the proposed active PV generator for a smart microgrid application is presented. Based on the weather prediction and the load forecasting, the power references are given by the grid operator. The real time power exchange of the APG with the microgrid was detailed. Different levels of the control system were studied and organized in a hierarchical control structure. Three main operating modes, other recovering modes that correspond to some faulty conditions, are highlighted

and analyzed. According to the state of the three sources, the energy management strategy chooses the corresponding operating mode and calculates the power reference for each source. Before passing the task to the batteries, the ultra-capacitors should undertake it; it is controlled to supply the required transient power from storage units. From the calculated power references, the electrical references (voltages, currents) are realized by the various control strategies. The regulation scheme of the DC-link depends on the chosen operating strategy, the grid following strategy is used when the APG is connected to the microgrid and the power dispatching strategy is used when the APG is disconnected, where the ultra-capacitors take up the task. Finally, the simulation results show that the energy management strategy is satisfied and works well with good performances of the APG, such as smooth power, fast dynamic compensation, optimum utilization of storage elements.

Further works can now be oriented to:

- ✓ Both steady-state operations (grid connected mode and island mode) have already been discussed in this thesis. Transient operation due to the switching between these two modes is also very advantageous for searching, for example, to reduce the transient current during switching;
- ✓ The integration of the artificial intelligent in management algorithms;
- ✓ The nonlinear optimization with multi optimization variables is required and may be studied in the future.

Apendices

Appendices

I. Design of the PI Controllers in Boost Converter

All PI controllers are similar and they are designed based on pole placement method. Therefore, to avoid the repetition we suffice with one example.

We consider the intermittent PV current (I_{PV}) coming from the PV generator as a disturbance signal, and the power converter as two linear subsystems with some disturbances signals. The first system is the PV capacitor (Fig.A.1.a) while the second is the PV inductor (Fig.A.1.b).

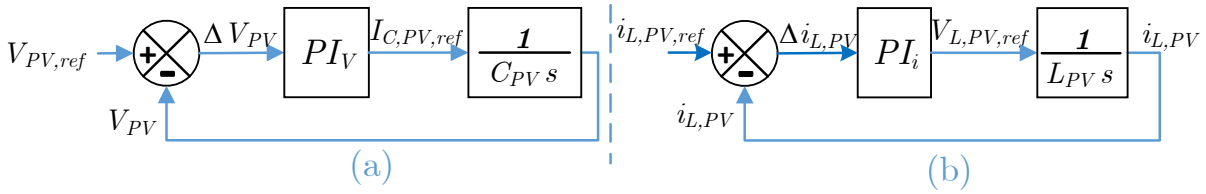

Fig.A.1. PV converter represented as two linear subsystems (a and b) after the simplification.

The mathematical model of the first sub system is simply given by

$$\frac{d}{dt}V_{PV} = \frac{1}{C_{PV}}I_{C_{PV}} \tag{a}$$

The second is

$$\frac{d}{dt}i_{L,PV} = \frac{1}{L_{PV}}V_{L,PV} \tag{b}$$

I.1. Voltage Control Loop

The open loop transfer function of the first system is given by,

$$T_{OL} = \left(Kp_v + \frac{Ki_v}{s}\right)\frac{1}{C_{PV}s} = \frac{Kp_v s + Ki_v}{C_{PV}s^2} \tag{c}$$

The closed loop transfer function is,

$$T_{CL} = \frac{Kp_v s + Ki_v}{C_{PV}s^2 + Kp_v s + Ki_v} \tag{d}$$

The general second-order transfer function looks like this:

$$T_{CL,g} = \frac{\omega_n^2}{s^2 + 2\xi\omega_n s + \omega_n^2} \tag{e}$$

If zeros does not affect the dynamic response, then, we can neglect them in terms of transient response. The system transfer function becomes,

$$T_{CL} = \frac{Ki_v}{C_{PV}s^2 + Kp_v s + Ki_v} = \frac{\frac{Ki_v}{C_{PV}}}{s^2 + \frac{Kp_v}{C_{PV}}s + \frac{Ki_v}{C_{PV}}} \tag{f}$$

Finally, we can easily choose the suitable gains (Ki and Kp) to get the desired closed loop response.

$$T_{CL} = T_{CL,g} \Rightarrow \frac{\omega_n^2}{s^2 + 2\xi\omega_n s + \omega_n^2} = \frac{\frac{Ki_v}{C_{PV}}}{s^2 + \frac{Kp_v}{C_{PV}}s + \frac{Ki_v}{C_{PV}}} \tag{g}$$

ξ : The dumping coefficient

ω_n : Natural frequency.

From (A.7),

$$\begin{cases} Ki_v = C_{PV}\omega_n^2 \\ Kp_v = 2C_{PV}\xi\omega_n \end{cases} \tag{h}$$

Equation (A.8) gives the relationship between the control gains and the 2nd order system parameters. It remains, how to determine these parameters (ω_n and ξ).

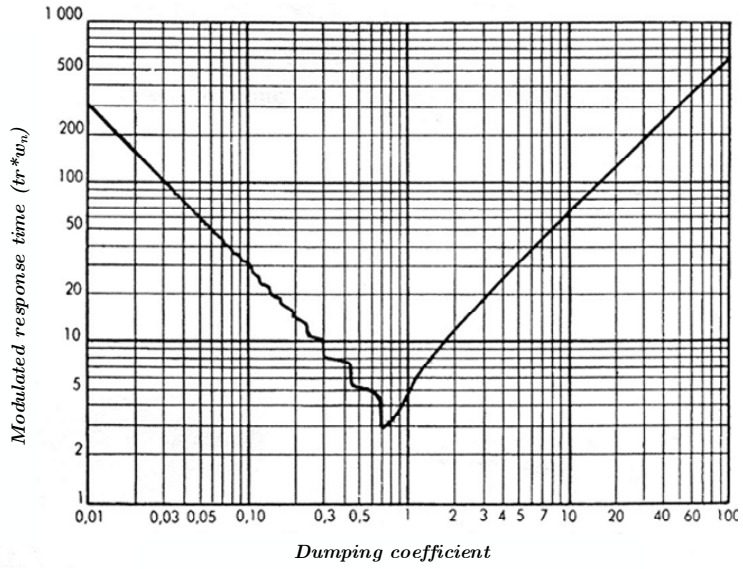

Fig.A.2. Response time curve of a second order system as a function of the dumping coefficient.

From the above curve ($tr_m = f(\xi)$), the minimum response time is obtained from the point $(\xi, \omega_n tr) = (\sqrt{2}/2, 3)$, by choosing the suitable response time we can get the resulting natural frequency on that point.

$$\begin{cases} \omega_n = \dfrac{tr_d}{3} \\ \xi = 0.707 \end{cases} \quad \text{(i)}$$

tr_d : Desired response time (selected by the designer).

I.2. Current Control Loop

Same as voltage control design, the only important difference here is that the current loop must be designed much faster than the voltage loop, because they are in cascade.

II. Electrical Design of a 100kw Peak Power PV Array.

II.1. Introduction

After we select one of the existing PV modules in the market (BPSX3200B in our case), we must estimate the required number of the PV modules for the specified AC output power, taking into account many criterion.

II.2. AC Energy Output of PV Array

The output of the PV array is affected by:

- ✓ Average solar radiation data for selected tilt angle and orientation;
- ✓ Manufacturing tolerance of PV modules;
- ✓ Temperature effects on the modules;
- ✓ Effects of dirt on the modules;
- ✓ System losses (eg. power loss in wiring cables);
- ✓ Conversion chain efficiency.

II.3. Power Yield

For a specified peak-power rating (kWp) for a solar array, a designer can determine the system's output power, it is known as the system's "Power Yield", which can be determined as follows:

$$P_{sys} = P_{array,STC} f_{temp} f_{man} f_{dirt} \eta_{pv,inv} \eta_{inv} \eta_{inv-sb} \quad \text{(j)}$$

$P_{array,STC}$: Rated output power of the array under standard test conditions, in watts;

f_{temp} : Temperature de-rating factor;

f_{man} : De-rating factor for manufacturing tolerance;

f_{dirt} : De-rating factor for dirt;

η_{inv} : Efficiency of the inverter;

η_{pv-inv} : Efficiency of the subsystem (cables) between the PV array and the inverter;

η_{inv-sb} : Efficiency of the subsystem (cables) between the inverter and the switchboard.

II.4. Solar Radiation

Solar irradiation is typically provided as kWh/m^2. However, it can be stated as daily Peak Sun Hours (PSH). This is the equivalent number of hours of solar irradiance of 1kW/m^2.

II.5. Allowable PV Voltage range

To insure the power balance, and the system stability, a minimum DC-link voltage is required (chapter 03). In addition, the PV boost converter have a safe operating range for the duty cycle (d). The duty cycle is depending on the voltage reference given by the tracking algorithms (MPPT, LPPT), which depends on climatic conditions (irradiation and temperature). Hereafter, a design procedure from an electrical viewpoint is given as a Matlab code.

II.5.1. Minimum Voltage at the PV output

When the temperature is at a maximum (Fig.A.4), then the Maximum Power Point Voltage (V_{MPP}) of the array should never fall below the minimum operating voltage of the boost chopper (ch.03, sec.3.2.7).

$$D_{\max} = 1 - \sqrt{\alpha} \quad \text{(k)}$$

Where: α is a non-ideality factor of the PV boost chopper.

It is recommended that the designer use maximum effective cell temperature of 70°C.

II.5.2. Maximum Voltage at the PV output

At the coldest daytime temperature the open circuit voltage of the array shall never be greater than the maximum allowed input voltage for the inverter. Therefore, the lowest

daytime temperature for the area where the system is installed shall be used to determine the maximum V_{OC}.

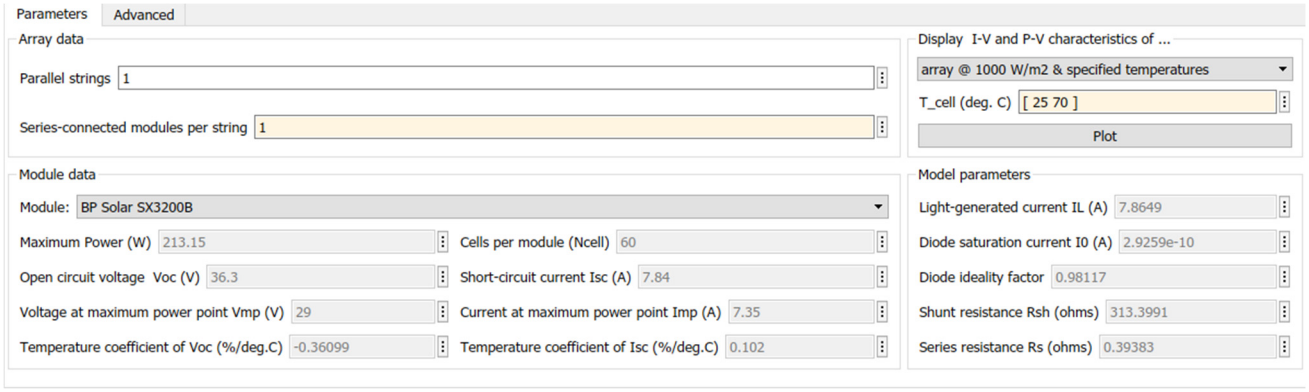

Fig.A.3. Data sheet for "BP Solar SX3200B" PV module obtain from Matlab-Simulink.

Fig. A.3 shows the technical data for the BP Solar SX3200B PV module.

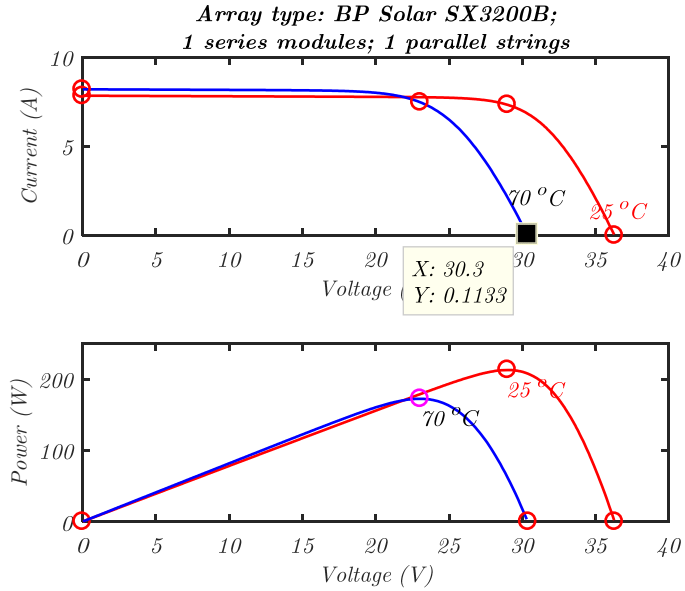

Fig.A.4. P-V and I-V curves of "BP Solar SX3200B" PV module for different temperature values.

```
%% Sizing of the BP_SX3200B based PV array for Pmax=100kW;

% Ta=25°C, G=1; from datasheet
vmpp_25=29; % Module voltage @MPP
Impp_25=7.35; % Module current @MPP
P_MPP_Mod_25=vmpp_25*Impp_25; % MPP
Voc=36.3; % Open circuit voltage
Isc=7.84; % short circuit current

% Ta=70°C, G=1; from model
vmpp_70=23.04;
Impp_70=7.486;
P_MPP_Mod_70=vmpp_70*Impp_70;
Voc_70=30.4;
Isc_70=8.154;

%% Design start here:-----------------------------------------------------------
P_desired=100e3;
Nu=0.8; % Nu include all de-rating factors and efficiencies
Pmpp_array_max=P_desired/Nu; % specified power
Vdc=1500; %required dc-link voltage
```

```
Rmin=Vdc^2/Pmpp_array_max; % maximum boost load
rL=10e-3;% internal resistance of the PV inductor
alfa_max=rL/Rmin; % non-ideality parameter (inductor) of the boost chopper
d_max=1-sqrt(alfa_max); % critical duty cycle (it corresponds to the maximum
voltage ratio)
d=0.7; % maximum allowable operating duty cycle (for safety)
ro=1/(1+alfa_max/((1-d)^2));% Efficiency for a given duty cycle
M_max=ro/(1-d); % Real voltage ratio
Msp=round(Pmpp_array_max/P_MPP_Mod_25); % number of PV modules to produce the
desired peak power
Vpv_array_min=Vdc/M_max; % minimum PV voltage to keep the duty cycle below its
maximum
Ms=round(Vpv_array_min/Voc_70); % the required number of series modules at the
worst temprature case Ta=70
Mp=round(Msp/Ms); % the required number of parallel strings at the worst temprature
case Ta=70.
```

Bibliography

Bibliography

[ABB11] ABB white paper, "Battery energy storage, Optimize integration of renewable energy to the grid", 2011

[Ay07] M.Y. Ayad et al, "Voltage regulated hybrid DC power source using supercapacitors as energy storage device", Energy Conversion and Management, vol. 48, 2007, pp. 2196-2202.

[Bel13] Beltran H., Bilbao E., Belenguer E., Etxeberria-Otaoui I., and Rodiguez P., "Evaluation of Storage Energy Requirements for Constant production in PV Power Plants",
IEEE Trans. on Industrial Electronics, vol. 60, no.3, March 2013. pp.1225-1234.

[Bha05] Bhatia, R.S., Jain, S.P., Jain, D. K. and Singh, B., "Battery Energy Storage System for Power Conditioning of Renewable Energy Sources", PEDS 2005, Proceedings of
the International Conference on Power Electronics and Drives Systems, 2005, vol. 1, pp. 501-506.

[Bps15] British Petroleum, "BP Statistical Review of World Energy", 2015
Available on: https://www.bp.com/content/dam/bp/pdf/energy-economics/statistical-review-2015/bp-statistical-review-of-world-energy-2015-full-report.pdf

[Cho15] A. Choudar, D. Boukhetala, S. Barkat, and J-M Brucker, "A local energy management of a hybrid PV-storage based distributed generation for microgrids", Energy Conversion and Management, vol. 90, 2015, pp. 21–33.

[DE08] U.S. Department of Energy, "The SMART GRID: an introduction" by Litos Strategic communication under contract, how a smarter grid works as an enabling engine for our economy, our environment and our future. 2008, No. DE-AC26-04NT41817, Subtask 560.01.04, available on:
https://www.smartgrid.gov/document/smart_grid_introduction.

[DE12] Department of Energy Office of Electricity Delivery and Energy Reliability. Summary Report: 2012 DOE Microgrid Workshop Report. 30-31 2012, Chicago, Illinois. Available on:
file:///C:/Users/choud/Desktop/2012%20Microgrid%20Workshop%20Report%2009102012.pdf.

[Ebk01] D. Linden, and T. B. Reddy, "Handbook of Batter", 3d ed, McGraw-Hill, 2001, available on:

http://www.etf.unssa.rs.ba/~slubura/diplomski_radovi/Zavrsni_rad_MarkoSilj/Literatura/Handbook%20Of%20Batteries%203rd%20Edition.pdf.

[Ebk13] S. Chakraborty, M. G. Simões and W. E. Kramer, "Power Electronics for Renewable and Distributed Energy Systems", Springer-Verlag, London, 2013.

[Ecp14] European Commission, "EU Energy in Figures, Statistical Pocketbook", 2014 Available on : *http://ec.europa.eu/energy/sites/ener/files/documents/2014_-pocketbook.pdf.*

[End01] M. Endo, T. Takeda, Y. J. Kim, K. Koshiba and K. Ishii, "High Power Electric Double Layer Capacitor (EDLC's); from Operating Principle to Pore Size Control in Advanced Activated Carbons", Carbon Science, 2001, vol. 1, pp. 117-128,

[EPRI01] Investigation of the Technical and Economic Feasibility of Micro-Grid Based Power Systems, EPRI, Palo Alto, CA, USA, 2001. 1003973.

[Fa11] H. Fakham, D. Lu, and B. Francois, "Power Control Design of a Battery Charger in a Hybrid Active PV Generator for Load-Following Applications", IEEE Transactions on Industrial Electronics, vol. 58, no. 1, 2011.

[GEI15] [What are the Benefits of the Smart Microgrid Approach? | Galvin Electricity Initiative. Available: http://www.galvinpower.org/resources/microgridhub/smartmicrogridsfaq/benfits., accessed Feb. 13, 2015.

[Haj 07] Hajizadeh, A. and Golkar, M. A., "Intelligent power management strategy of hybrid distributed generation system", Elsevier, electrical Power and Energy systems, 2007, pp. 783-795.

[Hat07] Hatziargyriou, N., Asano,H., Iravani, R. and Marnay, C., "Microgrids-an Overview of Ongoing Research, Development and Demonstration Projects", IEEE Power & Energy Magazine, July/August 2007, p. 78-94.

[Iea03] International Energy Agency, "Renewable Energy Working Party", 2003. Available on: http://library.umac.mo/ebooks/b1362376x.pdf.

[Iea14] International Energy Agency, "Key world energy statistics", 2014 Available on: http://www.iea.org/publications/freepublications/publication/keyworld2014.pdf

[IEC11] International Electrotechnical Commission, "Electrical Energy Storage", Switzerland, 2011. Available on: www.iec.ch/whitepaper/pdf/iecWP-energystorage-LR-en.pdf.

[IRE16] International Renewable Energy Agency, "Renewable Energy Benefits: Measuring the Economics", IRENA 2016, Abu Dhabi.
Available on : http://www.irena.org/DocumentDownloads/Publications/IRENA_Measuring-the-Economics_2016.pdf

[Kaz16] Marian K. Kazimierczuk, “Pulse Width Modulated DC-DC Power Converters”, Second Edition, John Wiley & Sons, Ltd, 2016.

[Li08] P. Li, B. Francois, Ph. Degobert, and B. Robyns, "Multi-level representation for control design of a super capacitor storage system for a microgrid connected application ", ICREPQ’08, Santander, 12-14 Mars 2008.

[Li08a] Li Peng, Degobert P., Robyns B., and Francois B. “Implementation of interactivity across a resilient microgrid for power supply and exchange with an active distribution network”, CIRED Seminar 2008: SmartGrids for Distribution, Frankfurt, June 2008.

[Lis10] M. Liserre, T. Sauter, and J. Y. Hung, “Integrating Renewable Energy Sources into the Smart Power Grid through Industrial Electronics”, IEEE Power and Energy Magazine, 2010.

[Lu09] D. Lu, and B. François, “Strategic framework of an energy management of a microgrid with a photovoltaic-based active generator”, Electromotion, EPE, joint symposium, Chapter “Electric drives”, Lille, France, 1-3 July 2009, pp. 342-347

[Lu10] D. Lu, T. Zhou, H. Fakham, and B. Francois, “Application of Petri Nets for the Energy Management of a Photovoltaic Based Power Station Including Storage Units,” 2010, Renew. Energy, vol. 35, no. 6, pp. 1117–1124.

[Mar01] M. Sc. Mariusz Malinowski, “Sensorless Control Strategies for Three-Phase PWM Rectifiers”, Ph.D. Thesis, Warsaw, Poland, 2001.

[Mass15] MassCEC. Microgrids—Benefits, Models, Barriers and Suggested Policy Initiatives for the Commonwealth of Massachusetts. [Online]. Available: http://www.masscec.com/content/microgrids-%E2%80%93-benefitsmodels-barriers-and-uggested-policy-initiatives-commonwealth, accessed Feb. 13, 2015.

[MFE13] L. Schmitt, J. Kumar, D. Sun, S. Kayal, and S.S. (Mani) Venkata, Microgrids and the Future of the European City, IEEE Power and Energy Magazine, 2013, 1540-7977.

[Mit06] Mitra, I., “A Renewable Island Life Electricity From Renewables on Small Islands”, Refocus, Volume 7, Issue 6, November-December 2006, pp. 38-41

[Mor 06] Moreno, J., Ortuzar, M. E., Dixon, J. W., "Energy Management System For A Hybrid Electric Vehicle, Using Ultra capacitors and Neural Networks", IEEE Transactions on Industrial Electronics, vol. 53, no.2, 2006, pp. 614-623,

[Mot14] M. Motevasel, and A. R. Seifi, “Expert Energy Management of a Micro-Grid Considering Wind Energy Uncertainty”, Energy Conversion and Management, vol. 83, 2014, pp 58-72.

[NAA12] National Alliance for Advanced Technology Batteries (NAATBATT), "Distributed Energy Storage Serving National Interests", 2012. Available on: http://naatbatt.org/naatbatt-white-paper-distributed-energy-storage-serving-national-interests-dec-4-2010/.

[Pal14] O. Palizbana, K. Kauhaniemia, and J. M. Guerrero, " Microgrids in Active Network Management- Part I: Hierarchical Control, Energy Storage, Virtual Power Plants, and Market Participation", Journal of Renewable and Sustainable Energy Reviews, vol. 36, 2014, pp. 428–439.

[Pen08] P. Li, P. Degobert, B. Robyns, and B. Francois, "Implementation of Interactivity Across a Resilient Microgrid for Power Supply and Exchange with an Active Distribution Network", CIRED Seminar 2008: Smart Grids for Distribution, Frankfurt, June 2008.

[Rif09] Riffonneau Y., "Gestion des Flux Energétiques dans un Système Photovoltaïque avec Stockage, Connecte au Réseau", Thèse de Doctorat de l'Université Joseph Fourrier, Grenoble, France, 2009.

[Rif09a] Riffonneau Y., Bacha S., Barruel F., and Delaille A. "Energy Flow Management in Grid Connected PV Systems with Storage - A Deterministic Approach", IEEE International Conference, 2009.

[SERI82] Paul Hersch; Kenneth Zweibel, "Basic Photovoltaic Principles and Methods", Solar Energy Research Institute, Technical Information Office , 1982

[Slo91] Jean-Jacques E. Slotine, and Weiping Li, "Applied nonlinear control", Prentice-Hall, Inc, 1991.

[Sma12] SmartGrids – CRE, "Smart Grid City : une Gestion Locale des Sources d'Approvisionnement et de Consommation", 2011, available on : http://www.smartgrids-cre.fr/index.php?p=smartcities-smart-grid-city

[Sur14] S. Suryanarayanan and E. Kyriakides, ''Microgrids: an Emerging Technology to Enhance Power System Reliability,'' IEEE Trans. Smart Grid, Mar. 2012. Available: http://smartgrid.ieee.org/march-2012/527-microgrids-an-emerging-technology-to-enhance-powersystem-reliability., accessed Nov. 13, 2014.

[Url13] Santiago Miret, "Storage Wars: Batteries Vs. Supercapacitors", 10 November 2013, available on: http://berc.berkeley.edu/storage-wars-batteries-vs-supercapacitors/.

[Url15] Kathie Zipp, "What is the best type of battery for solar storage?", Solar Power World Online, August 21, 2015, available on: http://www.solarpowerworldonline.com/2015/08/what-is-the-best-type-of-battery-for-solar-storage/.

[Vel14] R. Velik, P. Nicolay, “A cognitive decision agent architecture for optimal energy management of microgrids”, Elsevier, Energy Conversion and Management, vol. 86, 2014, pp. 831–847.

[Yan16] Xue Yang, Hao Niu, He Jiang, Qian Wang, and Fengyu Qu, “High Energy Density All-Solid-State Asymmetric Supercapacitor Based on Mos2/Graphene Nanosheet and Mno2/Graphene Hybrid Electrodes”, Journal of Materials Chemistry A, 2016

[Yu04] X. Yu, K. Strunz, “Combined Long-Term And Short-Term Access Storage For Sustainable Energy System”, IEEE Power Engineering Society General Meeting, vol. 2. 10 June 2004, pp. 1946-1951.

[Zho09] T. Zhou, P. LI, and B. François, “Power Management Strategies of a DC-Coupled Hybrid Power System in a Microgrid for Decentralized Generation”, EPE '09, 13th European Conference on Power Electronics and Applications, Barcelona, 2009.